University of Alberta

Effects of Closely-Spaced Buildings on Dispersion of Stack Exhaust Gases

By

Ian Fabris Ⓒ

A Thesis Submitted to the Faculty of Graduate Studies and Research in Partial Fulfillment of the Requirements for the Degree of Master of Science

Department of Mechanical Engineering

Edmonton, Alberta

Fall 1998

Canada

ABSTRACT

This thesis presents three publication manuscript papers dealing with the effect of closely spaced buildings on the dispersion of exhaust gases. The first paper develops a final-rise gaussian model with a limit on the amount of dilution produced by plume height. It is shown that this is a suitable model for predicting dilutions over buildings with the same roof height and dilutions of plumes from isolated stacks with no buildings present. In the second paper, the final-rise gaussian model is extended to produce a roof-level dispersion model for cases where a plume is emitted from a stack on a building downwind of a taller adjacent building. The model includes extra initial dilution and added vertical spread and a decrease, caused by building downwash, in the effective plume trajectory and if necessary a virtual origin shift of the plume. Criteria are developed to determine if the plume is trapped in a recirculation cavity formed in the wake of the upwind building. The third paper assesses the performance of the gaussian model in the first two papers in predicting dilutions on the wall of a building adjacent to a lower emitting building. The average dilution on the roof of the emitting building and the roof of the adjacent building is predicted using the roof-level theoretical model from the second paper as an estimate of the dilution on the wall.

TABLE OF CONTENTS

LIST OF TABLES

LIST OF FIGURES

LIST OF NOMENCLATURE

a	exponent for power law velocity profile
A_j	attenuation correction for pixels in row j
A_y	plume spreading rate in crosswind direction
A_z	plume spreading rate in vertical direction
B_j	plume rise constant
B_o	constant in initial plume spread Equation (2.24)
C	concentration, $[kg/m^3]$
C_{cal}	concentration of fluorescent dye in calibration box, $[mg/L]$
C_e	concentration of contaminant in stack exhaust gas, $[kg/m^3]$
C_{jet}	concentration of contaminant in jet, $[kg/m^3]$
C_r	centerline concentration at roof level, $[kg/m^3]$
C_s	concentration at source, $[kg/m^3]$
C_x	concentration of plume at downstream position x, $[kg/m^3]$
d	inside diameter at stack tip, $[m]$
D	dilution, ratio of concentration of exhaust gas to concentration at any point in space
D_{adj}	dilution at adjacent building roof level
D_{emit}	dilution at emitting building roof level
D_{ij}	dilution observed by camera pixel in column i and row j
D_{min}	minimum dilution at roof level at a particular downstream position
d_{plume}	effective diameter of plume for uniform profile, $[m]$
d_s	effective source diameter, $[m]$

d_{ref}	reference diameter used to normalize the product Md, [m]
F	fraction of available light collected by detector
G_{ij}	gain factor for pixel ij, [kg/(m^3·counts)]
h	plume height above concentration reflecting surface, [m]
H	reference building height, [m]
H_{adj}	adjacent building height, [m]
H_c	height of front edge roof recirculation zone, [m]
H_{cavity}	height of building wake recirculation cavity, [m]
h_f	final rise height of plume above concentration reflecting surface, [m]
h_s	stack height above concentration reflecting surface, [m]
h_{total}	total effective plume height including building downwash terms, [m]
I_e	laser light intensity, [W/m^2]
I_{ij}	laser light intensity at point ij, [W/m^2]
I_o	initial laser light intensity, [W/m^2]
$I_{o,ij}$	laser light intensity at point ij without attenuation , [W/m^2]
L_c	length of front edge recirculation zone, [m]
L_{cavity}	length of building wake recirculation cavity, [m]
L_v	Lagrangian turbulent eddy scale in crosswind direction, [m]
L_w	Lagrangian turbulent eddy scale in vertical direction, [m]
M	ratio of exhaust stack gas velocity to windspeed
N	number of counts
Q_e	volume flow rate of contaminant at stack exhaust, [m^3/s]
Q_{rot}	volume flow rate through rotameter, [m^3/s]

R	scaling length defined as $R=H^{2/3}Y^{1/3}$, [m]
R_d	scaling length defined as $R=\Delta H^{2/3}Y^{1/3}$, [m]
U	windspeed, [m/s]
U_c	windspeed at effective convection, [m/s]
U_H	windspeed at reference building height H , [m/s]
$U_{H.lab}$	windspeed at reference building height H in laboratory model, [m/s]
U_s	windspeed at stack height
v_{rms}	crosswind rms turbulence velocity
W_e	mean exhaust stack velocity at stack tip, [m/s]
$W_{e.lab}$	exhaust stack velocity at stack tip in laboratory model, [m/s]
w_{rms}	vertical rms turbulence velocity, [m/s]
x_{adj}	distance from stack to wall of upwind adjacent building, [m]
X_c	distance from front (upwind) edge of building to point where front edge recirculation zone reaches maximum height, [m]
X_{rot}	rotameter setting
x_{stack}	distance from front (upwind) edge of building to stack, [m]
x'	downwind distance from stack tip, [m]
$x'_{m.f}$	distance to final rise, [m]
y	crosswind position, [m]
Y	building width, [m]
z	vertical position above mass reflecting surface, either ground or roof level, [m]
z_c	effective plume convection height, [m]
z_{impact}	adjacent building height minus final plume height, [m]

z' plume height above mass reflecting surface, [m]

GREEK SYMBOLS

β_{eff} effective entrainment coefficient

Δh total plume height above stack tip, [m]

ΔH difference in emitting and adjacent building heights, [m]

Δh_d stack tip downwash correction, [m]

Δh_m plume rise due to exhaust gas jet momentum, [m]

$\Delta h_{m,f}$ final plume rise due to exhaust gas jet momentum, [m]

Δy_j distance from edge of calibration box, [m]

$\Delta\sigma_{o.edge}$ additional initial plume spread added to account for effect of front edge recirculation zone, [m]

$\Delta\sigma_{o.wake}$ additional initial plume spread added to account for effect of building wake recirculation cavity, [m]

$\Delta\sigma_z$ additional vertical plume spread, [m]

$\Delta\sigma_{z.wake}$ additional vertical plume spread added to account for building wake recirculation cavity, [m]

ε laser extinction coefficient, $[mg/L]^{-1}[mm]^{-1}$

λ_a peak absorption wavelength, [nm]

λ_f peak fluorescence wavelength, [nm]

ρ_a ambient fluid (air or water) density, $[kg/m^3]$

ρ_e density of stack exhaust gases, $[kg/m^3]$

σ_o initial plume standard deviation, [m]

σ_y crosswind plume standard deviation, [m]

σ_z vertical plume standard deviation, [m]

$\sigma_{z\,wake}$ vertical plume spread in building wake recirculation cavity, [m]

φ quantum yield of fluorescence

CHAPTER 1
INTRODUCTION AND LITERATURE REVIEW

OVERVIEW AND BACKGROUND

Exhaust gases ejected from stacks on a building roof can contain harmful chemicals or undesirable odors. Proper design of exhaust stack height, location, and exit velocity is required to prevent unacceptable concentrations of exhaust gas appearing in building air intakes. Knowledge of dispersion pattens around buildings is essential in determining the stack exhaust location, stack height and exhaust velocity needed to avoid unacceptable levels of exhaust gas being present on nearby building surfaces and ingested into building ventilation systems.

When two buildings are closely spaced, as is common in an urban industrial setting, there is the possibility of contamination between exhaust from vents on one building and intakes on either of the buildings. Even if an exhaust stack is designed to avoid contamination of intakes on the emitting building, intakes on a closely spaced adjacent building can be affected. Exhaust stack designs that improve conditions on one building often worsen the situation on a higher adjacent building. As well, if stacks were adequately designed to avoid unacceptable levels of contamination when a building was standing alone, the construction of a closely-spaced neighboring building can affect the flow pattens in such a way that the stacks are no longer adequate.

Three publication manuscript papers dealing with the effects of closely-spaced buildings on the dispersion of exhaust gases will be presented in the following chapters. These three papers present the results of part of a larger study on adjacent building effects reported in Wilson, Fabris, Chen, and Ackerman (1998).

1

CURRENT STATE OF KNOWLEDGE

Experimental Techniques

Previous investigators have used wind tunnel simulations to measure dilution of exhaust gases over scale model buildings. (Dilution at a particular point on the building is defined as the ratio of the contaminant concentration in the exhaust (source) gas to its concentration at a point on the building.) Snyder and Lawson (1976) and Huber and Snyder (1982) used a methane air mixture as a tracer gas that was detected by a flame ionization detector. Wilson (1976) used helium-air mixtures as the tracer gas with concentration measurements made by a thermal conductivity detector bridge. Robins and Castro (1977b) used flame ionization detector with a helium-propane tracer gas mixture. Here, the helium was used to obtain the proper density of the tracer gas. Samples were taken and passed through the flame ionization detector to determine propane concentration. Ogawa et. al. (1983) used sulfur hexafluoride tracer with sample concentrations determined by a gas chromatograph. Snyder (1994) used an air helium-ethane tracer gas mixture. Helium gas was used to give the correct exhaust gas buoyancy and a flame ionization detector was used to measure ethane concentrations.

Previous investigators have also made concentration measurements in a water channel. Snyder (1993) used neutrally buoyant dye released into the flow with samples collected at various locations. The sample concentrations were analyzed with a probe calorimeter. Laser induced fluorescence techniques have been developed by Lui (1996), and Johnston and Wilson (1997). These methods used disodium fluorescein dye tracer illuminated with laser sheet lighting. Fluorescent light was detected with a video camera calibrated against known concentrations of the tracer dye. The present study used a refinement of this technique.

2

Plumes on Single Buildings

Previous investigations have focused on dispersion patterns around a single building. The effects of the presence of a single building on the dilution of a plume from an upwind source have been investigated by Wilson and Netterville (1978), Wilson and Britter (1982), Li and Meroney (1983), and Thompson (1993). All of these studies considered only point sources upstream of the building and not emissions from a stack on the roof of a nearby building.

Wilson (1976) investigated the concentration over the roof a single buildings with intakes and exhausts on the same roof and developed a dilution model. This theoretical model dealt with exhaust and intake vents on the same roof and did not incorporate effects of exhaust gas momentum or exhaust stack height. The model was extended by Wilson (1977a) to predict dilutions on the sides of the buildings. These models did not account for air entrainment by the exhaust jet so they could not be used near the stack.

The initial dilution that accounts for exhaust jet and buoyancy-induced air entrainment near the source has been included in several theoretical models, c.f. Halitsky (1982), Wilson and Chui (1985), and Wilson and Lamb (1994). The initial dilution method places all the near-source jet dilution at the exhaust location and allows the model to be used close to the stack. These models still gave no credit for stack height or plume rise placing the plume centerline at the roof of the building. Wilson (1977b) and Wilson and Winkel (1982) considered an effective stack height that was the combination of an actual stack height plus plume rise due to exhaust jet momentum. Snyder and Lawson (1976) also investigated the effect of plume height and downwind concentration by specifying a minimum necessary stack height and did not consider variation of dilution with stack height.

The effect of wind direction at an angle to a building was investigated by Li and

3

Merony (1983) and Chui and Wilson (1988). Li and Meroney found that for low exhaust velocities there was a reduction in dilution by a factor of 3 to 9 when the building was placed at a 45 degree angle to the flow. These results were confirmed by Chui and Wilson who found similar reductions in dilution for low exhaust velocity. For high exhaust velocities with ratios of exhaust velocity to windspeed greater than 1.0, Chui and Wilson found that varying wind direction had a negligible effect on roof-level dilution.

SCOPE OF PRESENT STUDY

Measurement of Adjacent Building Effects

Previous investigations have not considered the effects of closely spaced neighboring buildings. The present study used water channel simulations to model dispersion around adjacent buildings. An existing laser induced fluorescence technique was refined to measure the concentrations of stack exhaust and determine the effect of the presence of adjacent buildings on the dispersion of a plume. A flourescent dye tracer was emitted from stacks on a model building to trace the dispersion of the plume. Fluorescent light from dye excited by a laser light sheet was filtered to remove the laser light frequencies, detected with a video camera, and time averaged by a digital frame grabber. A calibration technique was developed to determine the relationship between concentration and observed light intensity. Details of these experimental techniques can be found in Appendices A through G which deal with building configurations, laser induced fluorescence, rotameter settings, attenuation of dye fluorescence emission, light attenuation through plumes, video camera linearity, and data analysis procedures.

Concentrations were measured on building roofs and walls for several different building configurations. Parameters varied were: spacing between the emitting and adjacent buildings, the relative height of the two buildings, the exit velocity of the stack exhaust, the height of the stack, the position of the stack on the emitting building, the

4

width of the buildings and whether the adjacent building was upstream or downstream of the emitting building. In total, this resulted in over 1700 exhaust and building configurations being tested. See Appendix A for a description of all the different building configurations, although not all are discussed in this thesis. All building scenarios considered in the present study have the wind direction normal to the leading edge of both building.

Three papers are presented in this thesis to address different aspects of the investigations. In Chapter 2, the first paper contains selected data from plumes emitted from isolated stacks on a flat surface with no buildings, and from stacks on flat roof buildings, see for example Figure 2.2. A gaussian plume spread model is used to correlate the data for both these cases. Although recent investigators such as Brown et. al. (1993) and Genikhovich and Snyder (1994) have tried using non-gaussian plume models, the present study will show that a simple gaussian model can be adapted to produce realistic results on building roofs. A review of non-gaussian plume models can be found in Brown et. al. (1993)

Chapter 3 presents a paper with measured and predicted roof-level dilution data with a taller building upwind of the emitting building. The gaussian model developed in Chapter 2 is then extended to predict plume dispersion in the wake of the taller adjacent building. Chapter 4 presents a paper that deals with dilution measurements on the wall of the recirculation cavity formed between the emitting building and a higher upwind adjacent building. The gaussian plume model developed for roofs in Chapters 2 and 3 is tested in Chapter 4 to assess its ability to predict dilution on building walls.

REFERENCES

Brown, M., Arya, S.P. and Snyder, W.H. (1993) "Vertical dispersion from surface and elevated releases: An investigation of a non-Gaussian plume model" Journal of Applied Meteorology
32, 490-505.

Chui, E.H. and Wilson, D.J. (1988) "Effect of varying wind direction on exhaust gas dilution", Journal of Wind Engineering and Industrial Aerodynamics 31: 87-104.

Genikhovich, E.L. and Snyder, W.H. (1994) "A new mathematical model of pollutant dispersion near a building". 8th AMS Conf. on Appl. Air Poll. Meteorol.., with AWMA, Jan. 23-28, 1994, Nashville, TN.

Halitsky J (1982) "Atmospheric Dilution of Fume Hood Exhaust Gases", American Industrial Hygiene Association Journal, 43(3), 185-89

Huber, A.H. and Snyder, W.H. (1982) "Wind tunnel investigation of the effects of a rectangular-shaped building on dispersion of effluents from short adjacent stacks". Atmospheric Environment, 16, 2837-2848.

Johnston, C.R. and Wilson, D.J. (1997) "A vortex pair model for plume downwash into stack wakes" Atmospheric Environment 30 (accepted May 7/96) 8 journal pages.

Li, W.W. and Meroney, R.N. (1983) "Gas dispersion near a cubical model building. Part I. Mean concentration measurements". J. Wind Engr. Ind. Areo., 12, 15-33.

Liu, F. (1996) "Plume dispersion around a building from a ground-level source" Department of Mechanical Engineering, University of Alberta, Edmonton, AB, 147 pages.

Ogawa, Y., Oikawa, S. and Uehara, K. (1983) "Field and wind tunnel study of the flow and diffusion around a model cube II, near field and cube surface flow and concentration patterns". Atmospheric Environment, 17, 1161-1171.

Robins A.G. and Castro I.P. (1977b) "A wind tunnel investigation of plume dispersion in the vicinity of a surface-mounted cube – part II The concentration field". Atmospheric Environment, 11, 299-311.

Snyder, W.H. (1993) "Some observations on the influencing of stratification on diffusion in building wakes", Proceedings of the Institute of Mathematics and its Applications, Meeting on Stably Stratified Flows, Sept. 21-23, 1993, University of Surrey, Guildford, England, 24 pages.

Snyder, W.H. (1994) "Downwash of Plumes in the Vicinity of Buildings: A Wind Tunnel Study", Recent Research Advances in the Fluid Mechanics of Turbulent Jets and Plumes, 343-356

Snyder, W.H. and Lawson R.E. (1976) "Determination of Necessary Stack Height: A Wind Tunnel Study", Atmospheric Environment, 10, 683-691

Thompson, R.S. (1993) "Building amplification factor for sources near building: a wind tunnel study". Atmospheric Environment, 27A, 2313-2325.

Wilson, D.J. (1976) "Contamination of air intakes from roof exhaust vents", Trans. ASHRAE 82: 1024-38.

Wilson, D.J. (1977a) "Dilution of exhaust gases from building surface vents", Trans. ASHRAE 83: 157-166.

Wilson, D.J. (1977b) "Effect of vent stack height and exit velocity on exhaust gas dilution", Trans. ASHRAE 83: 157-166.

Wilson, D.J., and Britter, R.E. (1982) "Estimates of building surface concentrations from nearby point sources", Atmospheric Environment 16: 2631-2646.

Wilson, D.J. and Chui, E. (1985) "Influence of exhaust velocity and wind incidence angle on dilution from roof vents", ASHRAE Transactions 91 part 2B:1693-1706.

Wilson, D.J. and Lamb, B.K. (1994) "Dispersion of exhaust gases from roof level stacks and vents on a laboratory building", Atmospheric Environment 28: 3099-3111.

Wilson, D.J. and Netterville, D.D.J. (1978) "Interaction of a roof level plume with a downwind building", Atmos. Environment 12: 1051-1059.

Wilson, D.J., and Winkel, G. (1982) "The effect of varying exhaust stack height on contaminant concentration at roof level", ASHRAE Transactions 88, Part 1: 513-533.

Wilson, D.J., Fabris, I., Chen, J. and Ackerman, M.Y. (1998) "Adjacent Building Effects on Laboratory Fume Hood Exhaust Stack Design" Final Report of ASHRAE Research Project 897, 326 pages

CHAPTER 2
GAUSSIAN PLUME MODEL FOR CONCENTRATIONS ON FLAT ROOFED BUILDINGS AND FROM ISOLATED STACKS

INTRODUCTION

The objective in this chapter is to develop a simple gaussian plume model to predict the dispersion of a plume over same roof height buildings and near an isolated stack with no buildings present. Using a gaussian distribution for the vertical concentration profile is only strictly correct for the idealized case of dispersion in a uniform wind with speed U_c everywhere. For dispersion with no buildings present the windspeed U varies with height z above the ground raised to some power a, that is $U \propto z^a$ in the atmospheric boundary layer. However, considering its simplicity, a gaussian plume does remarkably well in capturing the fundamental physics of the dispersion process. See Brown et. al. (1993) for a comparison of non-gaussian to gaussian plume models.

Scale model atmospheric flow simulations were carried out in a water channel facility shown in Figure 2.1. Recirculating flow in the water channel passes through turbulence screens and then roughness elements that produce turbulence typical of an atmospheric boundary layer. The flow then passes over the scale model buildings. Fluorescein tracer dye stored in a tank on the side of the water channel is pumped through a flexible tube and out through stacks on the model buildings to simulate exhaust stack release. Laser light sheets were located above the building roofs to create illuminate the tracer dye. Fluorescent light from the tracer dye intersecting the light sheet was detected with a video camera above the water channel.

Figure 2.2 shows the different building configurations investigated in this chapter. Plumes were emitted from one of three different stacks numbered 1, 2, and 3. The reference building is a long flat roofed building used for comparison with the more

8

complicated building scenarios.

GAUSSIAN PLUME MODELS

The plume dispersion model developed in this chapter assumes a gaussian concentration profile. For contaminant concentration C_e in the exhaust gas, a volume flow rate at the stack of Q_e, and a uniform plume convection windspeed of U_c, plume spreads in the crosswind direction y and vertical direction z of σ_y and σ_z respectively, the concentration C at any point in space (x', y, z) in a gaussian plume is,

$$C = \frac{C_e Q_e}{2\pi U_c \sigma_y \sigma_z} \exp\left(\frac{-y^2}{2\sigma_y^2}\right) \left[\exp\left(\frac{-(z-h)^2}{2\sigma_z^2}\right) + \exp\left(\frac{-(z+h)^2}{2\sigma_z^2}\right)\right] \tag{2.1}$$

where x' is the downwind distance from the stack, y is the crosswind position, and z is the vertical position above the mass reflecting surface, either the ground or a building roof. The height of the plume centerline above the mass reflecting surface is given by h. The plume spreads σ_y and σ_z are the standard deviations of the gaussian concentration profile of the plume.

The second term in the square brackets in Equation (2.1) is the surface reflection term. When exhaust is carried down to ground level or roof level, it cannot penetrate the surface and the material is reflected back up. This is equivalent allowing the material to pass through the ground or roof and placing an image source below ground that is the same distance below ground as the actual plume is above ground. The vertical distance z between a point in space and the height of the image plume is then $z+h$ which appears in the surface reflection term.

The height h of the plume is a combination of the height of the stack h_s above $z=0$

9

and plume rise Δh above the stack tip caused by jet momentum or exhaust gas buoyancy so,

$$h = h_s + \Delta h \tag{2.2}$$

The present study is only concerned with roof level or ground level concentrations where $z=0$. Of particular interest are the concentrations along the plume centerline on the roof where the maximum concentrations occur. Using $z=0$ and $y=0$ in Equation (2.1) gives centerline concentrations C_r along roof level or ground level as

$$C_r = \frac{C_e Q_e}{\pi U_c \sigma_y \sigma_z} \exp\left(\frac{-(h_s + \Delta h)^2}{2\sigma_z^2} \right) \tag{2.3}$$

The dilution D can be defined as the ratio of concentration of the stack exhaust C_e to the concentration C at any point in space so that $D=C_e/C$. For maximum roof level concentration C_r, a minimum dilution is defined as $D_{min}=C_e/C_r$. The dilution can be normalized with the volume flow rate of effluent form the stack Q_e, the standard emitting building reference height H, and the velocity U_H at the reference height H in the approaching flow. Equation (2.3) can be rearranged to give normalized minimum dilution as

$$\frac{D_{min}Q_e}{U_H H^2} = \pi \frac{\sigma_y}{H} \frac{\sigma_z}{H} \left(\frac{U_c}{U_H} \right) \exp\left[\frac{(h_s + \Delta h)^2}{2\sigma_z^2} \right] \tag{2.4}$$

where H is an arbitrary length scale used to non-dimensionalize the dilution. The present study uses the height of the reference building as a convenient length scale although any length scale could have been chosen. The height of the reference building was

10

$H=2"=50.8$ mm in the laboratory models or 40' in the full scale for a scale ratio of 240:1. A single value of U_H was used in the laboratory flow simulations. The maximum possible value of U_H was used to give the highest possible Reynolds number Re_H. The results are applicable to situations with different windspeeds U_H since the plume rise only depends on the ratio of the exhaust velocity M.

As the plume moves downstream, the plume spread σ_z becomes much larger than the plume height h so that the exponential term in Equation 2.4 becomes negligible. It will be shown that the plume spreads σ_y and σ_z are linearly proportional to downstream distance x so that the normalization in Equation 2.4 produces a non-dimensional dilution that is only proportional to x^2 when far downstream of the source.

ISOLATED STACK

In addition to the scale model building water channel experiments, experiments were also carried out in which dye tracer was emitted from a short stack near ground level with no buildings present. The stack height $h_s=0.175H$ was at the same height above ground level as the shortest stacks used on the model buildings were above roof height. The stack protruded from a smooth surface and was $5.5H$ downstream from the end of the roughness element array that was used to produced turbulence in the flow typical of an atmospheric boundary layer. This put the isolated stack at the same position downstream of the roughness elements as the central stack on the reference building. Measurements of fluorescent dye tracer using a laser light sheet at $z=5$mm above the smooth floor of the water channel were made to measure concentrations near ground level.

To use Equation (2.4) to model dispersion from the isolated stack, appropriate functions for the plume spreads σ_y and σ_z, plume height h, and the ratio U_c / U_H of plume convection velocity U_c to reference velocity U_H at reference height $z=H$ above ground level are required. Although there was no building in the case of the isolated stack, the

11

reference height H was still used to normalize the dilution for comparison with cases in which buildings were present.

Effective Plume Convection Wind Speed U_c

Several options for evaluating the effective wind speed U_c were considered. It was found that evaluating U_c at half of the final plume height, $z_c = 0.5 h_f$, was most effective in fitting the water channel dilution measurements to a final-rise gaussian dispersion model. The final plume height h_f is the stack height h_s plus the final plume rise by jet momentum Δh_{mf} minus a correction for stack downwash Δh_d :

$$h_f = h_s + \Delta h_{mf} - \Delta h_d \tag{2.5}$$

The final plume rise by jet momentum depends on the inside stack diameter d, the plume convection velocity ratio U_H / U_c, and the density-weighted velocity ratio M that is defined as:

$$M = \left(\frac{\rho_e}{\rho_a} \right)^{0.5} \frac{W_e}{U_H} \tag{2.6}$$

where W_e is the mean velocity of the stack exhaust, ρ_e is the density of the stack exhaust, and ρ_a is the density of the approaching flow. Note that all velocity ratios are calculated using the windspeed U_H in the approaching flow at the reference height H. For all situations considered in the present study the density of the stack exhaust ρ_e and the density of the ambient fluid ρ_a were equal.

After being released from the stack, a plume continues to rise as it moves downstream until it reaches an equilibrium height beyond which there is no further plume rise. This is referred to as the point of final rise. From Briggs(1975), the final rise height

due to exhaust jet momentum Δh_{m_f} is,

$$\Delta h_{m_f} = B_3 \left(\frac{U_H}{U_C} \right) M d$$

(2.7)

where d is the inside diameter of the stack. A rise constant of B_3=3.0 was proposed by Briggs(1975) based on a survey of experimental data and this was found to work well in fitting a gaussian model to the present data.

For the isolated stack the effective convection velocity U_c is evaluated at an effective convection height z_c. It was found that taking the convection height z_c at a height of

$$z_c = \frac{h_s + \Delta h_{m_f}}{2} \quad \text{isolated stack}$$

(2.8)

gave good agreement in fitting the data to a gaussian model.

The velocity profile in the water channel upstream of the emitting stack or source as measured by a laser doppler velocimeter system was

$$U(z) = U_H \left(\frac{z}{H} \right)^{0.26}$$

(2.9)

where U_H =0.571 ft/s (0.174m/s) at H=2" (50.8 mm) in the water channel experiments.

Using Equation (2.9) to relate the effective plume convection velocity U_c at height z_c to the reference windspeed U_H at reference height H gives

13

$$U_c = U_H \left(\frac{h_s + \Delta h_{mf}}{2H} \right)^{0.26} \tag{2.10}$$

Plume Spread Model

Draxler (1975) gives approximations for crosswind plume spread σ_y and vertical plume spread σ_z as

$$\sigma_y = \frac{\dfrac{v_{rms}}{U_c} x'}{\left(1 + \dfrac{x'}{2L_v} \right)^{0.5}} \tag{2.11}$$

$$\sigma_z = \frac{\dfrac{w_{rms}}{U_c} x'}{\left(1 + \dfrac{x'}{2L_w} \right)^{0.5}} \tag{2.12}$$

for homogeneous turbulence with crosswind velocity fluctuations v_{rms} and vertical velocity fluctuations w_{rms}. The Lagrangian length scales L_v and L_w are the distances over which the turbulence velocities v_{rms} and w_{rms} remain correlated. For neutral atmospheric stability, the full scale atmospheric measurements of McElroy and Pooler (1968) used in the EPA model ISCST give

$$\frac{v_{rms}}{U_c} = 0.16 \quad \text{for 60 min. averages} \tag{2.13}$$

14

$$L_v = 1250 \text{ m} \tag{2.14}$$

$$\frac{w_{rms}}{U_c} = 0.14 \quad \text{for 60 min. averages} \tag{2.15}$$

$$L_w = 1670 \text{ m} \tag{2.16}$$

The Lagrangian length scales L_v and L_w are both large compared to the distance x' traveled by a plume over adjacent building roofs, so the denominators in Equations (2.11) and (2.12) are close to 1.0 implying that close to the stack (for $x' < 10H$, where reference height $H=2''$ (50.8mm)), both the crosswind plume spread σ_y and vertical plume spread σ_z vary linearly with distance:

$$\sigma_y = A_y \, x' + \sigma_o \tag{2.17}$$

$$\sigma_z = A_z \, x' + \sigma_o \tag{2.18}$$

where σ_o is the initial source size that accounts for dilution by exhaust jet air entrainment during rise and for the stack diameter. The initial spread σ_o has been shown to add linearly to distance dependent spread, see Wilson and Chui (1985). The crosswind spreading rate is $A_y = v_{rms}/U_c$ and vertical spreading rate is $A_z = w_{rms}/U_c$.

Measurements of σ_y in the water channel were used to verify the use of linear plume spread Equations (2.17) and (2.18). Ground level concentration measurements for a short stack with no buildings present were used. The plume spread was calculated at each downstream position as the standard deviation of the concentration in the crosswind

15

direction y. A gaussian profile was fitted to the concentration profile with the tails clipped off below a concentration threshold of 10% of the centerline concentration, with a correction applied to account for the effect of this threshold concentration cutoff on σ_y.

Figure 2.3 shows measured spread plotted against downstream distance x. A line with a slope of 0.08 plotted through the data shows that the linear model fits the data very well except for near the stack, where there could be a possible systematic error in determining plume spread from the data because the plume from a stack is highly diluted at ground level and can have its tails excessively cut off by the threshold correction calculation method. In addition, the initial dilution spread σ_o will be increasing as the plume gradually rises, causing some of the non-linearity in σ_y seen near the stack.

The initial spread σ_o results from entrainment into a rising plume jet. Wilson and Lamb(1994) show that the initial dilution C_e / C_{jet} is

$$\frac{C_e}{C_{jet}} = 1 + \frac{U_c}{W_e} \left(\frac{2\beta_{eff}\Delta h}{d} \right)^2 \qquad (2.19)$$

where d is the inside diameter of the stack and Δh is the plume height above the stack tip with no correction for stack tip downwash. If the surface reflection term in the exponential is neglected in Equation (2.1) then C_{jet} can be calculated as

$$C_{jet} = \frac{C_e Q_e}{2\pi U_c \sigma_o^2} \qquad (2.20)$$

where the volume flow rate Q_e is

16

$$Q_e = W_e \frac{\pi d^2}{4} \tag{2.21}$$

Combining Equations (2.20) and (2.21) with Equation (2.19) and solving for initial plume spread σ_o gives

$$\frac{\sigma_o^2}{d^2} = \frac{W_e}{8U_c} + \frac{\beta_{eff}^2}{2} \left(\frac{\Delta h}{d} \right)^2 \tag{2.22}$$

where β_{eff} is the effective entrainment constant. The value of the effective entrainment used to fit the data is taken from Johnston and Wilson (1996) where

$$\beta_{eff} = 0.6 \left(\frac{1 + 0.015M^2}{1 + 0.04M^2} \right) \tag{2.23}$$

In the present study a slightly modified version of Equation (2.22) that includes an initial source size $B_0 d$. The term is included so that the plume still has some initial size in the limit of zero exhaust velocity, ie. $M=0$. The dependence of the initial spread σ_o on rise Δh with no stack tip downwash can then be estimated by

$$\sigma_o = \left[\left(\frac{U_H}{U_c} \right) \frac{M}{8} + \frac{\beta_{eff}^2}{2} \left(\frac{\Delta h}{d} \right)^2 + B_o^2 \right]^{0.5} d \tag{2.24}$$

At the lowest exhaust velocity to windspeed ratio $M=1$, the initial spread σ_o varied from about $0.7d$ to $2.0d$ as the plume gradually rose to its final-rise height. This is one source of the non-linearity in spread seen near the stack in Figure 2.3. The line fit through measurements of crosswind spread σ_y in Figure 2.3 gave an initial spread $\sigma_o = 0.125H =$

17

2.5d, which is in reasonable agreement with the final-rise prediction of $\sigma_o = 2.0d$ from Equations (2.7), (2.23) and (2.24).

When fitting the data with the gaussian dispersion model, good agreement was found using $B_0 = 0.5$ in Equation (2.21). This implies that for the case of M equal to zero, such as would occur in the case of a stack with a rain cap for example, there is still an effective source size, σ_o, equal to half the diameter of the stack.

Dispersion Model Using Final-Rise

Two options considered in modeling the plume rise are referred to as final-rise and transitional-rise. After traveling a certain distance downstream from the stack, the plume reaches an equilibrium final-rise height beyond which it no longer rises. The final-rise model forces the plume immediately to its final-rise height on exiting the stack, see Figure 2.4 The plume height h, is equal to the stack height h_s, plus the final momentum rise $\Delta h_{m,f}$, less a correction for stack tip downwash, Δh_d. The final-rise is calculated using Equation (2.7). The stack tip downwash correction is given by

$$\Delta h_d = A_1\left(3.0 - \left(\frac{U_H}{U_c}\right)M\right) \qquad (2.25)$$

where the constant $A_1 = 1.0$ for $M(U_H / U_c) \leq 3.0$ and $A_1 = 0$ for $M(U_H / U_c) > 3.0$. This is a slightly modified version of the downwash equation recommended by Briggs (1974). Equation (2.25) was used since it gave a better fit to the data in the current study.

Using the equations for spread, velocity ratio and plume height, Equation (2.4) for dilution can be used to calculate theoretical final-rise curves. However, because the rise is constant even as σ_z approaches a small initial source size σ_o, the ratio $h^2/2\sigma_z^2$ in

18

Equation (2.4) becomes very large and the exponential term causes large over predictions of the dilution factor D_{min}. To avoid this overprediction in our model, the ratio $h^2/2\sigma_z^2$ was limited to 5. This cutoff limits the amount of dilution allowed due to plume rise to $\exp(5.0)=148$ near the source. This is physically realistic since there is less actual plume rise near the stack than is predicted by final-rise. Limiting $h^2/2\sigma_z^2$ to 5 means h is limited to $h=3.16\sigma_z$. In effect the limit of $h^2/2\sigma_z^2 \leq 5$ does not allow the model to calculate dilutions more than three standard deviations below the plume centerline.

Dispersion Model Using Transitional Plume Rise

A transitional plume rise model allows the plume to rise gradually to its final-rise height. The plume transitional-rise height due to momentum is proportional to downwind distance from the stack to the 1/3 power, $\Delta h_m \propto x^{1/3}$. The plume continues to rise in this manner until it reaches the final-rise height given by Equation (2.7) at a final-rise distance x_{mf}. The transitional-rise also uses the stack tip downwash correction in Equation (2.25) that was used for final-rise.

Briggs (1975) gives the distance to final rise x_{mf}' as

$$x_{mf}' = \left(\frac{4\beta^2 B_3^3}{3} \right) Md \tag{2.26}$$

so that the transitional rise due to momentum is

$$\Delta h_m = \Delta h_{mf} \left(\frac{x'}{x_{mf}'} \right)^{1/3} \tag{2.27}$$

It will be shown that the transitional-model produces results that are much poorer than the final-rise model for roof level dilution near the stack. Even though the transitional rise model was more physically realistic in terms of predicting plume

19

trajectory, it was eventually abandoned because it is not mathematically robust.

The transitional-rise Equation (2.27) and Equation (2.10) for effective velocity ratio with Equations (2.17) and (2.18) for plume spread were used in Equation (2.4) to calculate theoretical plume centerline roof level dilution curves for seven different values of stack exhaust velocity to windspeed ratio M emitted from the isolated stack. The spread was calculated using A_y=0.08, determined from the plume spread measurements.

Different values of A_z were tried and it was found that the best agreement between the theoretical model and the data could be obtained using A_z=0.07. Figure 2.5 shows the theoretical lines for transitional-rise plotted along with the measured dilution. The inflection points in the theoretical curves correspond to the point where the plume reached final-rise height. One can see that the model transitional-rise dispersion poorly predicts dilution near the stack, and only begins to give reasonable estimates far downstream when the plume has reached its final-rise height.

Part of the failure of the transitional-rise model can be attributed to the instability of the exponential of the ratio of plume height to plume spread squared in the gaussian model. This is particularly unstable near the stack where the plume spread approaches its small initial value σ_o. This exponential term is sensitive to small changes in any of the parameters, making thus makes it difficult to create a robust model for dilution near the source.

Comparison of Figure 2.5 (transitional-rise) with Figure 2.6 (final-rise) shows that downstream the models are nearly identical. Near the stack the final-rise model with the exponential cutoff that limits $h^2/2\sigma_z^2 \leq 5$ produces a much more realistic estimate of dilution. The cutoff-limited model predicts both closer dilutions and the proper shape of the dilution curves close to the stack where $h > 3.16\sigma_z$.

20

REFERENCE BUILDING

The reference building as shown in Figure 2.2, with a long flat roof downwind of the 3 stacks, was used as a simple baseline configuration to see how a building affects the plume spreads σ_y and σ_z. Figure 2.7 shows dilution contours over the roof of the reference building emitted from stack 2 with a stack height $h_s=0.175H$ and a stack exhaust velocity to windspeed ratio M of 1.0. The reference building is an emitting building with a long flat roof downwind of the stacks.

Figure 2.8 shows plume spread fit with a line of slope 0.08. As in the case of the isolated stack, the line fits the data quite well except for near the stack where it is expected that the gaussian model can break down. This means that the same linear plume spread assumptions in Equations (2.17) and (2.18) that were used for the isolated stack may be used for the reference building.

Effective Plume Convection Windspeed U_c

The effective wind speed U_c, is difficult to evaluate for the reference building. The flow accelerates over the upwind edge of the building changing the vertical velocity profile over the roof. The convection velocities seen by the plume will depend on stack height and plume rise, and vary as the plume is dispersed back down to the roof. After trying several alternatives for estimating the plume convection speed U_c, and the stack height windspeed U_s, it was found that a good estimate for both U_c and U_s was the velocity of the approaching flow at roof height H, so that $U_c=U_s=U_H$ on the buildings.

Transitional vs. Final-Rise Dispersion Models

As in the case of isolated stack, the data for the reference building was fitted with both transitional and final-rise models. Equation (2.4) was used with height h as height

21

above roof instead of height above ground level. Figure 2.9 shows data from plumes emitted at stack 2 at six different velocity ratios on the reference building plotted with theoretical lines for transitional-rise. Transitional-rise dilution predictions were inaccurate except for far downstream where the plume had reached final-rise. The transitional-rise model drastically underestimated the dilution near stack and then overestimates the dilution farther downstream for higher velocity ratios.

Figure 2.10 shows the same data plotted with a final-rise model, that produces a closer fit to the measurements than the transitional rise model. The benefits of using a final-rise model can be seen more clearly by comparing Figures 2.11 and 2.12 that show data plotted from stack 2 on the reference building with a stack height equal to half of the building height and six different velocity ratios. Figure 2.11 shows the transitional-rise model while Figure 2.12 shows the final-rise model. The transitional-rise model was a poor fit to the measured data, with values that are several orders of magnitude too large for the first few building heights downstream of the stack.

Exponential Cutoff for Final-Rise Gaussian Models

By using a final-rise model and limiting the ratio $h^2/2\sigma_z^2$ to 5, more realistic estimates of the dilutions were obtained as shown in Figure 2.12. As discussed before, the limit $h^2/2\sigma_z^2 \leq 5.0$, effectively prevents the model from calculating dilutions at more than three standard deviations from the centerline. If the plume were truly gaussian however, for high stacks with $h_s=0.5H$ the roof level would be more than 10 plume standard deviations below the plume trajectory at the stack position, and one would expect very high dilutions near the stack.

The fact that low dilution was observed near the stack, illustrates that the plume does not follow a gaussian profile and some other mechanism must be responsible for dispersing the plume down to ground level near the stack. This would also explain the

failure of the transitional-rise model. Even though the plume trajectory used in the transitional-rise dispersion model is more related to the physics of real plume behavior than simply using the final-rise height, the transitional model assumes gaussian plume spread that does not provide reasonable estimates close to the plume origin. Using a final-rise model and exponential cutoff limit $h^2/2\sigma_z^2 \leq 5$ simply makes the gaussian model produce reasonable estimates near the source.

ROOF EDGE RECIRCULATION ZONE

Effluents emitted from a stack near the upwind edge of the building can be trapped in a recirculation zone near this leading edge. Recall that Figure 2.7 shows dilution contours from the centerline stack 2 with no plume trapping. Compare this to Figure 2.13 dilution for the same velocity ratio $M=1$ and stack height $h_s=0.175H$ but emitted from stack 1 close to the upwind edge of the building. The effect of this roof edge recirculation zone is clearly evident by comparing these two figures, particularly in the regions near the stack. In Figure 2.13, exhaust from stack 1 is carried upstream from the stack and there is a much larger plume width near the source. This increase in crosswind spread is also shown in Figure 2.14 where there is a sharp increase near the leading edge of the building. Beyond a few stack heights downstream, however, the plume spread is still linear and can be fitted with a slope of 0.08 as in the previous cases.

The crosswind plume spread σ_y calculated by fitting a gaussian to y direction profiles, is shown in Figure 2.14. The exhaust from the short stack $(h_s=0.175H)$ with its lowest exhaust to windspeed ratio $M=1$, allowed the plume to be trapped in the roof edge recirculation cavity and carried upwind to the roof edge. This recirculation and large increase in plume spread in the roof edge cavity has only a modest effect on the plume farther downwind. The plume growth rate A_y, in Equation (2.17) was still at 0.08, the value found for an isolated stack, and for stack 2 on the reference building, where roof edge recirculation did not trap the plume. The only effect of roof edge cavity trapping

23

was an increase in initial plume to $\sigma_o=3.5d$ for the trapped plume in Figure 2.14 This added spread and virtual origin shift will be included in the dispersion model.

In order to adjust the model to emulate the effect of this recirculation zone, the virtual origin was shifted back to the upwind edge of the building and extra initial spread was added to the plume. If maximum height of the cavity is H_c, and L_c is the length of the cavity, and X_c is the distance from the leading edge of the building where the cavity reaches its maximum height H_c, the dimensions of the recirculation cavity are as $H_c=0.22R_d$, $X_c=0.5R_d$, and $L_c=0.9R_d$ where the scaling length $R_d=\Delta H^{0.67}Y^{0.33}$ when building width Y larger than the change in roof level ΔH at the upwind wall where the cavity exists. These dimensions are taken from 1997 ASHRAE handbook based on measurements by Wilson (1979). The shift of the origin in the model was made only if the stack position fell within the recirculation zone and the final plume height was less than H_c.

$$X_{stack} < X_c = 0.5R_d \tag{2.28}$$

$$h_s + \Delta h_{m,f} - \Delta h_d \leq H_c \tag{2.29}$$

On the buildings used in the current study the criteria in Equations (2.28) and (2.29) shift the origin for the upstream stack 1, but not for stack 2 or stack 3.

The extra spread due to the recirculation cavity is

$$\Delta\sigma_{o,edge} = \frac{0.05R}{1+4.0\left(\dfrac{x_{stack}}{X_c}\right)^3} \tag{2.30}$$

24

In Equation (2.30), $R_d = \Delta H^{0.67} Y^{0.33}$ is based on the width and height increase ΔH of the front face of the building. For the reference building there was no upwind adjacent building and $\Delta H = H$. Here, Y is the crosswind width of the building and H is the emitting building height. The cavity position X_c, and stack position x_{stack} are measured from the upwind edge of the roof so that this produces a correction equal to $0.05R$ on the leading edge that decreases as the stack location moves out of the recirculation cavity. For the central stack location 2, $x_{stack} = 0.125H$ and for $2.5H$ wide reference building, $X_c = 0.68H$. At stack 2, the correction in Equation (2.30) is reduced to only 4% of its initial value.

The source size correction $\Delta \sigma_{o,edge}$ in Equation (2.30) contains no dependence on stack height, so for all stack heights there will always be some additional plume spread added. It may seem unrealistic that extra plume spread is added even if the stack is above the recirculation zone, but for plumes that begin just above the zone, some of the stack exhaust can still be caught in the recirculation zone as the plume is diffused downward giving an apparent initial spread. For plumes much higher that the front edge roof cavity, the extra spread does not affect the prediction at roof level significantly.

Measurements of Added Plume Spread and Dilution

The increase of measured initial spread σ_o from $2.0d$ to $3.5d$ with edge cavity trapping, shown in Figures 2.8 and 2.14, gives a measured value of $\Delta \sigma_{o,edge} = 1.5d$. Equation (2.30) for the edge trapping effect was developed from roof level dilution measurements, not plume spreads σ_y, and so is independent of the measured values of $\Delta \sigma_{o,edge}$. For stack 1, $x_{stack} = 0.25H$, the scaling length $R_d = 1.35H$ for the $2.5H$ wide building, so the cavity position is $X_c = 0.68H$. Using these values in Equation (2.30), the predicted increase in initial spread is $\Delta \sigma_{o,edge} = 1.13d$, in reasonably good agreement with the measured values of $1.6d$, considering that the predicted value is an adjustment for all the effects recirculation of final-rise gaussian plume model.

25

The effect of this correction can be seen by comparing Figures 2.15 and 2.16. Figure 2.15 shows data from plumes emitted at stack 1, stack height h_s=0.175H, and six different values of exhaust velocity to windspeed ratio M plotted together with theoretical lines calculated using an uncorrected final-rise model. Note that these curves will be identical to the final-rise model dilution curves for stack 2. Figure 2.16 shows the theoretical curves calculated with final-rise with the origin shifted back to the leading edge of the building and extra initial spread has been introduced. For high values of M, the agreement between predicted and measured dilution values is about the same but at lower M values the theoretical model with the front edge correction does a better job of predicting dilutions near the stack.

The most significant effect in plume trapping correction is produced by the addition of extra spread. The shift of the virtual origin alone would only produce a small change in the predicted dilution downstream of the stack, but forces the model to produce the required concentrations upstream of the stack where the plume is trapped in a front edge recirculation cavity.

BUILDINGS SEPARATED BY A GAP

The next case considered was two buildings separated by a gap equal to the building height and whose roofs are at the same height. These building configurations are referred to as step across buildings. The same theoretical model used for the reference building was applied to see how well it would work for gap between the buildings. In the first case, the downwind and emitting building were separated by one building height. Figure 2.18 shows plots of dilution data measured on the emitting and adjacent building. Data and theoretical models appear in Figure 2.18 for three different values of Md/d_{ref}. This ratio is used so that results are applicable to different stack diameters. Since plume rise depends on the ratio Md, see Equation 2.7 , different combinations of M and d that produce the same value product Md should have the same plume rise and dilution. Since

26

the value of d is specific to this experiment, Md is normalized by using this as the reference diameter d_{ref}. In the present study, the stack diameter d and reference diameter were always equal so that $Md/d_{ref} = M$.

Even though no adjustments were made to the model for the effect of the gap, it still predicts dilutions quite well, within 20% in most cases and at most a factor of 2. This is quite good considering that the measured dilutions on the buildings varied over a range of 300:1. That the presence of a gap has little effect on the measured dilutions seems to indicate that the gap can quickly be filled with concentration close to the roof level value and that for each bit of exhaust gas that is dispersed down into the gap, the same amount is dispersed back up producing the same effect as if the plume had been reflected from the roof.

The same model is used to predict dilutions for building widths of both $2.5H$ and $5.0H$. In Figures 2.18 and 2.19 the dilution data for both building widths is almost the same and small differences could be attributed to run to run variations. (Note that the data in Figures 2.18 and 2.19 is plotted with different scales for downwind distance.) The model accurately predicts through its weak dependence on width Y in the initial plume spread $\Delta\sigma_{v,edge}$ that is proportional to $R_d = \Delta H^{0.67} Y^{0.33}$.

Plume Spreading Rates

Figure 2.17 shows the plume spread measured over the emitting and adjacent building with a stack exhaust velocity to windspeed ratio M of 3, at stack 1 and a stack height of $0.25H$. The crosswind spread σ_y measured on the reference building for the same velocity ratio M, and stack height are also shown. In the gap there is an increase in spread likely due to leaking of the concentration out the sides. However, over the roofs of the two buildings, the spreads are almost identical, both linear with distance and having a slope of 0.08.

STACKS ON DOWNWIND ADJACENT BUILDING

The final case examined was buildings with the same roof height with the emitting building downstream of the adjacent building. Figure 2.19 shows measured dilutions for the step across case where there is a gap between the buildings with gap width equal to the building height H. Also plotted are the theoretical curves for dilution calculated with the final-rise model. Data is shown for three different values of stack exhaust velocity to windspeed ratio M, emitted from stack 1, the upstream stack. In the cases where the emitting building was upstream, virtual origin shifts were made for stack 1; however, since the adjacent building height is only one emitting height upstream for the situation in Figure 2.19, the flow streamlines are not forced up from ground level in front of the emitting building. The stream lines are already at roof height on the adjacent building and do not have a chance to move back to ground level as they move across the space separating the buildings. As a result, no correction for the roof edge recirculation zone was made when the emitting building was downstream.

The theoretical model plotted in Figure 2.19 shows good agreement with the data, but is slightly conservative in most cases. One would expect the presence of the upwind building would increase the turbulence in the flow and create higher dilutions, and in fact observed dilutions were slightly higher than the predictions. No attempt is made to incorporate this effect into the model since the effect is minor and the simple approach produced reasonable estimates of dilution for this case as well as the reference building.

CONCLUSIONS AND DESIGN GUIDELINES

A gaussian plume model was developed to predict dilutions for the simple cases of dispersion from isolated stacks and stacks on flat roofed buildings. This model will serve as a starting point when dealing with more complicated building configurations in subsequent chapters. Five main points were be established:

- Dilution close to the stack is poorly predicted by a transitional-rise model. Using a final-rise model with a limit on the amount of dilution from plume height near the stack produces better estimates of the minimum dilution.

- Plumes emitted from stacks near the upwind edge of a building are caught in a recirculation zone which forms at this leading edge. This requires that the plume be simulated with a larger initial source size and a shift in the virtual origin back to the upwind edge of the building.

- The presence of a gap between buildings of the same roof height has little effect on the dilutions and spreading rates on the roofs of the two buildings. In the gap, the crosswind spread is increased; however, over the building roofs the spread show the same distance dependence as on a long flat-roofed buildings.

- The presence of a building has very little effect on the spreading rate of the plume in the cross stream direction.

- Note that all the cases discussed in this chapter there was virtually no change in the cross stream spreading rate A_y. The spreading rates for the reference building and step across building with a gap were the same as those from the isolated source. Based on these observations in can be concluded that the presence of the buildings has almost no effect on the turbulence in the cross stream direction and as a result, plume spread σ_y remains constant.

REFERENCES

ASHRAE. (1997) "Air flow around buildings", Chapter 15 in 1997 ASHRAE Handbook of Fundamentals. American Society of Heating, Refrigerating and Air-Conditioning Engineers, Atlanta, Georgia.

Briggs, G.A. (1974) "Diffusion estimation for small emissions" in ERL, ARL, USAEC Report ATDL-106. U.S. Atomic Energy Commission, Oak Ridge, Tennessee.

Briggs, G.A., (1975) "Plume rise predictions" Chapter 3 Lectures on Air Pollution and Environmental Impact Analyses, American Meteorological Society, Boston, 29 Sept - 3 Oct, 1975: 59-111.

Brown, M., Arya, S.P. and Snyder, W.H. (1993) "Vertical dispersion from surface and elevated releases: An investigation of a non-gaussian plume model" Journal of Applied Meteorology
32, 490-505.

Draxler, R.R. (1976) "Determination of atmospheric diffusion parameters" Atomospheric Environment 10: 99-105.

EPA (1995a) "User's guide for the Industrial Source Complex (ISC3) dispersion models: volume 2 - description of model algorithms" U.S. Environmental Protection Agency, Research Triangle Park, North Carolina, document EPA-454/B-95-003b.

McElroy, J.L. and Pooler, F. (1968) " The St. Louis dispersion study". US Public Health Services, National Air Pollution Control Administration, Report AP-53.

Johnston, C.R. and Wilson, D.J. (1996) "A vortex pair model for plume downwash into stack wakes" Atmospheric Environment 30 (accepted May 7/96) 8 journal pages.

Wilson, D.J. (1979) "Flow patterns over flat roofed buildings and application to exhaust stack design", Trans. ASHRAE 85, Part 2: 284-295.

Wilson, D.J. and Chui, E. (1985) "Influence of exhaust velocity and wind incidence angle on dilution from roof vents", ASHRAE Transactions 91 part 2B:1693-1706.

Wilson, D.J. and Lamb, B.K. (1994) "Dispersion of exhaust gases from roof level stacks and vents on a laboratory building", Atmospheric Environment 28: 3099-3111.
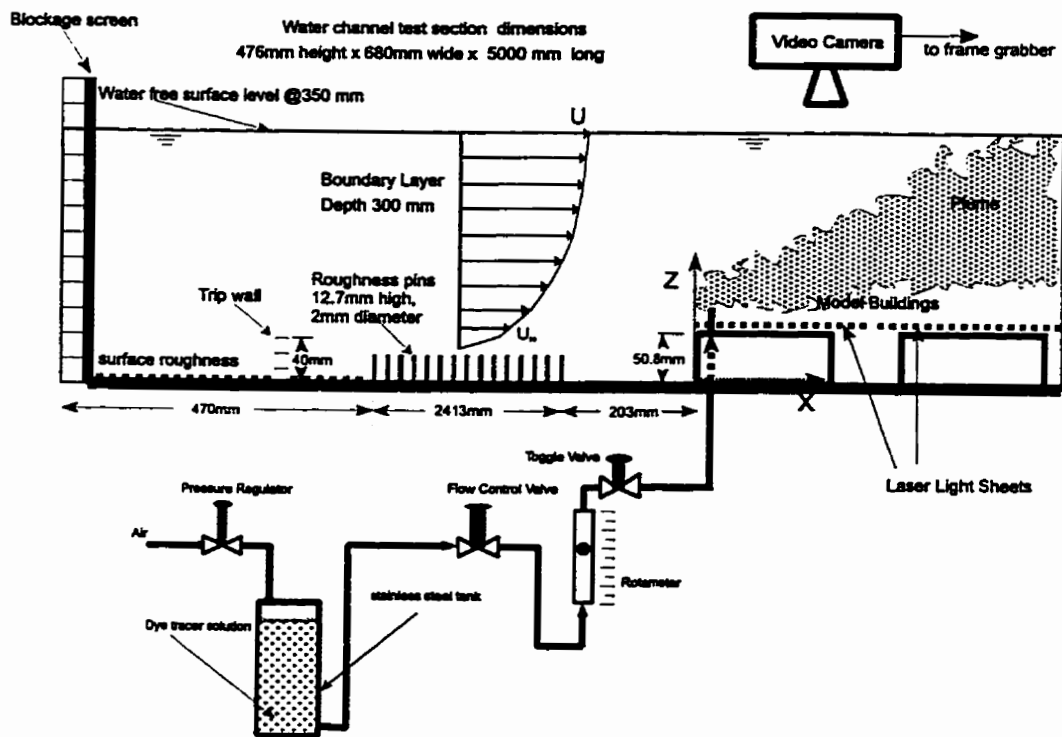
Figure 2.1   Schematic of water channel facility used to simulate atmospheric flow

31

reference
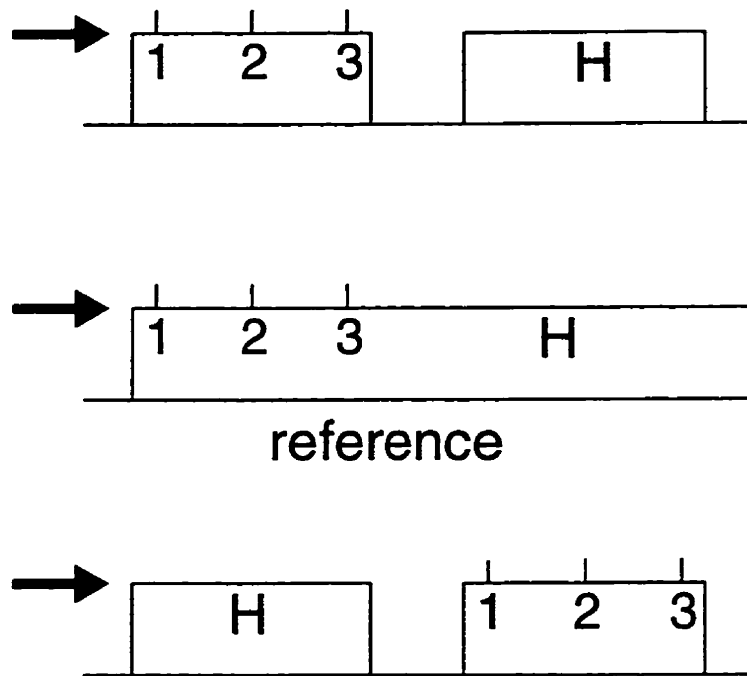
Figure 2.2   Building configurations investigated for Chapter 2.
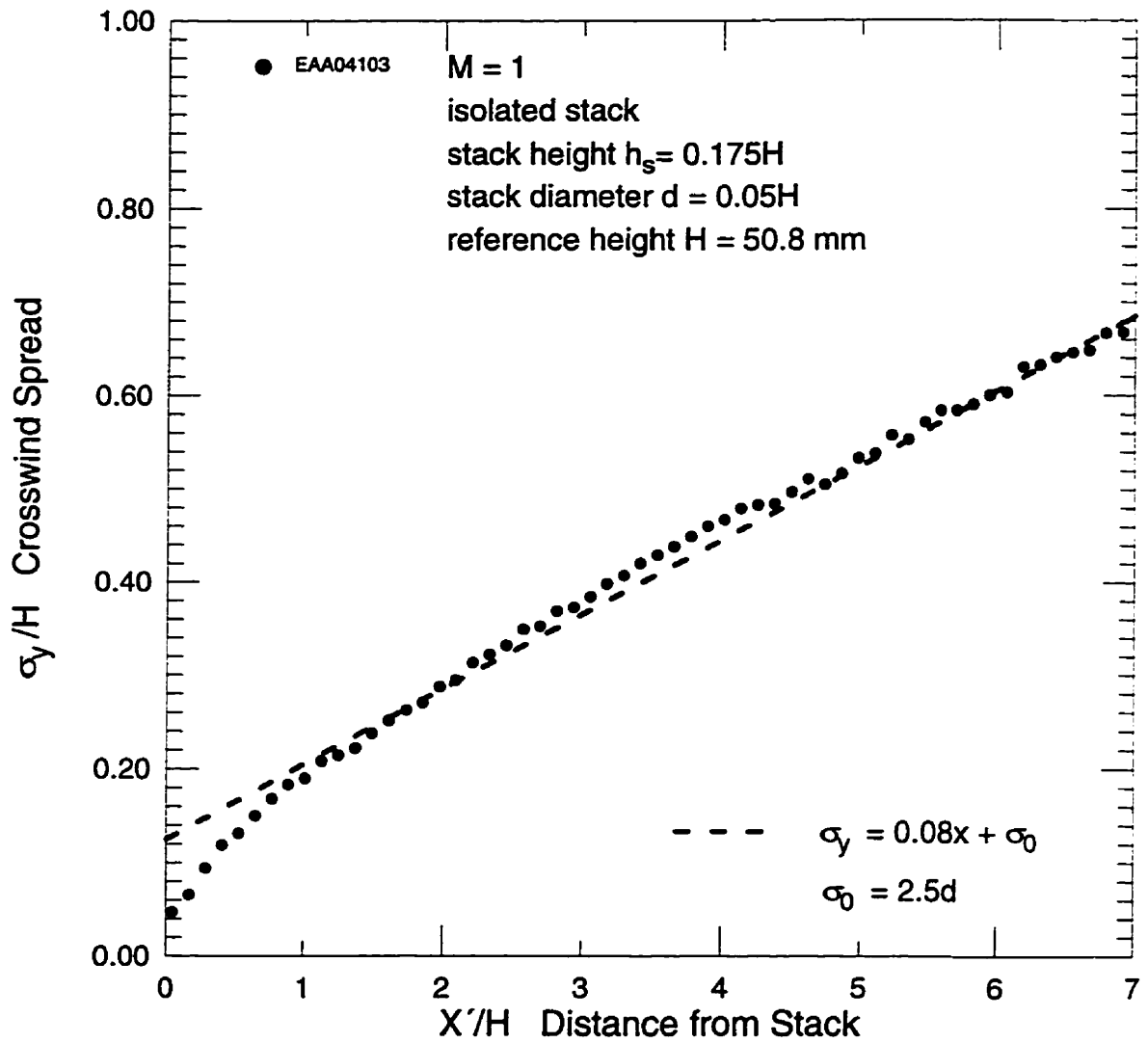
Figure 2.3   Plume spread measured at ground level from an isolated stack release at
a stack exhaust velocity to windspeed ratio of 1.0 and a stack height of
0.175*H*.

Proposed Model

edge cavity
increases
initial dilution

plume trajectory

U_H

h_s

H

virtual origin shifts to upwind
edge if final rise origin falls
inside edge cavity trapping zone

34
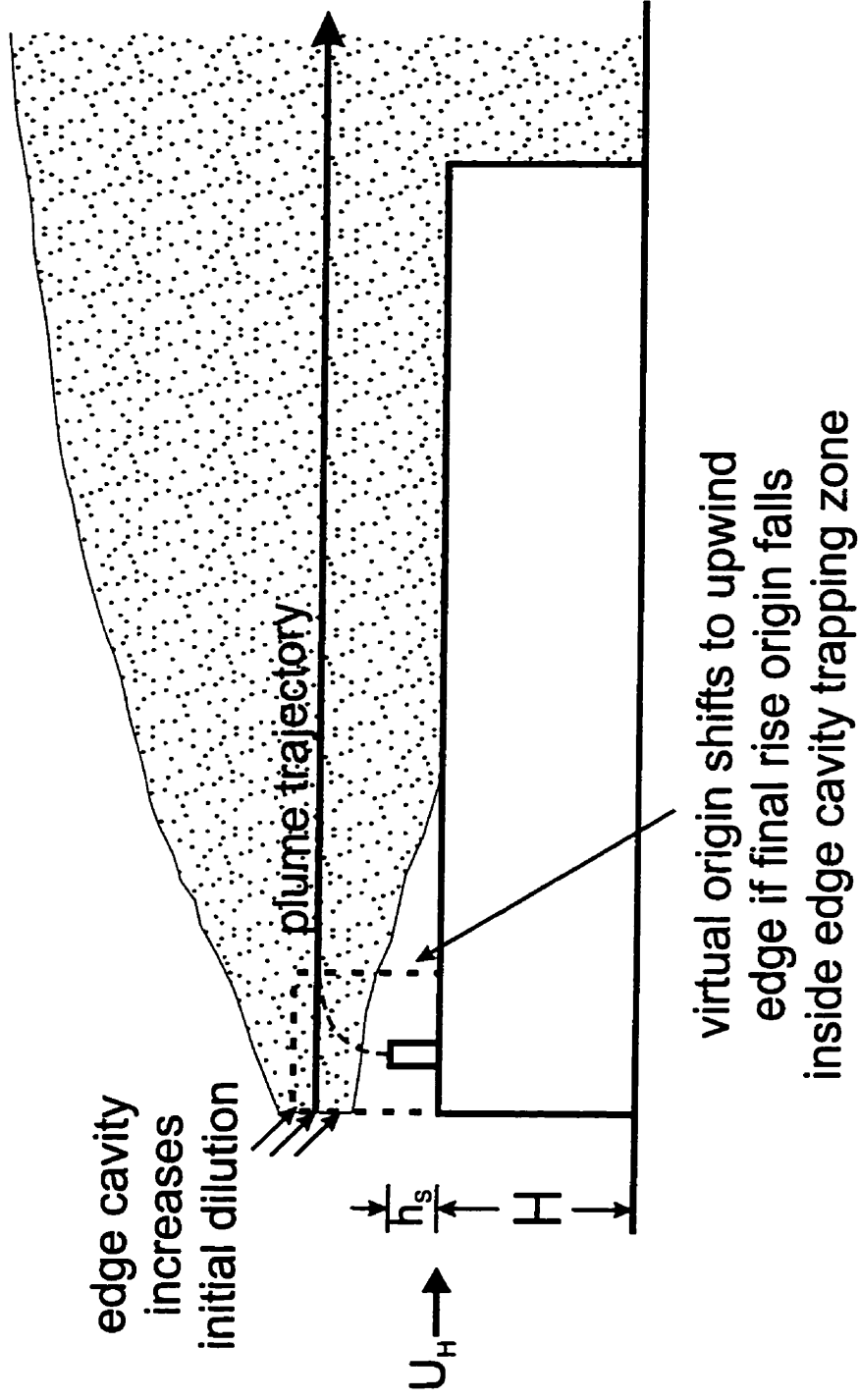
Figure 2.4   Proposed model for a plume emitted over a flat roofed building
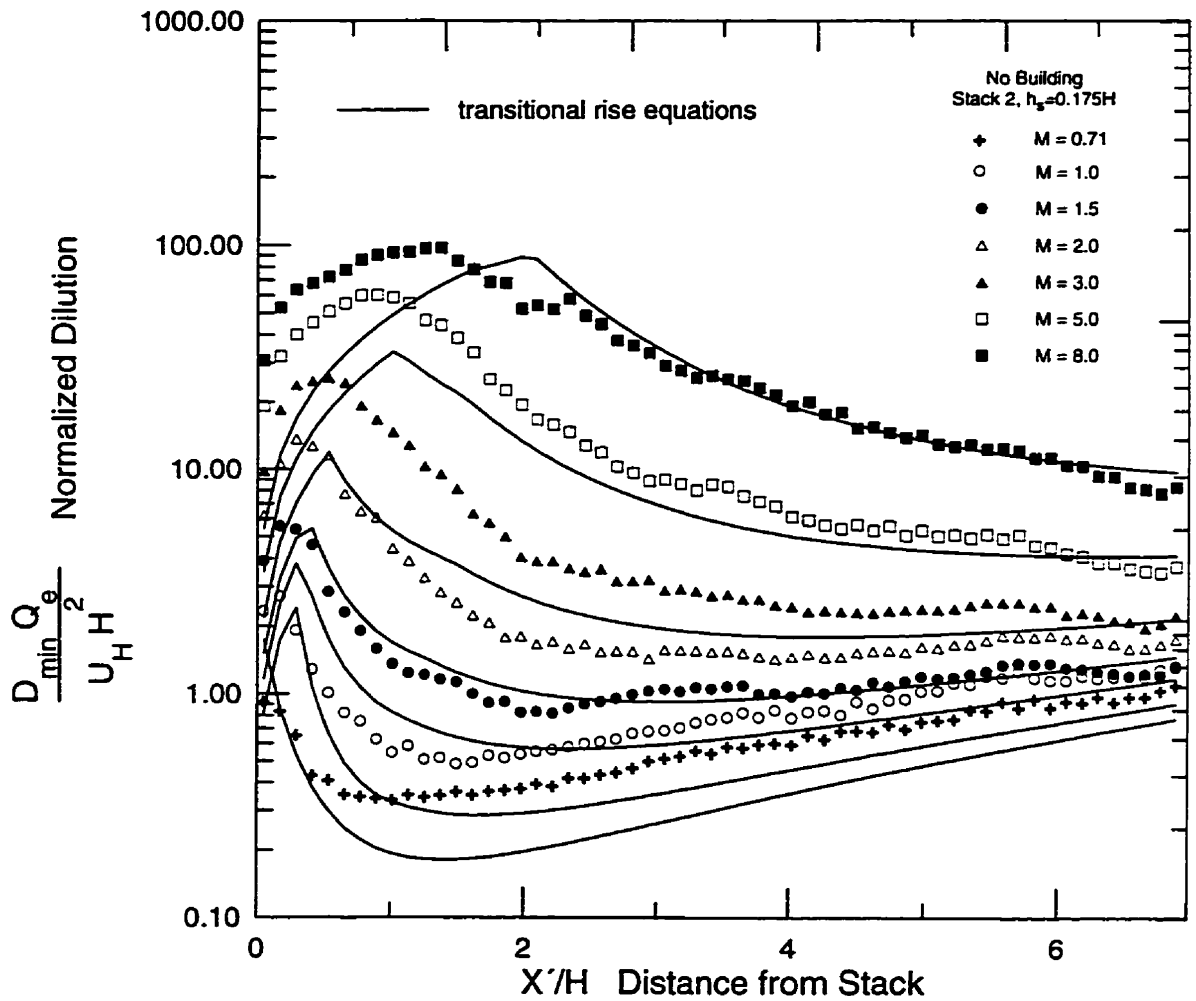
Figure 2.5   Dilutions from an isolated stack for 7 different values stack exhaust
velocity to windspeed ratio M with theoretical curves calculated from
transitional rise model. Compare to Figure 2.4 showing final rise
curves for the isolated stack

35
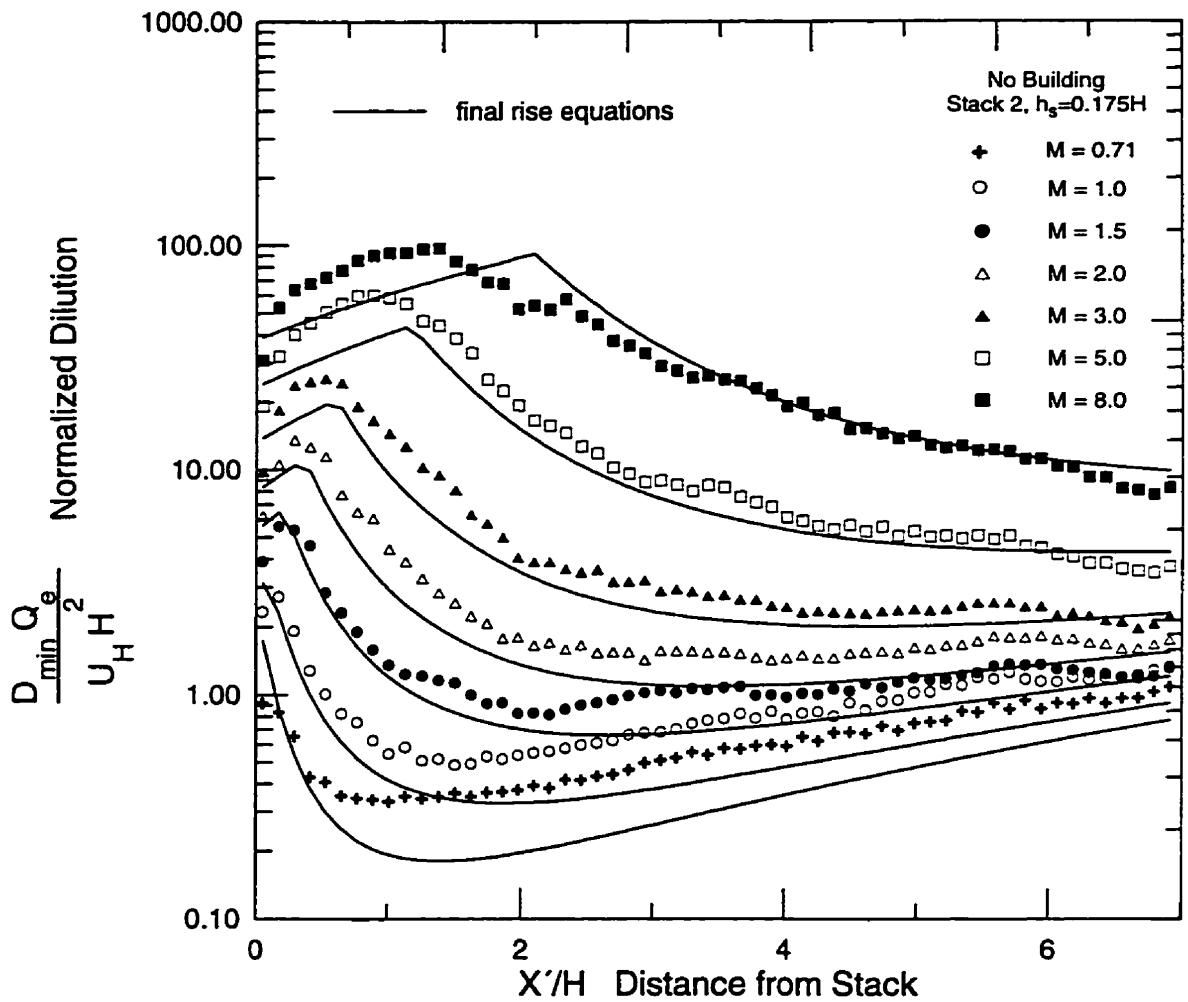
Figure 2.6   Dilutions from an isolated stack for 7 different values stack exhaust
              velocity to windspeed ratio M with theoretical curves calculated from
              final rise model. Compare to Figure 2.3 showing transitional rise
              curves for the isolated stack.

36

$$\frac{D_{min} Q_e}{U_H H^2}$$

10.0
5.0
2.0
1.0
0.5
0.2
0.1

reciculation cavity

emitting stack

U_H
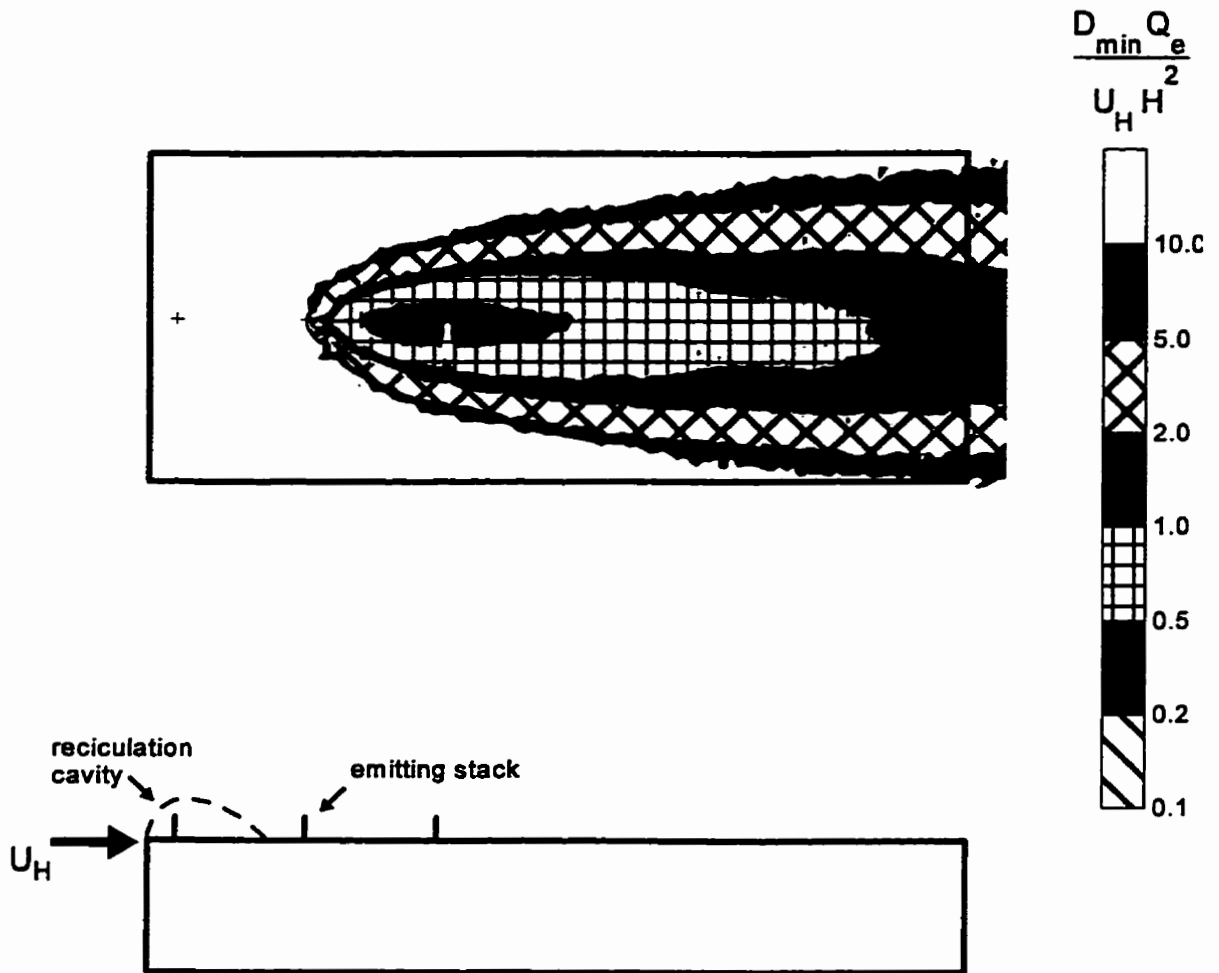
Figure 2.7   Dilution contours over reference building for plume emitted from center stack 2 at a stack exhaust velocity to windspeed ratio M of 1 and a stack height of $0.175H$.
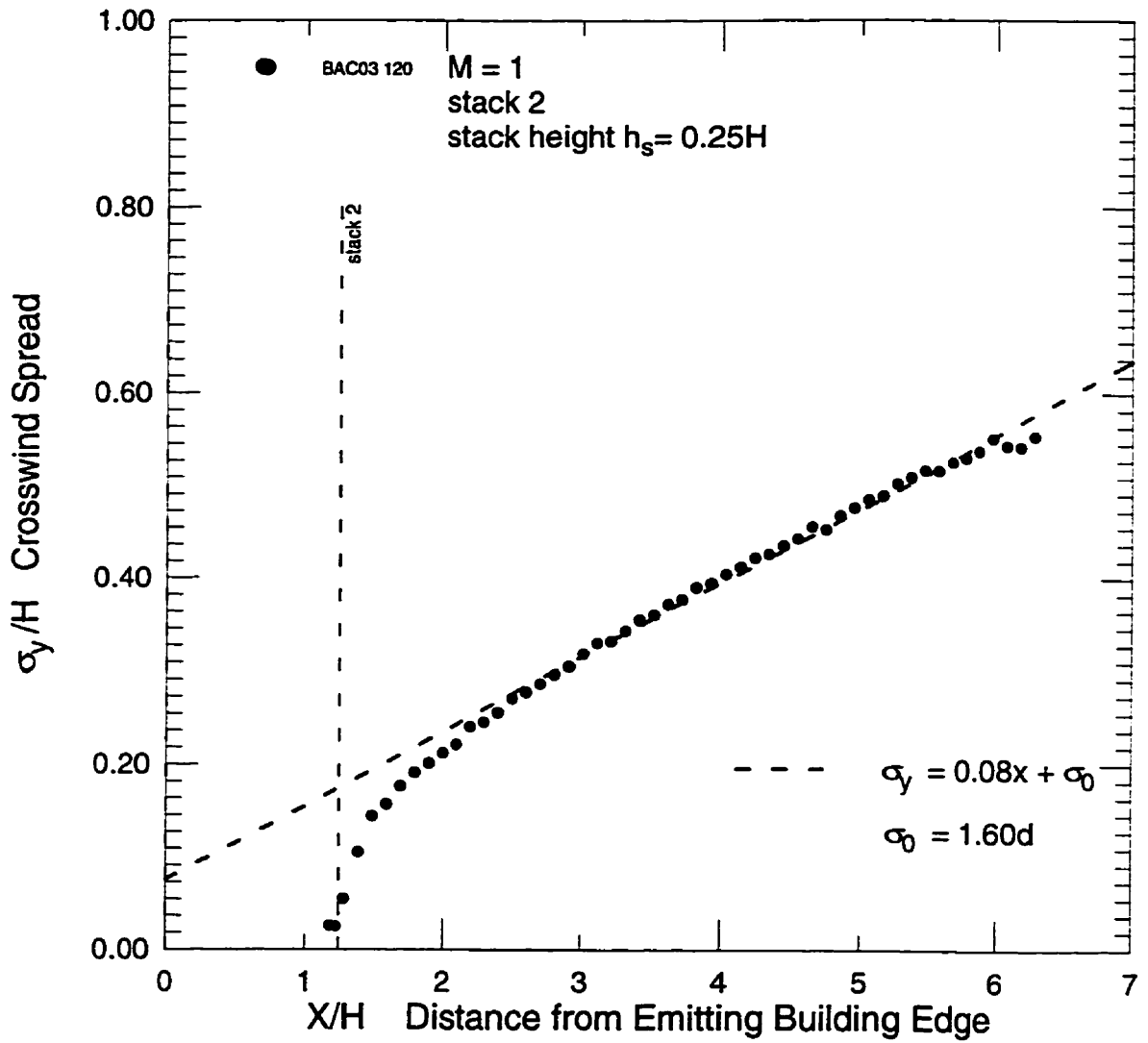
Figure 2.8   Plume Spread in cross stream direction measured over reference
building for plume emitted from center stack 2 at a stack exhaust
velocity to windspeed ratio M of 1 and a stack height of $0.25H$.

38
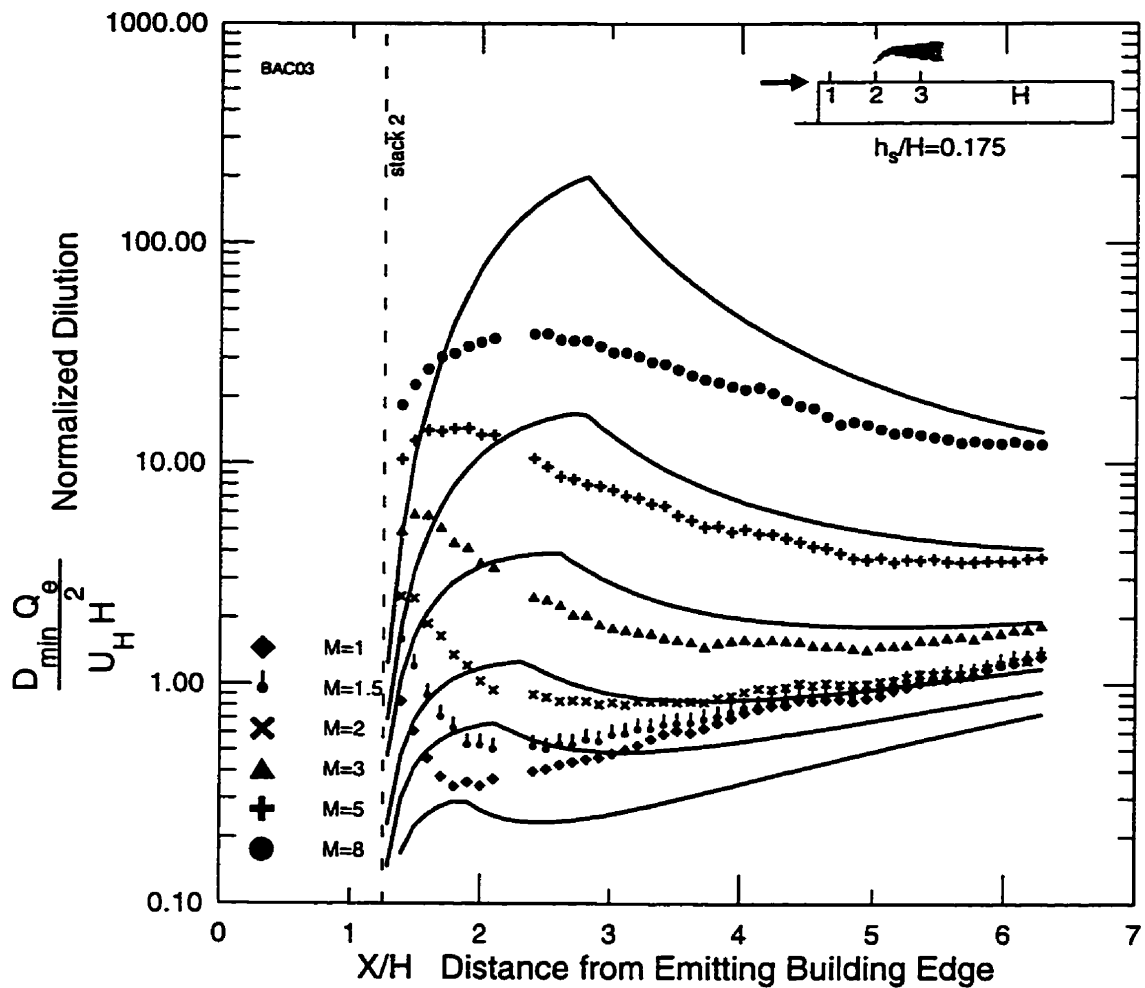
Figure 2.9   Dilutions over reference building for plume emitted from stack 2 at six different values of stack exhaust velocity to windspeed ratio M and a short stack height of $0.175H$. Theoretical curves are calculated using **transitional** rise model.

39
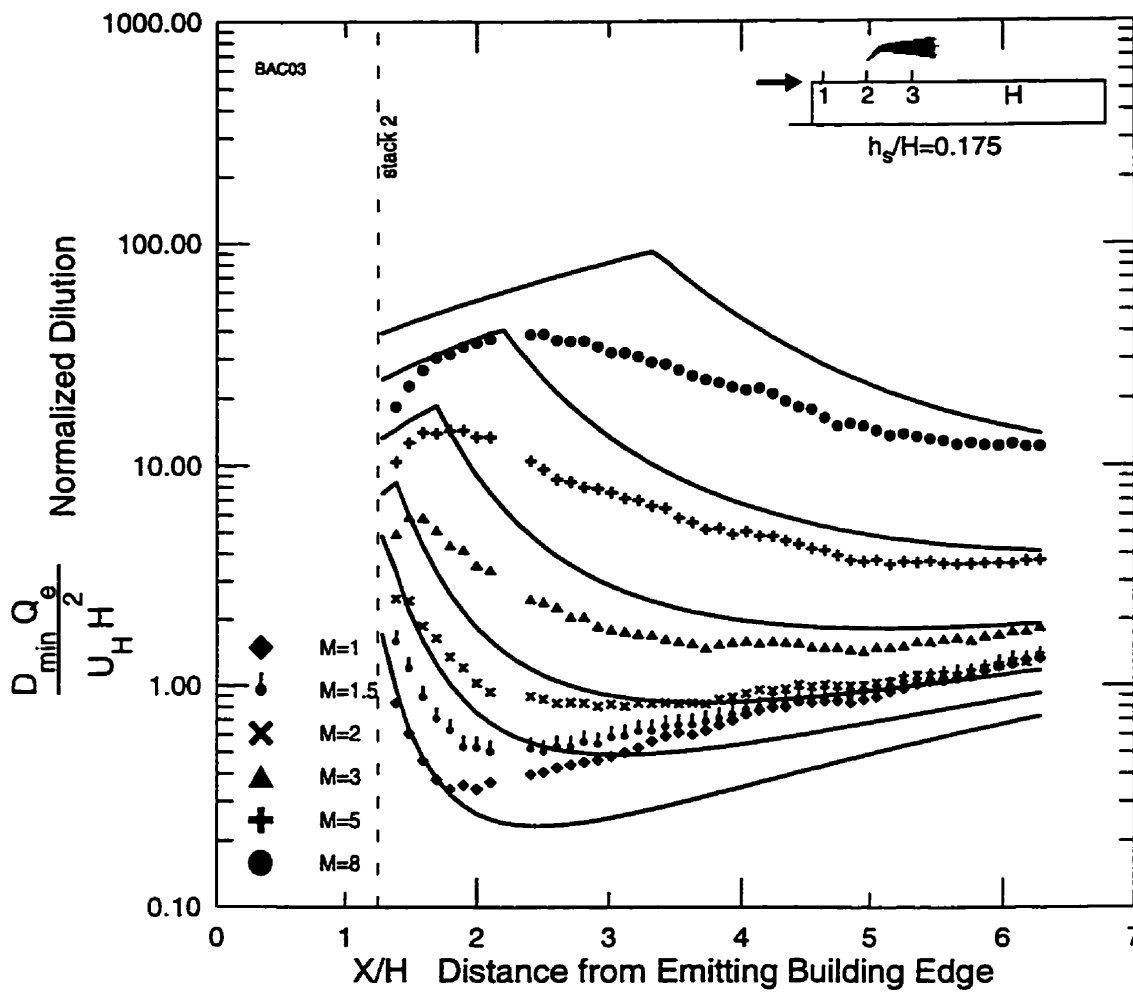
Figure 2.10   Dilutions over reference building for plume emitted from stack 2 at six different values of stack exhaust velocity to windspeed ratio M short stack height of $0.175H$. Theoretical curves are calculated using **final** rise model. Compare to Figure 2.7 showing transitional rise for the same situation to see the effectiveness of using the final rise model.

40
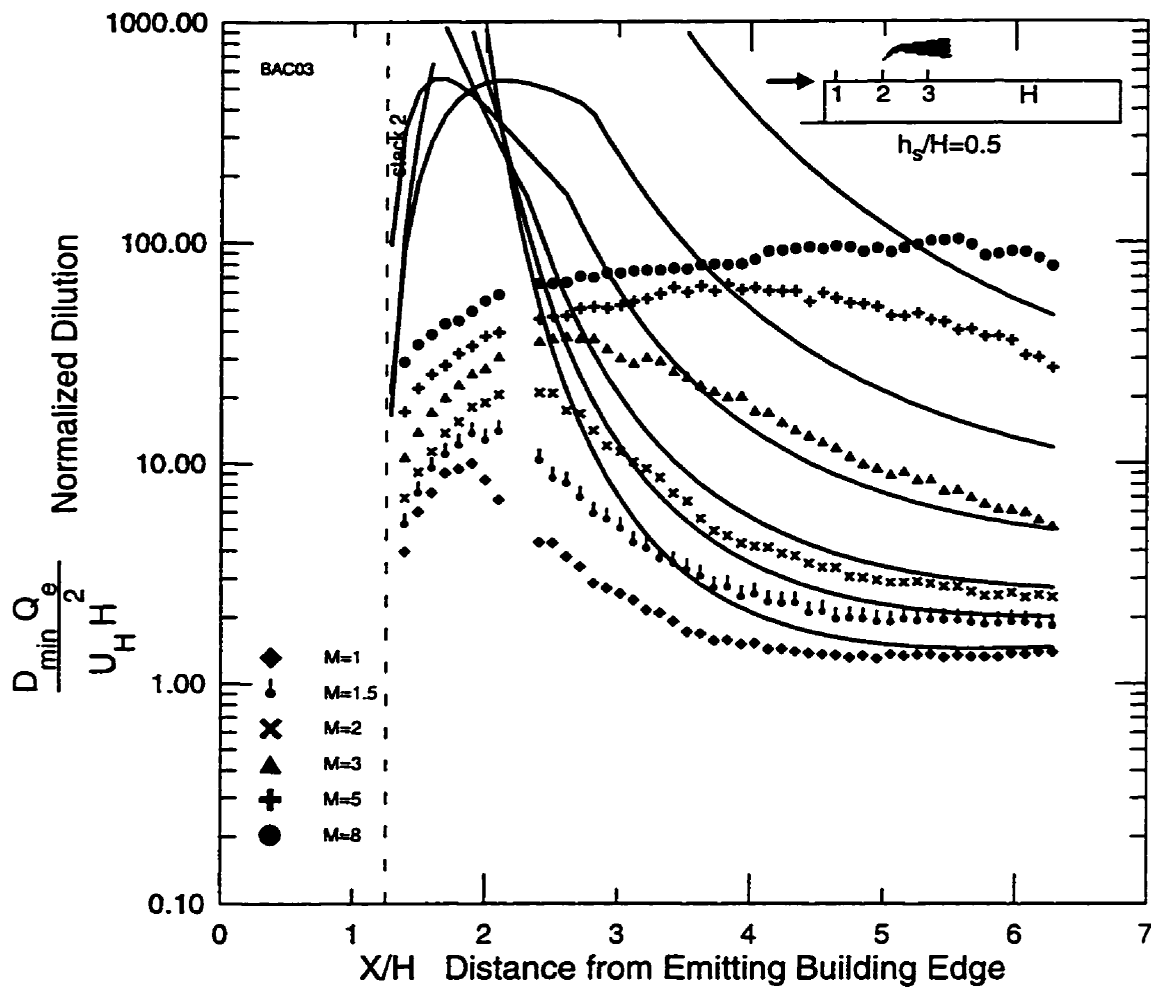
Figure 2.11   Dilutions over reference building for plume emitted from stack 2 at six different values of stack exhaust velocity to windspeed ratio M and a tall stack height of $0.5H$. Theoretical curves are calculated using **transitional** rise model.

41
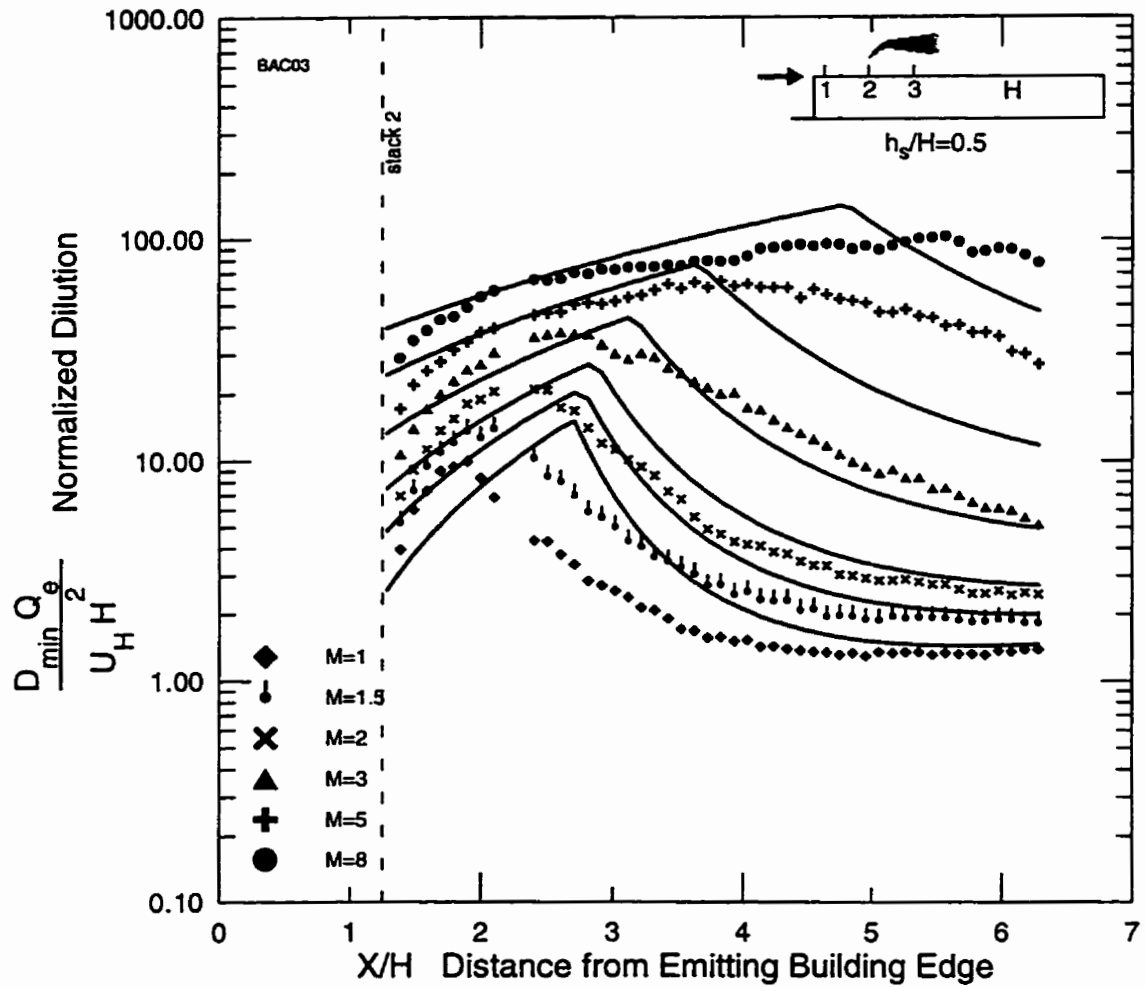
Figure 2.12   Dilutions over reference building for plume emitted from stack 2 at six
different stack exhaust velocity to windspeed *M* and a tall stack height
of 0.5*H*. Theoretical curves are calculated using **final** rise model.
Compare to Figure 2.9 showing transitional rise for the same situation
to see the effectiveness of using the final rise model.

42

$$\frac{D_{min} \, Q_e}{U_H \, H^2}$$

reciculation
cavity

emitting stack

U_H
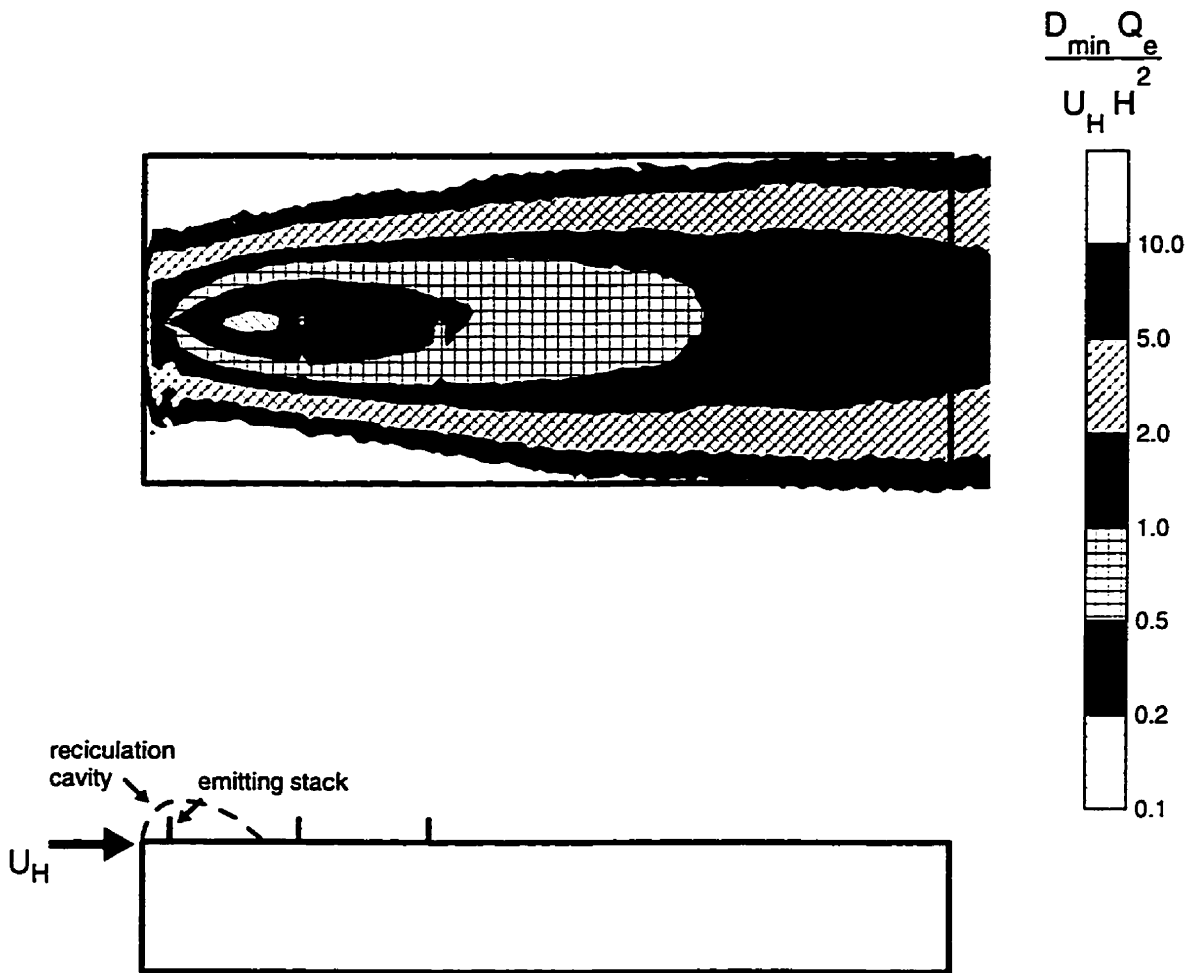
Figure 2.13   Dilution contours over reference building for plume emitted from upwind stack 1 at a stack exhaust velocity to windspeed ratio M of 1 and a stack height of $0.175H$. Compare to Figure 3.5 showing contours from center stack 2 to see the increased initial plume spread when emitting from stack 1.
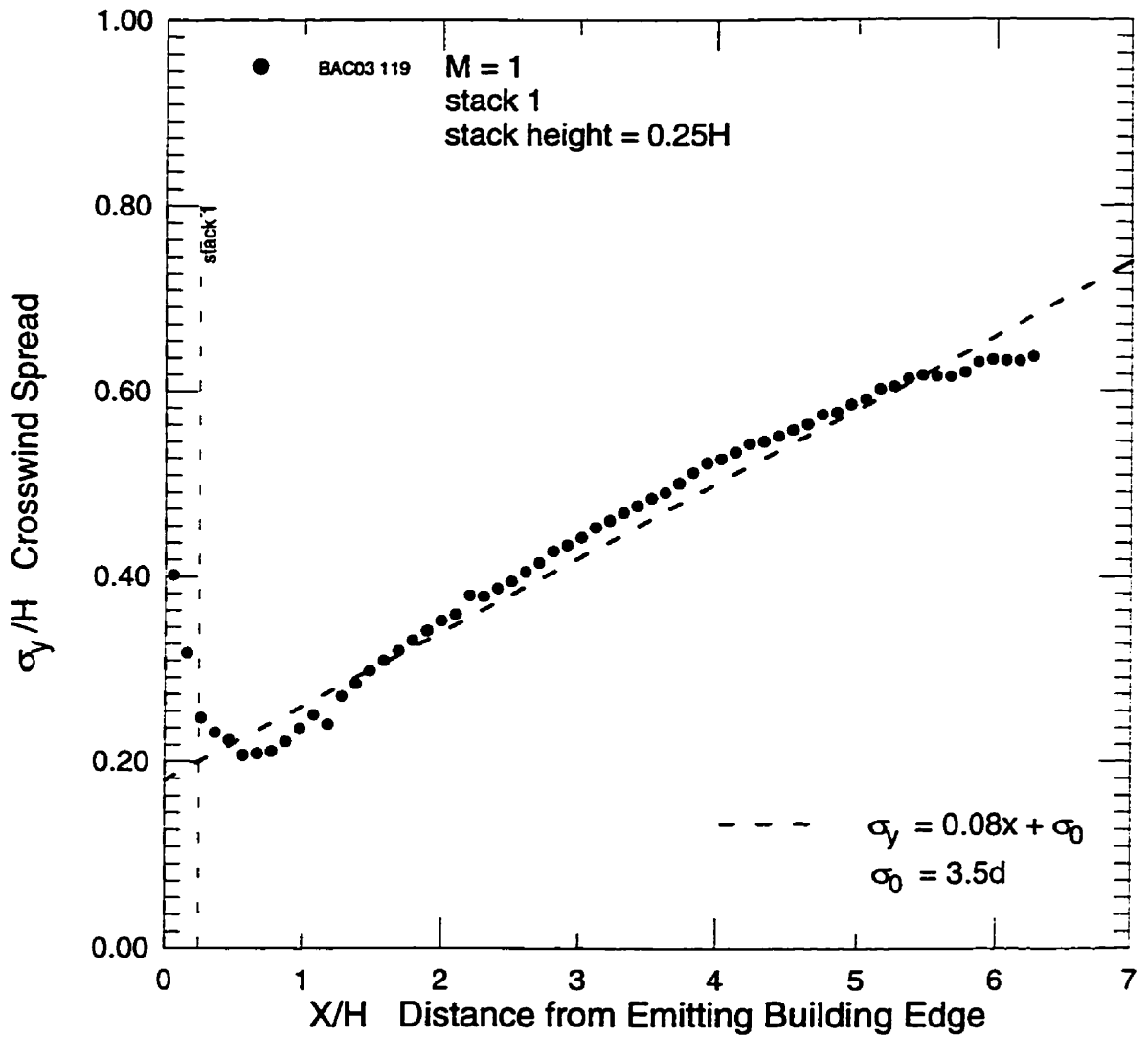
Figure 2.14   Plume Spread in cross stream direction measured over reference building for plume emitted from upwind stack 1 at a stack exhaust velocity to windspeed ratio M of 1 and a stack height of $0.25H$. Note increased spread near the front edge of the building.

44
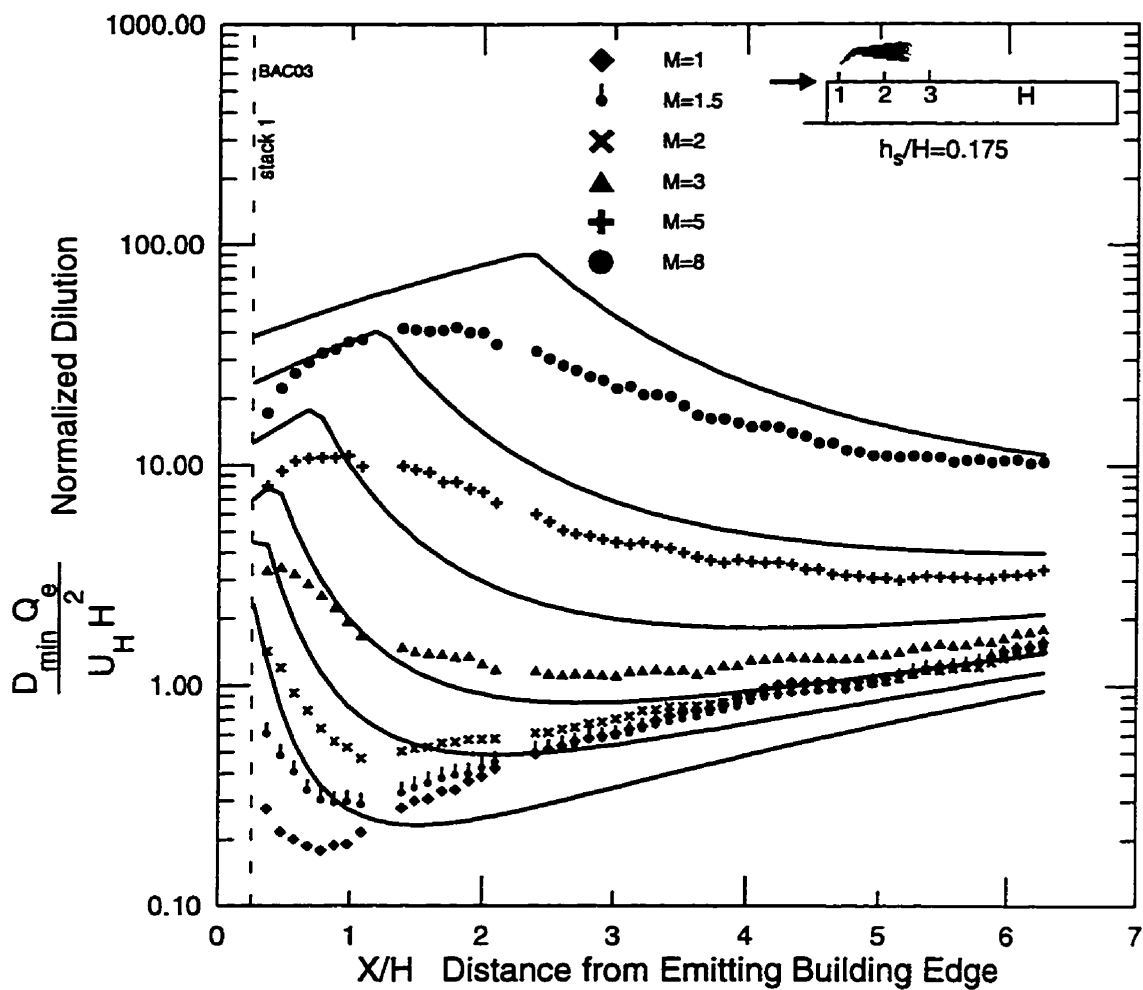
Figure 2.15   Dilutions over reference building for plume emitted from stack 2 at six different values of stack exhaust velocity to approaching windspeed M and a short stack height of $0.175H$. Theoretical curves are calculated using **final** rise model **without** front edge correction.

45
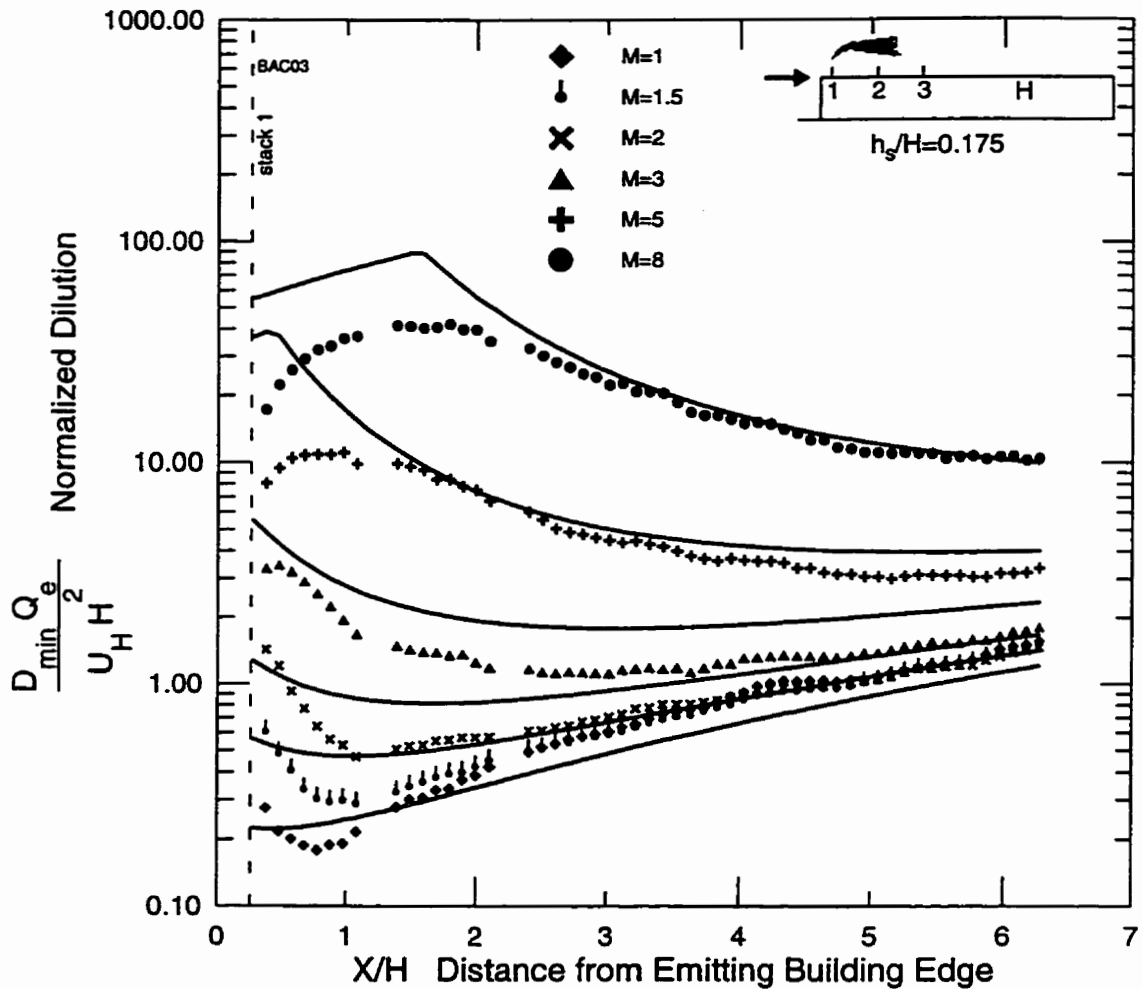
Figure 2.16   Dilutions over reference building for plume emitted from stack 2 at six different values of stack exhaust velocity to approaching windspeed M and a short stack height of $0.175H$. Theoretical curves are calculated using **final** rise model **with** front edge correction. Compare with Figure 2.13 to see improvement using front edge correction, particularly near the stack at low M.

46
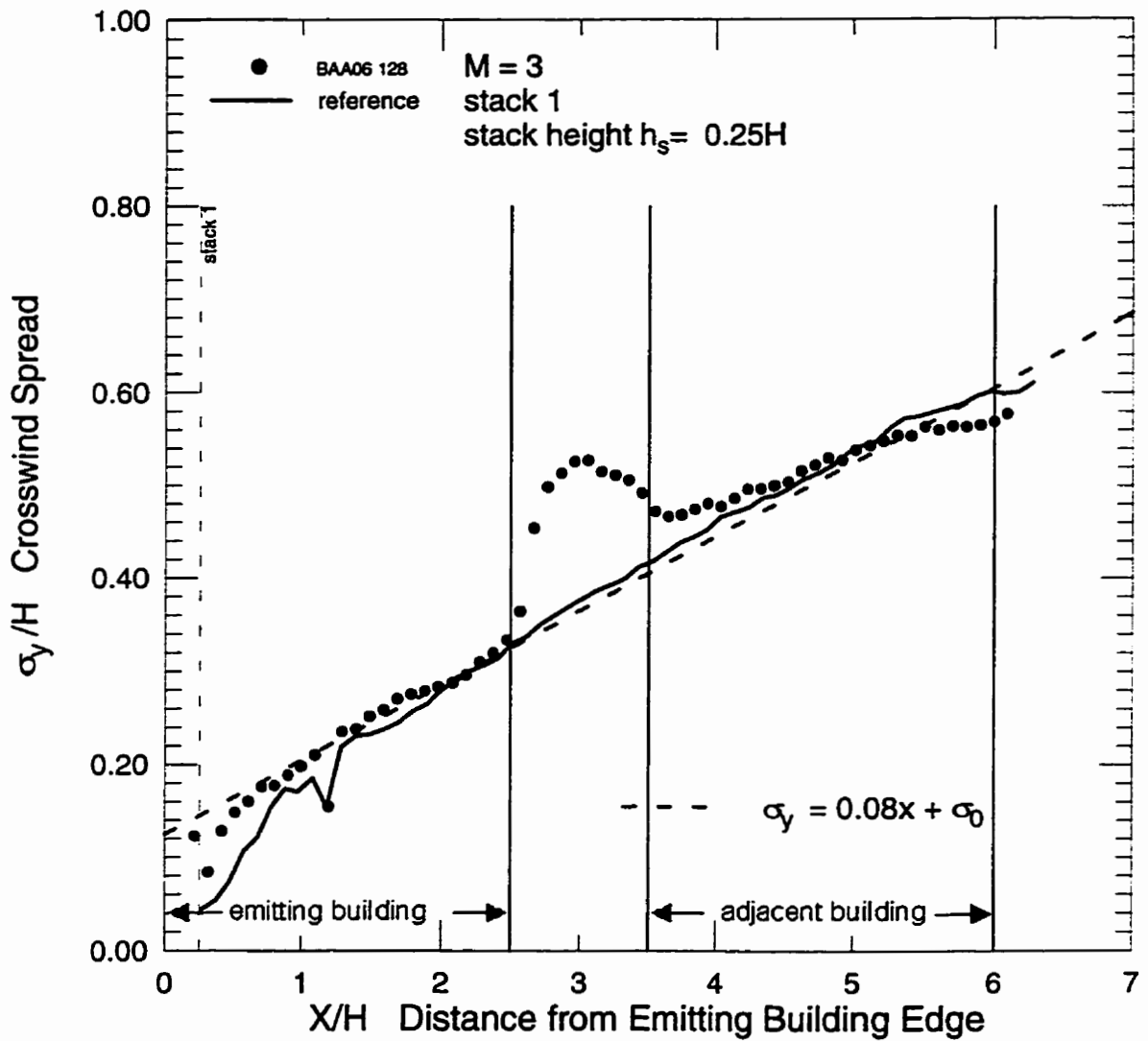
Figure 2.17   Plume Spread in cross stream direction measured over step across buildings for plume emitted from upwind stack 1 at a stack exhaust velocity to windspeed ratio M of 3 and a stack height of $0.25H$. Note close match between plume spreads measured on reference building and step across buildings over the building roofs.
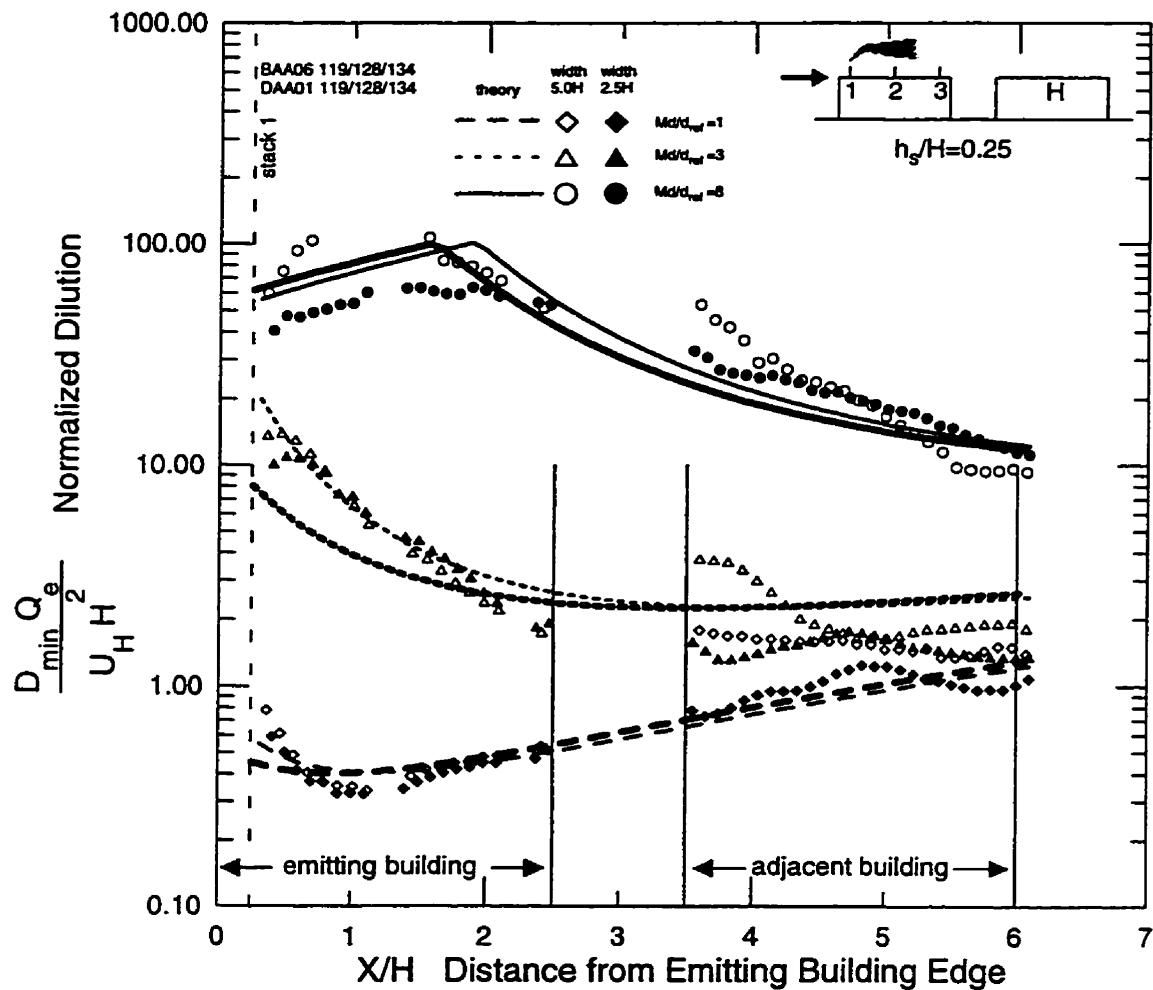
Figure 2.18   Dilutions over emitting and adjacent buildings for same height roofs
with emitting building **upstream.** Plume emitted with stack exhaust to
approaching flow velocity ratio M of 1, 3, and 8 from upstream stack 1
with stack height of $0.175H$. Theoretical dilution curves calculated with
final rise model used for reference building. Thick lines on the graph
correspond to 5.0H wide buildings and the thin lines on the graph
correspond to 2.5H wide buildings.

48
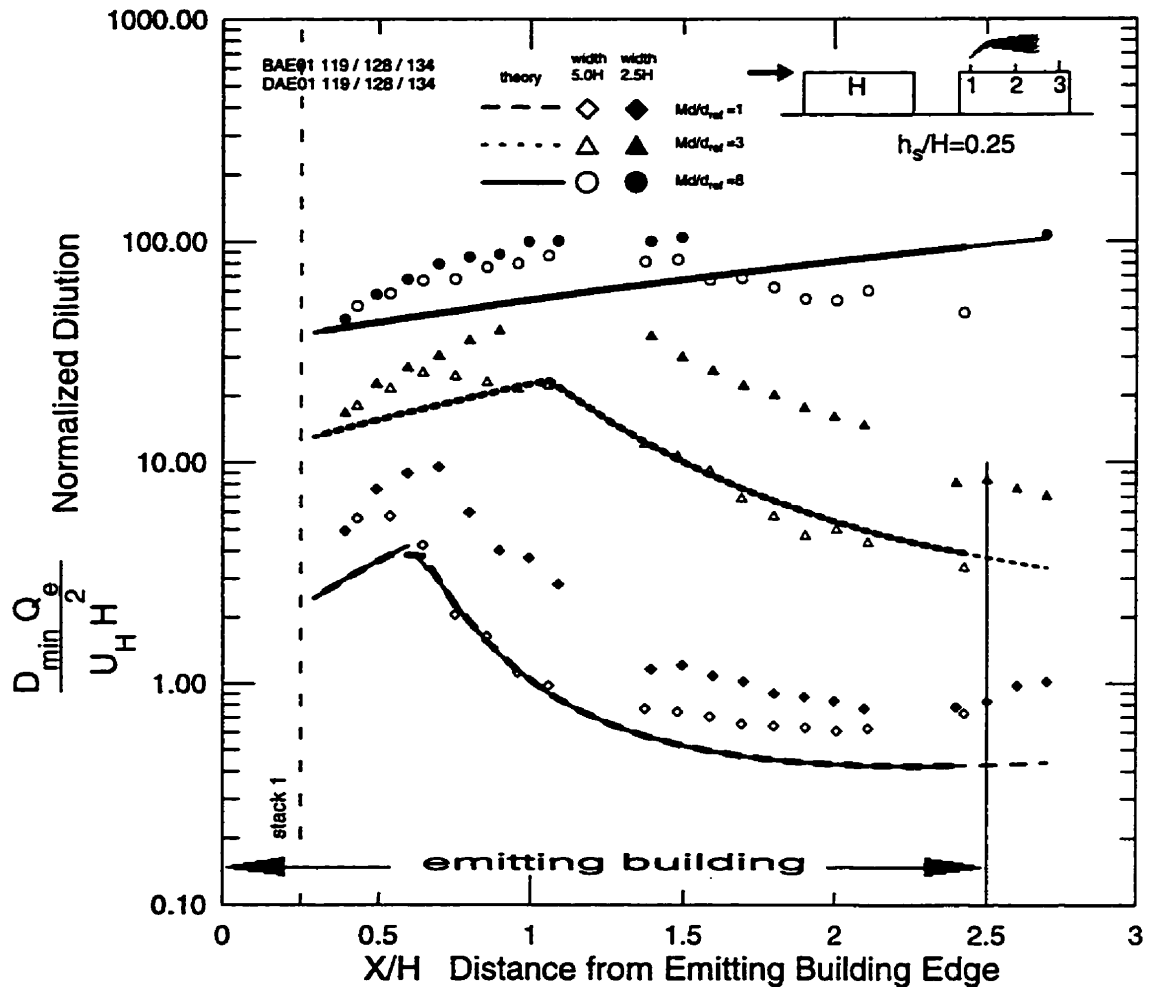
Figure 2.19   Dilutions over emitting and adjacent buildings for same height roofs
with emitting building **downstream**. Plume emitted with stack exhaust
velocity to windspeed ratio M of 1, 3, and 8 from upstream stack 1 with
stack height of $0.175H$. Theoretical dilution curves calculated with
final rise model used for reference building. Thick lines on the graph
correspond to 5.0H wide buildings and the thin lines on the graph
correspond to 2.5H wide buildings.

49

CHAPTER 3
INFLUENCE OF UPWIND BUILDINGS ON GAS DISPERSION FROM ROOFTOP STACKS

INTRODUCTION

In Chapter 2 a gaussian model was developed to predict plume dispersion over same roof height buildings and isolated stacks with no buildings present. The object in this Chapter is to test the model from Chapter 2 for cases where there is a taller building upwind of the building emitting an exhaust plume, and determine necessary adjustments to the model for predict dilutions on the roof of the emitting building.

Scale model atmospheric flow simulation were carried out for situations where a plume is emitted from a building downstream of a taller adjacent building. Measurements of concentration of the downwind building roof were carried out using a laser induced fluorescence technique. A schematic of the water channel facility used to carry out the flow simulation is shown in Figure 3.1. Recirculating flow in the water channel passes through turbulence screens and then roughness elements that produce turbulence typical of at atmospheric boundary layer. The flow then passes over the scale model buildings. Fluorescein tracer dye stored in a tank on the side of the water channel is pumped through a flexible tube and out through stacks on the model buildings to simulate exhaust stack release. Laser light were sheets located above the building roofs to create illuminate the tracer dye. Fluorescent light from the tracer dye intersecting the light sheet was detected with a video camera above the water channel.

Figure 3.2 depicts the complicated reversing trajectory of the plume. The stack exhaust is trapped inside the wake recirculation cavity behind the upwind adjacent building. Part of the plume is carried upstream from the stack back toward the downwind wall of the adjacent building and is mixed in the recirculation cavity before finally

escaping downstream.

The amount of exhaust gas trapped in this cavity will depend on stack location, stack height, stack exhaust momentum ratio, and the relative height difference and crosswind width of the buildings. The flow patterns in and around the wake are quite complex and significant simplifications will be made to produce a stack design-oriented model estimating dilution on the buildings.

PROPOSED MODEL

With an emitting building downwind of a taller upwind adjacent building there are two different situations that must be simulated by the theoretical model. The first deals with a plume that is fully trapped in the wake recirculation cavity behind the upwind adjacent building, as shown in Figure 3.3. The second deals with plumes that are able to fully escape the recirculation cavity, as shown in Figure 3.4. Both cases will assume a gaussian plume model of the form developed in Chapter 2. The equation for minimum dilution along roof or ground level from Chapter 2 is

$$\frac{D_{\min}Q_e}{U_H \, H^2} = \pi \frac{\sigma_y}{H} \frac{\sigma_z}{H} \left(\frac{U_c}{U_H} \right) \exp \left[\frac{(h_s + \Delta h)^2}{2\sigma_z^2} \right] \tag{3.1}$$

In Equation (3.1), Q_e is the volume flow rate at the stack, H is the reference building height, U_c is the effective plume convection windspeed, U_H is the windspeed at reference height H in the approaching flow. The plume height above the mass reflecting surface, either the roof or the ground is a combination of the stack height h_s and is the plume rise Δh due to exhaust gas buoyancy or jet momentum. Plume spreads in the crosswind direction y and vertical direction z are σ_y and σ_z respectively. Several adjustments to Equation (3.1), described in the following section, are required to account for the presence of the upwind adjacent building.

51

Proposed Model With Wake Cavity Trapping

When the plume is trapped inside the building wake recirculation zone, stack exhaust gases become mixed throughout the zone and concentrations appear upstream of the stack. To model this, the virtual origin of the plume is moved from the stack location to the downwind wall of the adjacent building. The EPA wake dispersion model uses a similar virtual origin displacement, see EPA (1995). Mixing in the turbulent recirculation requires that the plume have a larger initial dilution σ_o. Extra vertical plume spread $\Delta\sigma_z$ is also added. The final rise height of the plume is reduced to account for building wake downwash.

If the initial location of the plume is within the cavity trapping zone as shown in Figure 3.3, then the origin is shifted to the downwind wall of the upwind adjacent building. The dimensions of this recirculation cavity trapping zone were determined empirically by examining roof level dilution to see if exhaust had been carried upwind. The height H_{cavity} and the length L_{cavity} where recirculation was observed to be present at roof level were roughly estimated as,

$$H_{cavity} = 1.5 R_d \qquad (3.2)$$

$$L_{cavity} = 2.0 R_d \qquad (3.3)$$

where $R_d = \Delta H^{0.67} Y^{0.33}$ for a difference in roof heights of ΔH and a building width Y that is greater than ΔH. The height H_{cavity} and the length L_{cavity} where determined by observing for which cases measurable dilutions were appearing upstream of the stack. If dilutions were present upstream of the stack, the plume was assumed to be trapped in the building recirculation cavity. The length of the cavity could be determined by observing which

stack locations plumes could be trapped for each R_d. The height of the cavity was estimated by identifying values of total plume height h_f at which plumes would be trapped.

The virtual origin of the plume is shifted if x_{adj} in Figure 3.3 and 3.4 is less than $2.0R_d$ and the final height h_f of the plume above the emitting roof is less than $1.5R_d$. The undisturbed height h_f of the plume is calculated as stack height h_s plus final momentum rise Δh_{mf} minus a correction for stack tip downwash Δh_d so

$$h_f = h_s + \Delta h_{mf} - \Delta h_d \tag{3.4}$$

No building wake downwash is included in the undisturbed height h_f. From Briggs(1975), the final rise height due to exhaust jet momentum Δh_{mf} is,

$$\Delta h_{mf} = B_3 \left(\frac{U_H}{U_C} \right) Md \tag{3.5}$$

where B_3 is the momentum rise constant. A rise constant of $B_3=3.0$ was proposed by Briggs(1975) based on a survey of experimental data and was found to work well for the present study.

Extra initial spread $\Delta\sigma_{o,wake}$ is added to plume spreads σ_y and σ_z. The proposed function for the extra initial spread $\Delta\sigma_{o,wake}$ is

$$\Delta\sigma_{o,wake} = \frac{0.2R_d}{1+4.0\left(\dfrac{x_{adj}}{L_{cavity}} \right)^3} \tag{3.6}$$

53

Here the the extra initial spread $\Delta\sigma_{o,wake}$ is adjusted for the decreasing effect of the roof level change with distance by including an empirical cubic decay term. Extra vertical plume spread $\Delta\sigma_{z,wake}$ is also added to the vertical plume spread σ_z

$$\Delta\sigma_{z,wake} = \frac{0.4R_d}{\left(1+\frac{k_{impact}}{R_d}\right)\left(1+4.0\left(\frac{x_{adj}}{L_{cavity}}\right)^3\right)} \tag{3.7}$$

The crosswind spread σ_y and plume convection speed U_c are assumed to be unaffected by the building wake, so the plume convection velocity U_c is the windspeed U_H at roof level in the approaching flow. In reality σ_y increases and U_c decreases but it is assumed that the product $\sigma_y U_c$ is the same so dilution D_{min} is unaffected. The difference between final plume height h_f and the adjacent height is z_{impact}.

The height of the plume is shifted down to account for downwash behind the upwind building. The decrease in plume height Δz_{wake} is

$$\Delta z_{wake} = \frac{0.2R_d\left(1-\frac{|z_{impact}|}{\Delta H}\right)}{1+4.0\left(\frac{x_{adj}}{L_{cavity}}\right)^3} \tag{3.8}$$

Equations (3.7) and (3.8) use the cubic decay term in the dominator to ensure that the adjustment falls quickly to zero once the stack location is past L_{cavity}.

Proposed Model Without Wake Cavity Trapping

Figure 3.4 depicts the case where the plume is allowed to escape the cavity. The plume origin is no longer moved to the downwind wall of the adjacent building, and the

54

plume simply originates at the stack location. The presence of the wake still increases the initial dilution slightly through $\Delta\sigma_{o,wake}$. Small corrections were still added for plume downwash Δz_{wake} and increased vertical spread $\Delta\sigma_{z,wake}$ but the adjustments are small because of the cubic decay terms in the denominators of Equations (3.6), (3.7) and (3.8)

WATER CHANNEL MEASUREMENTS

Figure 3.5 depicts the different building configurations upon which measurements of dilution were made using laser light sheet illumination of fluorescent dye tracer, described Appendix B, for the case of a downwind emitting building with a taller upwind adjacent building. Adjacent building heights of $1.5H$ and $2.0H$ were used where H is the height of the emitting building. Tests were performed with and without a $1.0H$ gap between the buildings, and with building widths of 2.5H and 5.0H were test for each of the four situations depicted in Figure 3.5. Plumes from one of three possible stacks numbered 1, 2, and 3 with stack 1 being the most upstream stack. All the stacks were on the centerline of the building.

In Figure 3.6 contours of constant dilution are shown for a plume emitted from stack 2, central stack, with a stack height of $0.25H$ (short stack) with an exhaust momentum ratio $M=1$. The plume is significantly wider upstream of the stack, showing where exhaust has been caught in the wake recirculation cavity. As the plume escapes downstream, the dilution remains relatively constant.

NEW MODEL VS. SIMPLE GAUSSIAN MODEL

Figure 3.7 shows dilution measurements for $M=1$, 3, and 8 over the roof of the emitting building with an adjacent building $2H$ high upstream and no gap between the buildings. The plume was emitted from stack 1 (upstream stack) with a stack height of $0.175H$ (short stack). Here one also sees relatively constant dilution with downwind

distance.

Solid symbols show dilutions over the 2.5H wide buildings and open symbols show dilutions over the 5.0H wide buildings. There is at most a factor of 2 and often less than 20% difference between dilution measured on the 2.5H and 5.0H wide buildings. Measured dilution is almost the same exhaust velocity to windspeed ratio, M=8, and is only slightly higher on the 5.0H width buildings for M=1 and M=3 since the larger building wake will give a larger initial dilution.

The lines from the theoretical model in Figure 3.7 were calculated using the simple gaussian plume model in Equation (3.1). The only adjustment made is to shift the origin back to the wall of the adjacent building. No other corrections were made to account for the presence of the adjacent building. This model that includes only a virtual origin shift does a very poor job of predicting dilutions, with errors of more than a factor of 10 in most cases.

For the same data shown in Figure 3.7, the complete wake recirculation dispersion model is plotted in Figure 3.8 with all corrections for $\Delta\sigma_{n,wake}$, $\Delta\sigma_{z,wake}$, and Δz_{wake} applied. The new model does a much better job at predicting the measured dilutions. The predictions of the complete model were well within a factor of 2 of measurements, compared to Figure 3.7 where the predictions were over a factor of 10 in error.

The complete model shown in Figure 3.8 also produces the correct trend in the data, with dilution being more or less constant over the roof with slight increases as one moved downstream. The relative effects of building width were also predicted well by the model. Both measurements and the model show almost no difference between the predicted dilutions for the highest stack exhaust velocity to windspeed ratio, M=8. For M=1 and M=3 the model predicts that single width buildings will have about a factor of 1.5 to 2 less dilution than the 5.0H buildings, which is also what is observed from the

data.

EFFECT OF STACK HEIGHT

Figure 3.9 shows dilutions measured for the same situation as Figure 3.8 except that the stack height is $h_s=0.5H$ (tall stack). Note that the data from Figure 3.8 and 3.9 are very similar, indicating that even for the tall stack, the plume is caught in the wake recirculation zone. Once again the theoretical model does a good job of predicting the dilutions and relative effects of changing momentum ratio M, building width Y, and stack height h_s.

EFFECT OF STACK POSITION

To see what happens as the stack location is moved farther downstream, compare Figure 3.8 for plumes from a $0.175H$ high stack at location 1, Figure 3.10 that shows dilutions from plumes at stack 2 and Figure 3.11 that shows plumes from stack 3. At stack 2 the plume is still caught in the recirculation cavity for both building widths as low diltutions are appearing upstream of the stack, however, at $M=8$ the measured dilutions become larger as one moves upstream, indicating that some portion of the plume is beginning to escape without first being carried upstream. At $M=1$, there is not enough momentum for the plume to escape and low dilutions appear upstream of the stack. Dilutions around stack 2 are lower when the plume is emitted from stack 2 than when the plume is emitted from stack 1. Around stack 2 the mean flow would be opposite the free stream flow carrying the plume upstream of the stack onto the roof. At stack 1 the mean flow would be upward, carrying more stack exhaust away from the roof and giving higher dilutions than observed when the plume was emitted from stack 2. The theoretical lines plotted in Figure 3.10 and 3.11 are identical. The theoretical model puts both stacks inside the wake recirculation cavity and moves the origin to the same position on the back wall of the adjacent building adding the same extra spread and downwash. No attempt is

made to account for the effects of moving the stack around within the recirculation cavity since the interactions within the cavity are complex and this would required adding even more complication to the model. Mixing within the cavity removes most of the variation within the cavity. Measured dilutions differ by a factor of two when the stack is moved from position 1 to position 2, an effect not accounted for by the model.

EFFECT OF BUILDING WIDTH

When moving to the stack 3 in Figure 3.11, the data only shows concentrations appearing upstream of the stack only for the $5.0H$ wide buildings, or for the exhaust velocity to windspeed ratio $M=1$ for the $2.5H$ wide buildings. This implies that for the $2.5H$ wide buildings, the stack is at the edge of the recirculation cavity. A plume exhausting at $M=1$ doesn't have enough momentum to completely escape the cavity, and a small portion of the plume is carried slightly upstream. For $M=3$ and $M=8$ the plume has enough momentum to completely escape the cavity. The $5.0H$ buildings have a larger wake recirculation cavity and some of the plume is trapped for all three M values. Being near the end of the cavity, however, some of the plume will escape before being mixed into the wake recirculation, especially for higher M values. The theoretical model predicts dilutions around the stack quite well, but underestimates the dilution more and more as one moves upstream. This occurs since the model assumes all of the plume becomes trapped and mixes in the wake recirculation whereas some of the plume actually escapes without being mixed in the cavity.

The model has no provision to account for fractional trapping of part of the exhaust mass flow. It simply assumes that if the stack is near enough to the adjacent building that some of the plume could be trapped, then all of the plume will be trapped. This means that for cases where part of the plume is escaping and part is trapped, the model will always underpredict dilutions upwind front from the emitting stack. It was accepted that the model will underpredict dilution and overpredict concentration in these

cases rather then trying to simulate the complicated fluctuating flow near the downwind edge of the recirculation cavity.

EFFECT OF A GAP

To see the effect of a gap between the buildings compare Figure 3.12 to Figure 3.10. The spacing between stacks 1 and 2 is $1.0H$ so that removing the gap between the buildings in Figure 3.10 puts stack 2 at the same distance from the downwind wall of the upwind adjacent building as stack 1 would have been if there was a gap width of H between the building. The proposed model makes no adjustment for the presence of the gap, so the theoretical model predicts the same dilutions relative to the stack locations in both Figures 3.10 and 3.12.

The gap must fill up with concentration and the amount of concentration leaking into the gap is more or less equaled by concentration leaking back into the wake recirculation cavity. Some of the concentration must leak out the sides of the cavity reducing the concentration in the recirculation zone, and there are slightly higher dilutions shown downstream of the stack in Figure 3.12 where there is a gap between buildings. This is similar to the case shown in Figure 2.17 discussed in Chapter 2 where an increase in the crosswind spread σ_y was observed in the gap between the buildings indicating that stack exhaust may be filling up in the gap and leaking out the sides. This is not a major effect and no effort is made to account for it in the model. Note that comparisons should be only made between the dilutions downstream of the stack in each case.

EFFECT OF ADJACENT BUILDING HEIGHT

All previous discussion has been for cases where the adjacent building height $H_{adj}=2H$, twice that of the emitting building. The behavior of the model when the upwind adjacent building height $H_{adj}=1.5H$ will now be examined.

Figure 3.13 shows data from a short stack $h_s=0.175H$ at stack position 1 with an adjacent building $1.5H$ high and no gap between the buildings. In this case the stack will still be caught in the recirculation cavity. The data shows the dilution to be relatively constant with distance, typical of mixing within a recirculation cavity. The theoretical model still does a good job of predicting the magnitude of the dilution and the relative effect of changing different parameters. The model is within at least a factor of 2 everywhere, and within 20% in most places. The relative differences between dilution for $M=1$, 3, and 8 are the same as those predicted by the model. There is only a small difference in dilution measurements for single and double width buildings and indeed the theoretical model predicts only a small dependence on building width. The theoretical model predicts slightly higher dilutions on the $2.5H$ wide buildings for exhaust velocity to windspeed ratios of $M=1$ and $M=3$ and slightly lower dilutions on the $2.5H$ wide buildings for $M=8$ than is actually what is observed near the stacks.

PLUME TRAPPING AND ESCAPE

Figure 3.14 shows dilutions for a short stack $h_s=0.175H$ emitted from stack position 2 on the emitting building with an $1.5H$ upwind adjacent with no gap between the buildings. Here the stack is near the edge of the wake recirculation cavity with some of the plume being trapped and some of the plume escaping. Near the downwind end of the building the theoretical model does a reasonable job of predicting dilutions, but upwind of the stack the measured dilutions are consistently higher than the theoretical model predicts, since not all of the plume is being trapped in the wake recirculation cavity as is assumed by the theoretical model.

Due to the complexity of flow patterns near the edge of the cavity, no attempt is made to model this situation where a fraction escapes. As for the $2H$ high adjacent building, when there is a chance of some plume trapping, the model assumes that all the plume is being trapped and thus underestimates the dilution upstream of the stack. Since

60

the area near the edge of the recirculation cavity is a region of high uncertainty, it was accepted that the proposed model will be a conservative design tool for predicting dilutions upstream of the stack.

It should be noted that for a exhaust velocity to wind speed ratio of $M=8$ on the single width buildings, the theoretical model predicts that the plume will escape the cavity and predicts no concentrations upstream of the stack and indeed this is what was observed. The model does a very good job of predicting concentrations downstream of the stack.

CONCLUSIONS

The gaussian plume spread model presented in Chapter 2 has been adapted for predicting dilutions on the roof of an emitting building when there is a taller emitting building present. The following modifications to the theoretical model were required to account for the effect of the upwind building:

- additional initial plume spread

- additional vertical plume spread

- a decrease in the effective plume height caused by building wake downwash

- a shift in the virtual origin of the plume back to the downwind wall of the upwind building if the plume was determined to be trapped in the building wake recirculation zone

Based on dilution measurements over the emitting building roof, criteria were developed to determine for which values of stack location and undisturbed plume height

that plume would be considered trapped in the building recirculation cavity. The theoretical model predictions were within a factor of 2 of measured dilutions in most cases.

REFERENCES

Briggs, G.A. (1975) "Diffusion estimation for small emissions" in ERL, ARL, USAEC Report ATDL-106. U.S. Atomic Energy Commission, Oak Ridge, Tennessee.

EPA (1995) "SCREEN3 model user's guide" U.S. Environmental Protection Agency, Research riangle Park, North Carolina, document EPA-454/B-95-004.
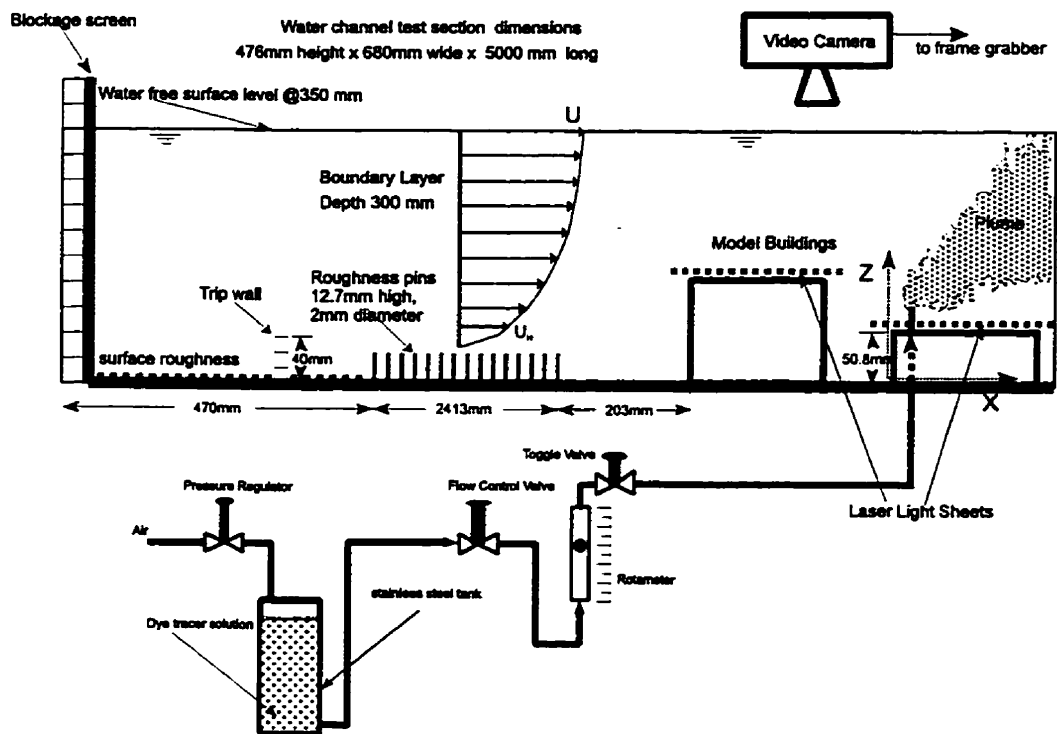
Figure 3.1   Schematic of water channel facility used for atmospheric flow
simulation

Actual Plume
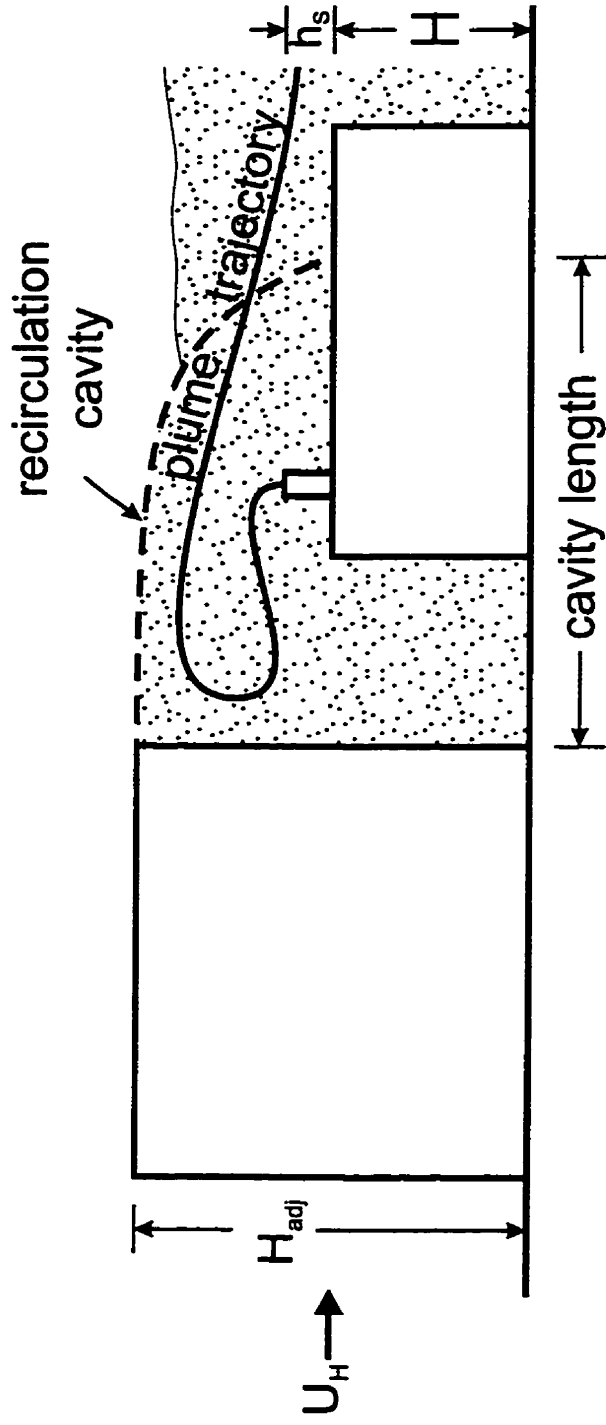
Figure 3.2   Actual plume behavior for a downwind emitting building when trapped in wake of a higher upwind adjacent building.
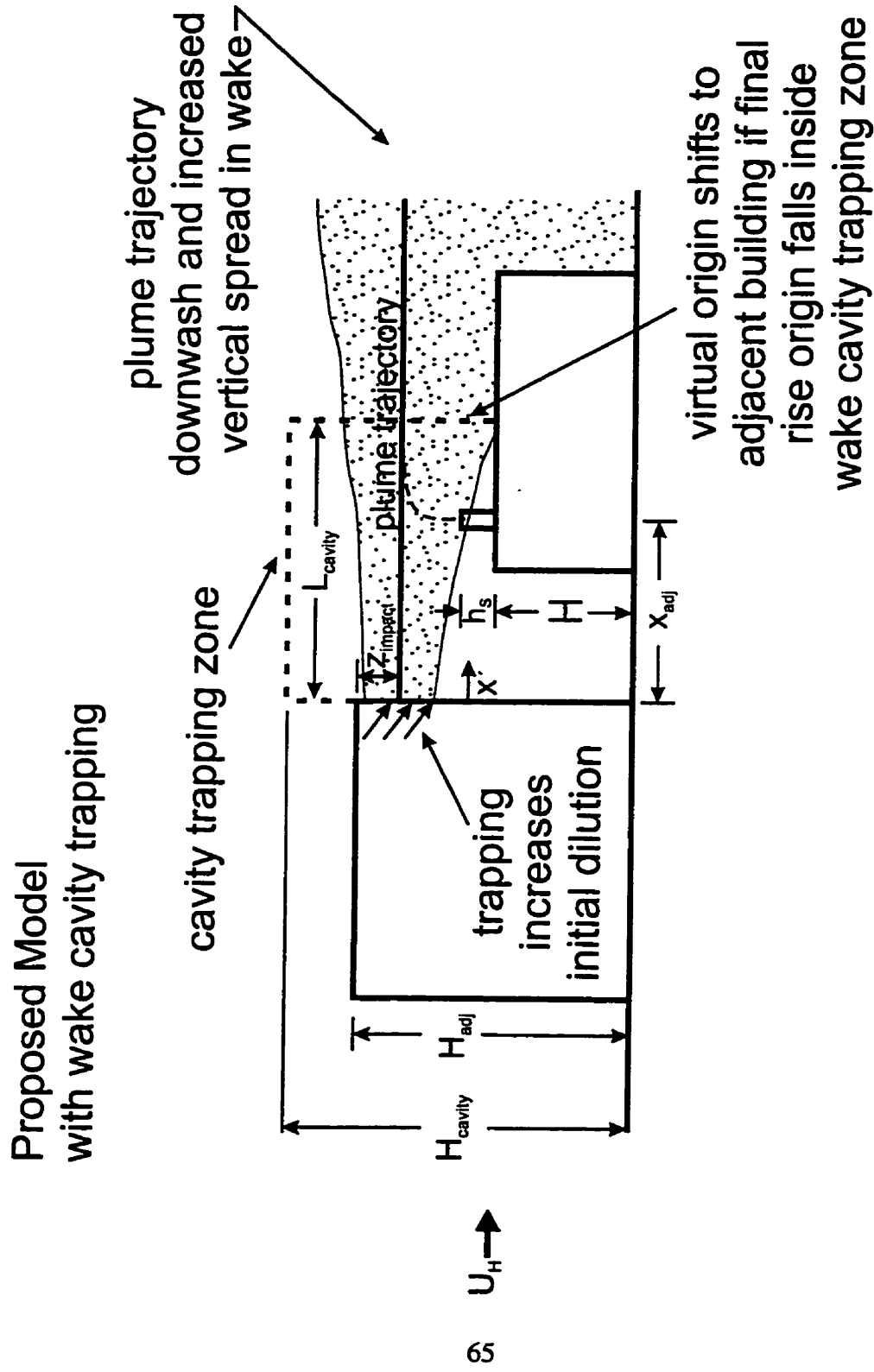
Figure 3.3   Proposed model for plume from a downwind emitting building trapped in wake cavity of an upwind adjacent building.

Proposed Model
no wake cavity trapping

plume trajectory downwash
and increased vertical
plume spread in wake

cavity trapping zone

wake increases
initial dilution

plume trajectory

L_{cavity}

Z_{impact}

H_{cavity} H_{adj}

U_H

$\overline{h_s}$

H

X_{adj}

no shift in virtual origin if
final rise origin falls outside
wake cavity trapping zone

66
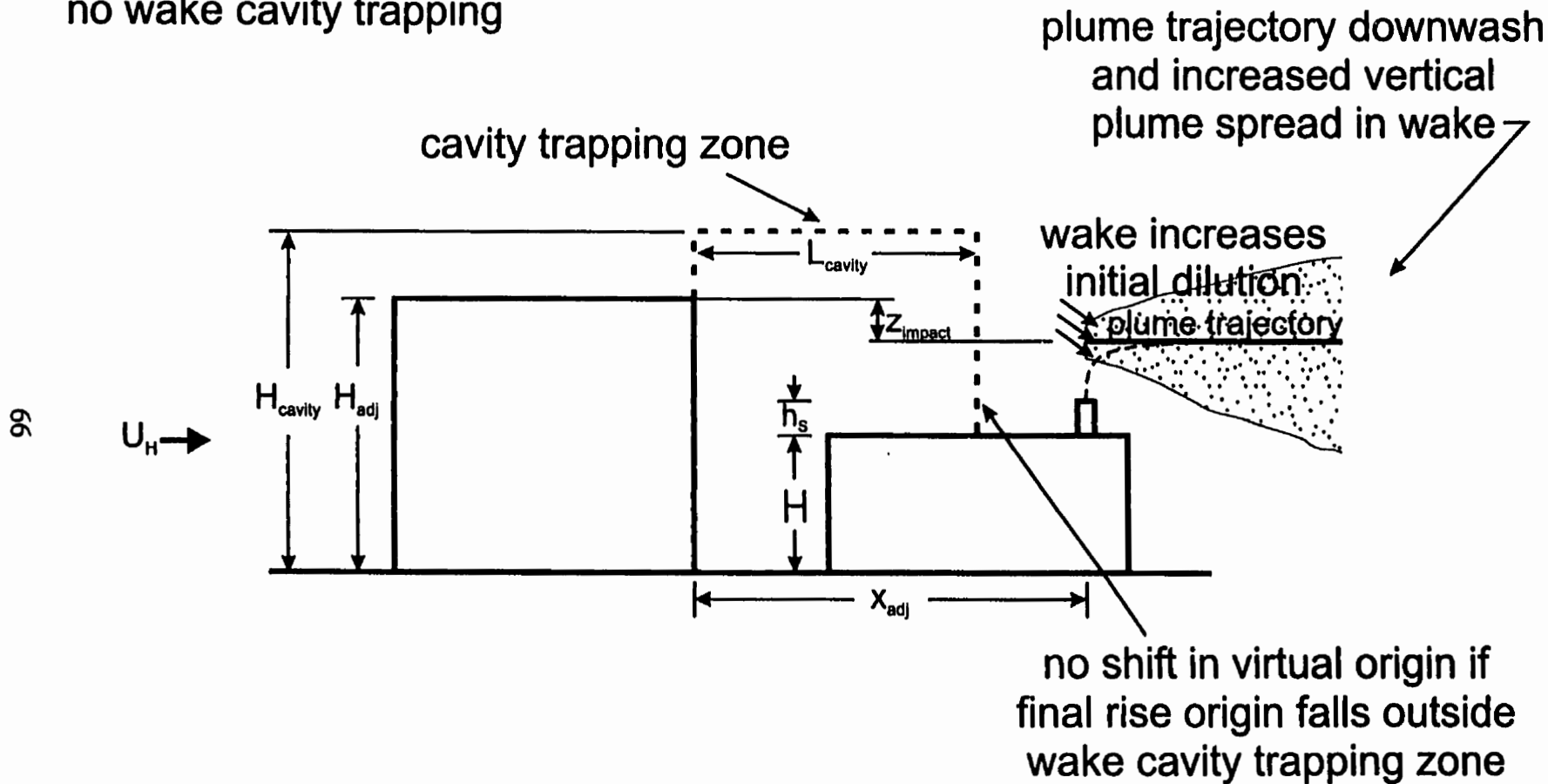
Figure 3.4   Proposed model for plume from a downwind emitting building where plume escapes
wake cavity of upwind adjacent building
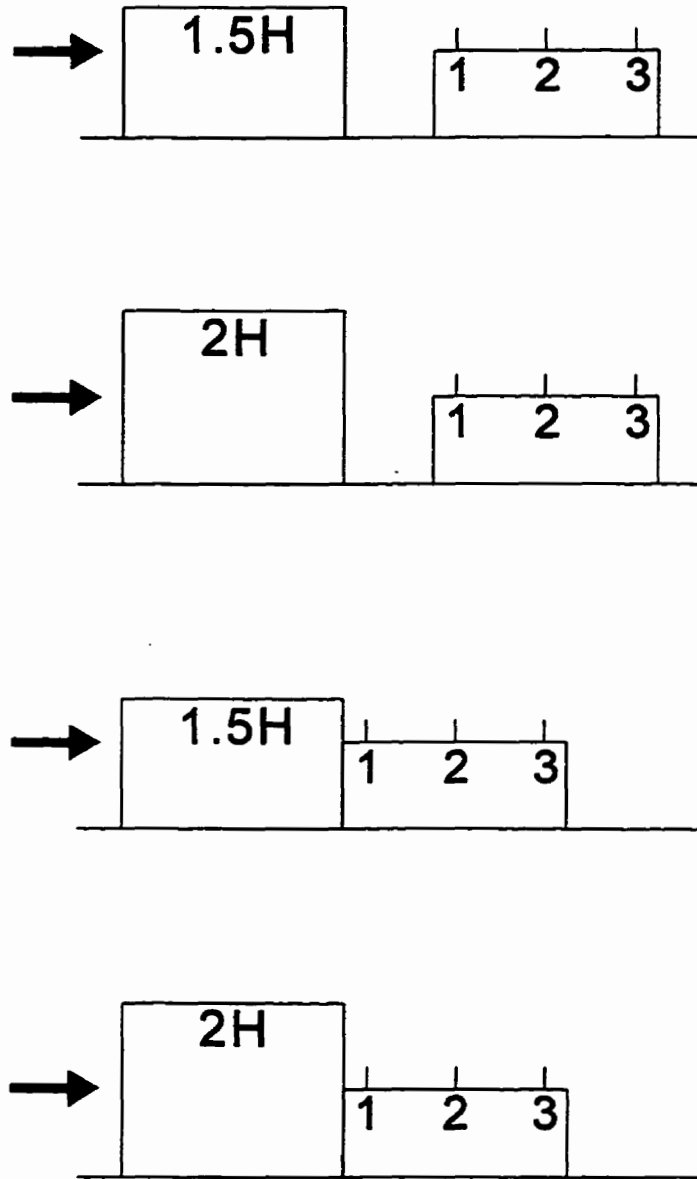
Figure 3.5   Building configurations used to measure plume dispersion form a
downwind emitting building with a taller upwind adjacent building

67
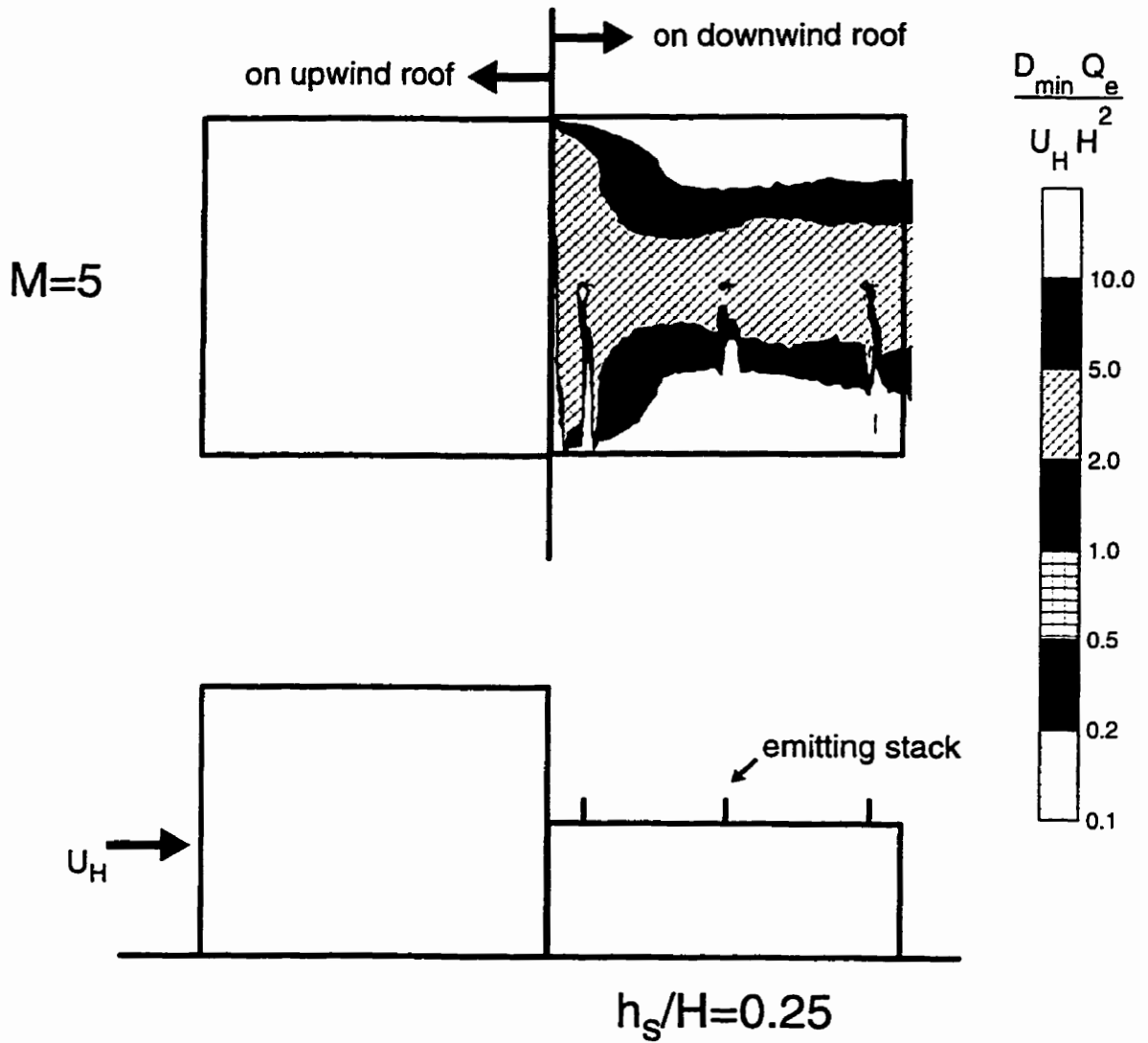
Figure 3.6   Dilution contours with plume emitted from stack 2 (central stack) on downwind building with $M=5$ and stack height $h_s=0.25H$.
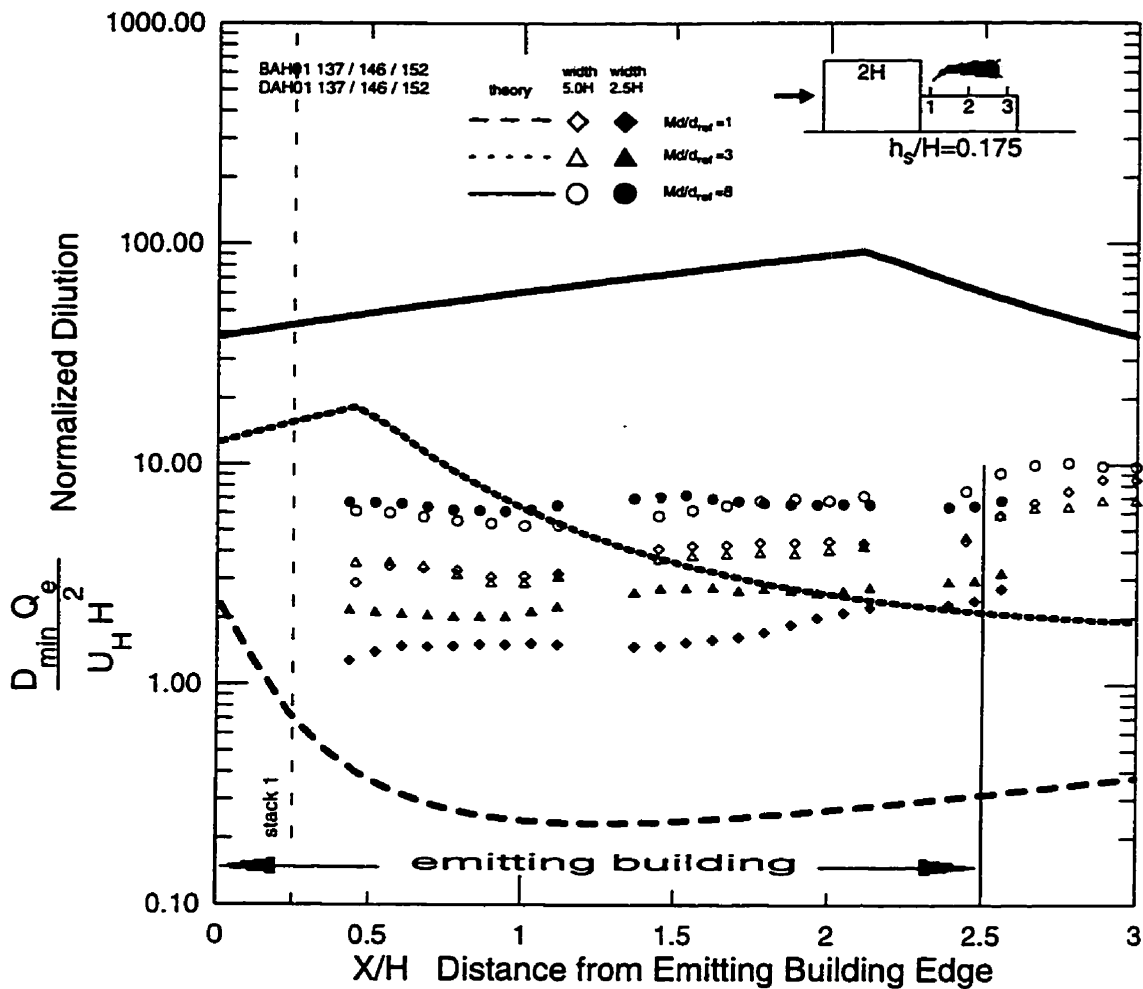
Figure 3.7   Model for short stack (stack height $h_s=0.175H$), stack 1 (upwind stack), no gap with no corrections for effects of the upwind building except a shift in the virtual origin to the downwind wall of the upwind adjacent building.
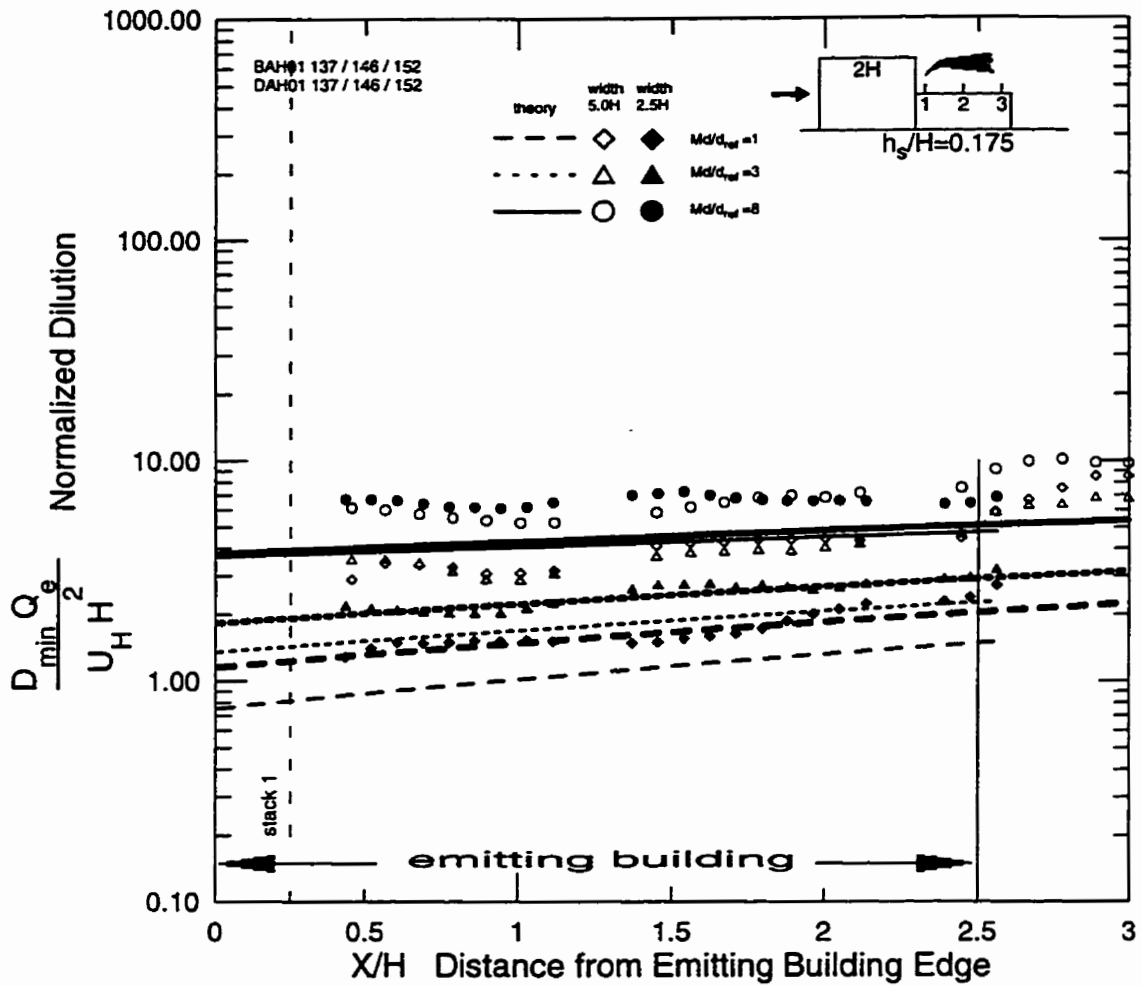
Figure 3.8   Complete model for short stack (stack height $h_s=0.175H$) , stack 1 (upwind stack), no gap, with added initial spread $\Delta\sigma_{o,wake}$, added spread $\Delta\sigma_{z,wake}$, and building downwash Δz_{wake} , all with downwind decay factors. Thick lines on the graph correspond to 5.0H wide buildings and the thin lines on the graph correspond to 2.5H wide buildings.

70
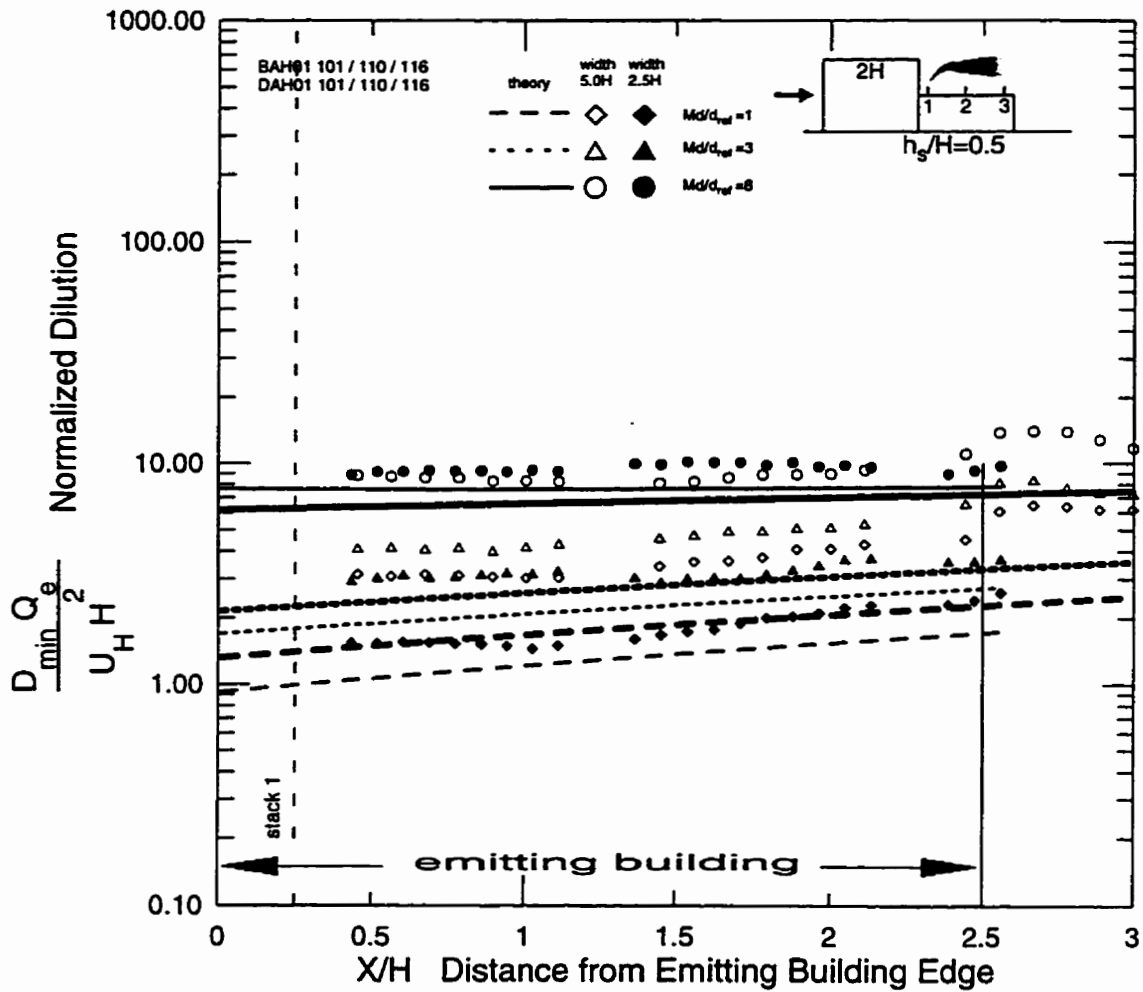
Figure 3.9   Complete model for tall stack (stack height $h_s = 0.5H$) , stack 1 (upwind stack), no gap, with added initial spread $\Delta\sigma_{o,wake}$, added spread $\Delta\sigma_{z,wake}$, and building downwash Δz_{wake} , all with downwind decay factors. Thick lines on the graph correspond to 5.0H wide buildings and the thin lines on the graph correspond to 2.5H wide buildings.

71
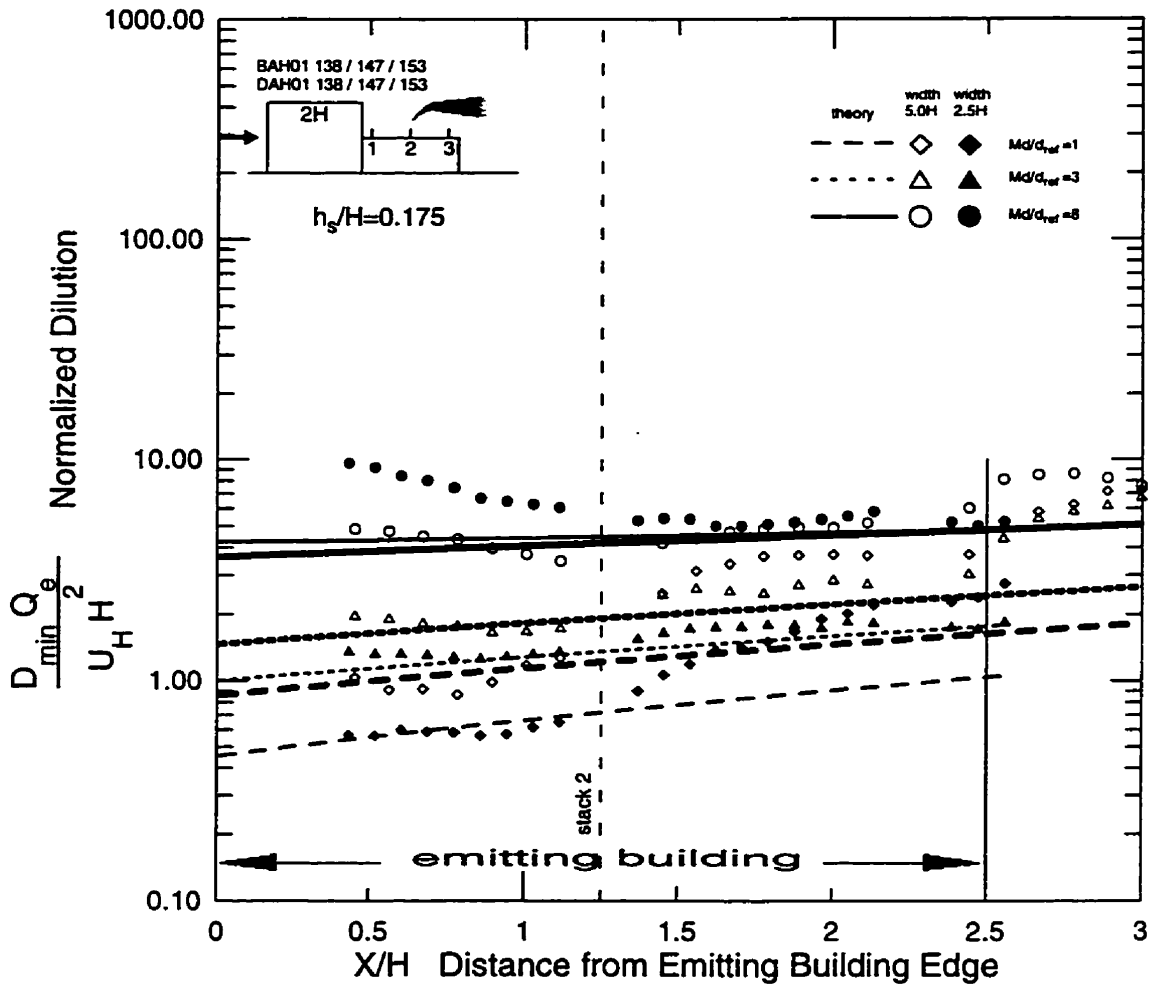
Figure 3.10   Complete model for short stack (stack height h_s=0.175H) , stack 2 (central stack), no gap, with added initial spread $\Delta\sigma_{o,wake}$, added spread $\Delta\sigma_{z,wake}$, and building downwash Δz_{wake} , all with downwind decay factors. Thick lines on the graph correspond to 5.0H wide buildings and the thin lines on the graph correspond to 2.5H wide buildings.

72
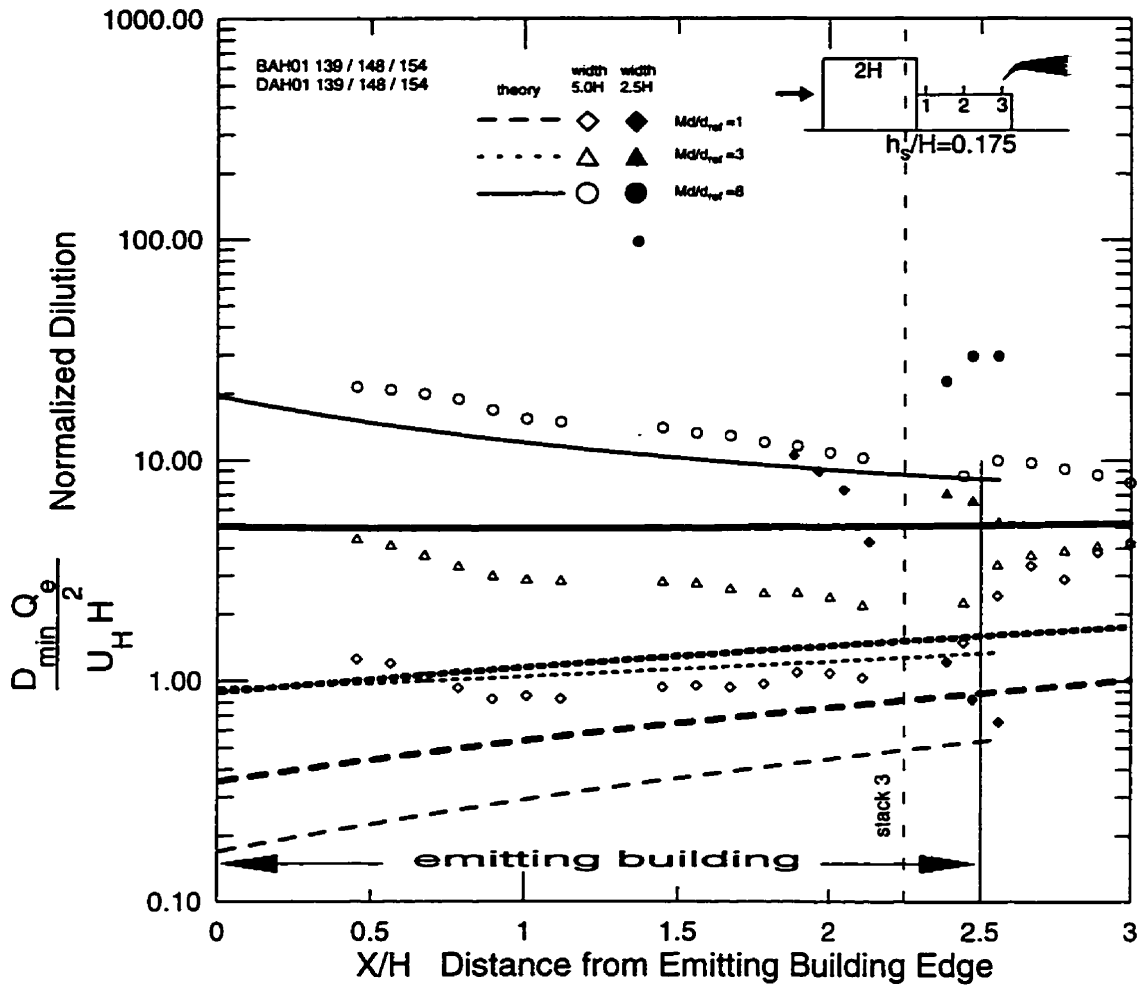
Figure 3.11   Complete model for short stack (stack height $h_s=0.175H$) , stack 3 (downwind stack), no gap, with added initial spread $\Delta\sigma_{o,wake}$, added spread $\Delta\sigma_{z,wake}$, and building downwash Δz_{wake} , all with downwind decay factors. Thick lines on the graph correspond to 5.0H wide buildings and the thin lines on the graph correspond to 2.5H wide buildings.
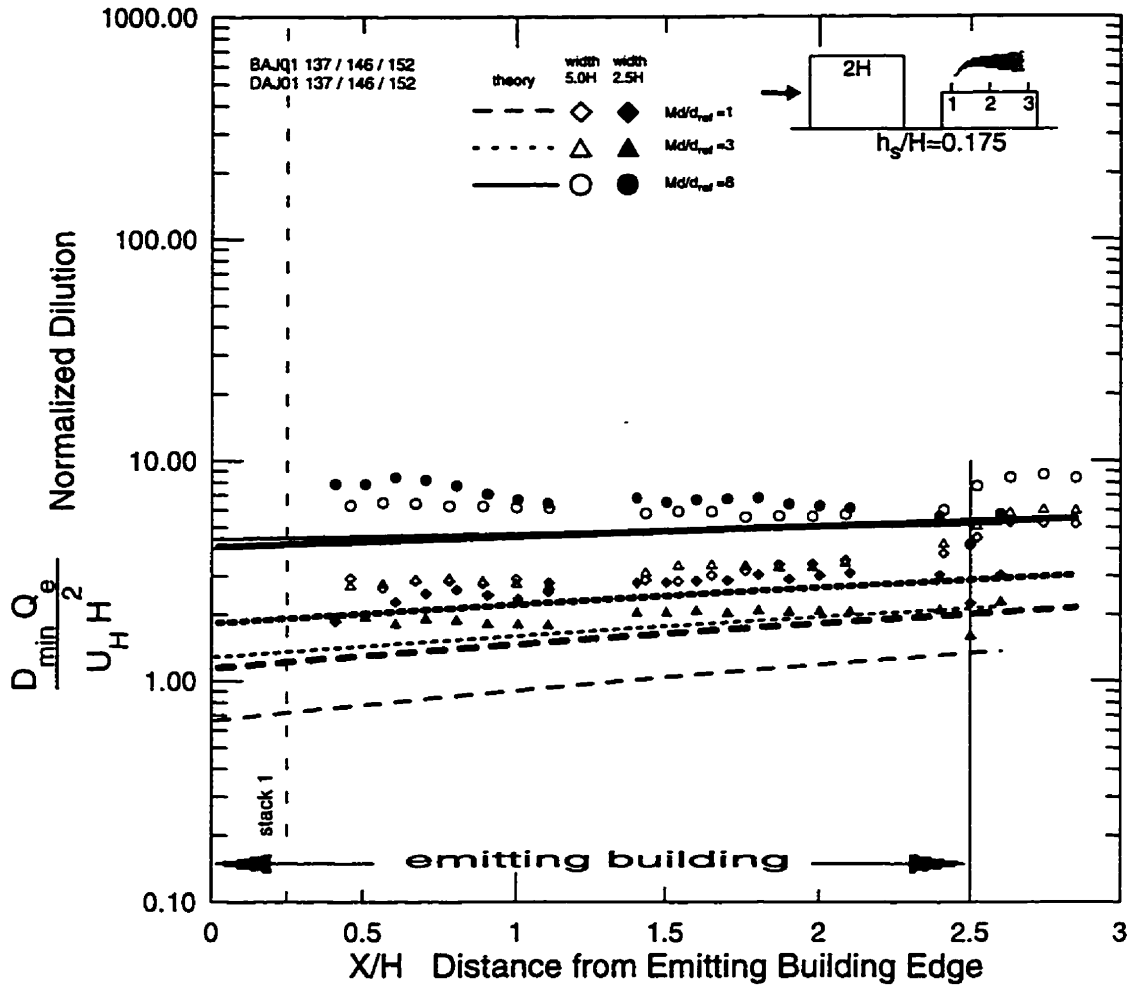
Figure 3.12   Complete model for short stack (stack height = 0.175H) , stack 1
(upwind stack) and gap width H between buildings. Model includes
added initial spread $\Delta\sigma_{o,wake}$, added spread $\Delta\sigma_{z,wake}$, and building
downwash Δz_{wake} , all with downwind decay factors. Thick lines on the
graph correspond to 5.0H wide buildings and the thin lines on the graph
correspond to 2.5H wide buildings.

74

BAM01 137 / 146 / 152
DAM01 137 / 146 / 152

	theory	width 5.0H	width 2.5H
$Md/d_{ref}=1$	– – –	◇	◆
$Md/d_{ref}=3$	······	△	▲
$Md/d_{ref}=8$	———	○	●

1.5H   1 2 3

$h_s/H=0.175$

Normalized Dilution

$$\frac{D_{min} Q_e}{U_H H^2}$$

1000.00

100.00

10.00

1.00

0.10

stack 1

◄——— emitting building ———►

0   0.5   1   1.5   2   2.5   3

X/H   Distance from Emitting Building Edge
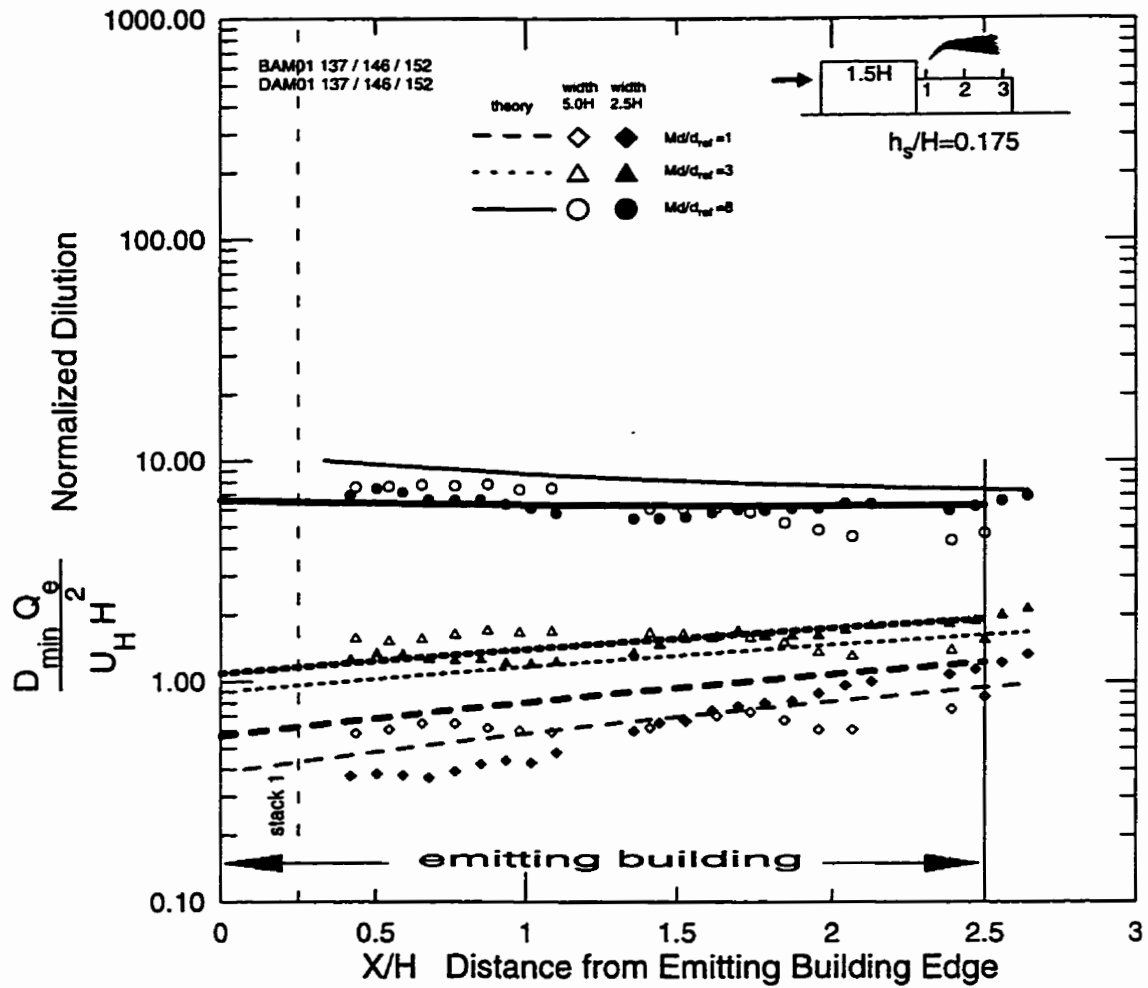
Figure 3.13   Complete model for short stack (stack height $h_s=0.175H$) , stack 1
(upwind stack), no gap with adjacent building height 1.5H. Model
includes added initial spread $\Delta\sigma_{o,wake}$, added spread $\Delta\sigma_{z,wake}$, and
building downwash Δz_{wake} , all with downwind decay factors. Thick
lines on the graph correspond to 5.0H wide buildings and the thin lines
on the graph correspond to 2.5H wide buildings.

75
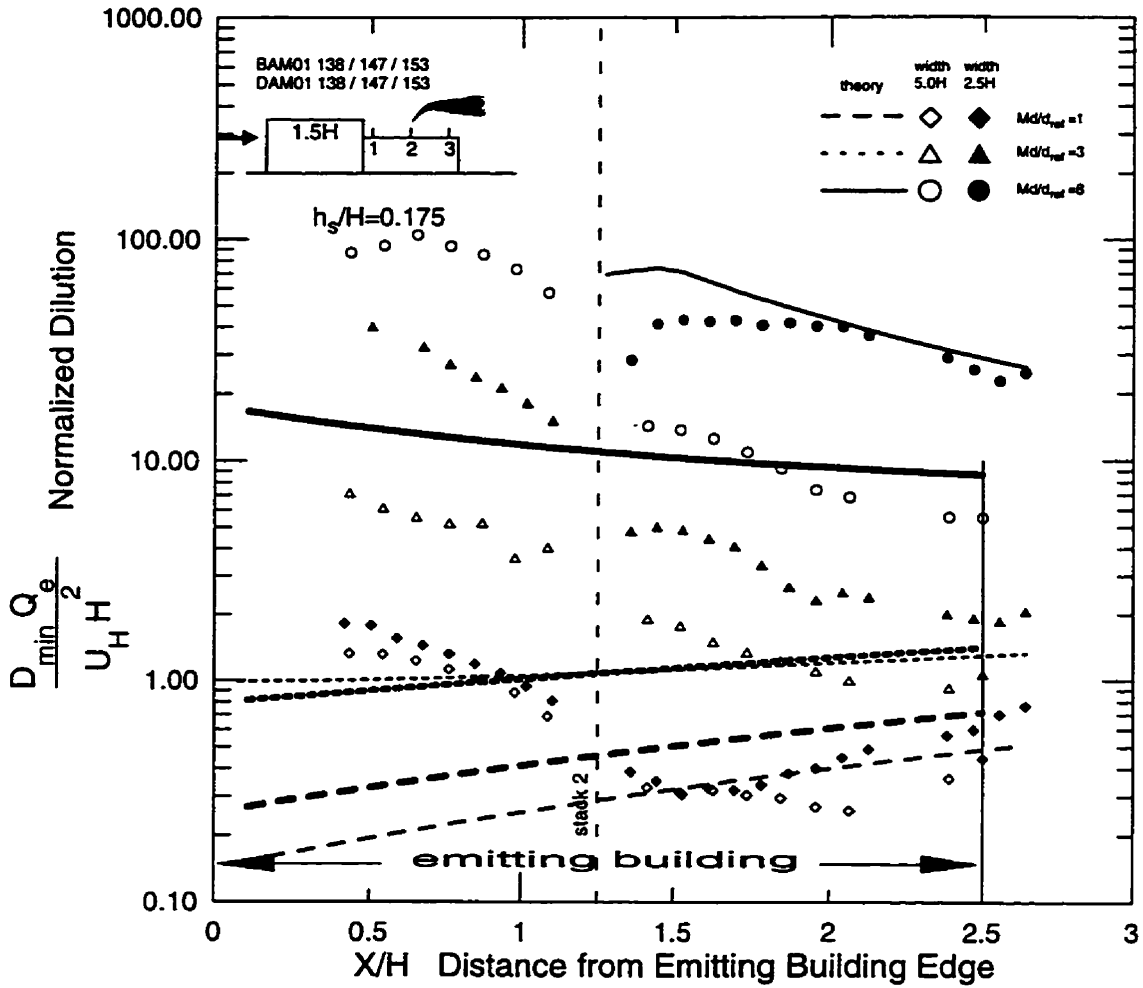
Figure 3.14   Complete model for short stack (stack height h_s=0.175H) , stack 2 (central stack), no gap with adjacent building height 1.5H. Model includes added initial spread $\Delta\sigma_{o,wake}$, added spread $\Delta\sigma_{z,wake}$, and building downwash Δz_{wake} , all with downwind decay factors. Thick lines on the graph correspond to 5.0H wide buildings and the thin lines on the graph correspond to 2.5H wide buildings.

76

CHAPTER 4

ESTIMATING WALL CONCENTRATIONS ON AN UPWIND ADJACENT BUILDING USING A MODIFIED ROOF LEVEL DILUTION THEORY

INTRODUCTION

Chapter 3 modified a theoretical model used to predict plume dispersion on the flat-roofed buildings and from isolated stacks. The modifications allowed the model to predict dilutions on the roof of an emitting building when there is a taller upwind adjacent building within a factor of 2 or better. The objective of this chapter is to assess the ability of this theoretical model to predict plume dispersion on the wall of the upwind adjacent building.

Figure 4.1 shows the building configurations used to measure and predict wall dilutions of a building with a lower emitting building downwind. Measurements were made on the wall closest to the emitting building using a laser induced fluorescence technique in a water channel simulation. A schematic of the water channel facility used for the simulations is shown in Figure 4.2. Recirculating flow in the water channel passes through turbulence screens and then roughness elements that produce turbulence typical of at atmospheric boundary layer. The flow then passes over the scale model buildings. Fluorescein tracer dye stored in a tank on the side of the water channel is pumped through a flexible tube and out through stacks on the model buildings to simulate exhaust stack release. Laser light sheets were located above the building roofs to create illuminate the tracer dye. Fluorescent light from the tracer dye intersecting the light sheet was detected with a video camera above the water channel. Plumes were emitted from one of three possible stacks numbered 1, 2, and 3 as in Figure 4.1 .All the stacks were on the centerline of the building. These are the same configurations used in Chapter 3 for roof level concentrations. The laser sheet lighting used to illuminate fluorescent dye tracer was placed on the back wall of the adjacent building, marked as the data plane in

Figure 4.1.

The actual behavior of a trapped plume is shown in Figure 4.3. The some stack exhaust is trapped inside the building recirculation cavity behind the upwind adjacent building and carried upstream from the stack back toward the downwind wall before finally escaping downstream. The theoretical model is shown schematically in Figure 4.5. The theoretical model shifts the virtual origin of the plume to the downwind wall of the upwind building. Extra initial spread and extra vertical spread are added to the plume to account mixing in the building recirculation cavity, and there is in the effective plume height to account for downwash in the building wake.

DILUTION MEASUREMENTS IN WATER CHANNEL SIMULATIONS

The experimental technique for measuring wall concentrations is described in Appendix B. Figure 4.4 shows the scale model setup for an adjacent building upwind of a lower emitting building. The upwind adjacent building was constructed with a transparent glass roof and a transparent glass wall on the side closest to the emitting building. The building contained a $45°$ mirror that reflected light from dye in front of the glass wall up to a video camera looking down on the building. The laser light sheet was located 2mm $(0.04H)$ in front of the glass wall to illuminate flourescent tracer dye.

PROPOSED DISPERSION THEORY

The theoretical model used for predicting dilution is the same one developed in Chapter 3 for an emitting building but now with a taller upwind adjacent building. Chapter 3 considered separate cases where the plume was trapped in the building recirculation cavity and where the plume was able to escape the cavity . For dilutions on the back wall of the adjacent building, only the case where the plume is trapped is considered because, if most of the stack exhaust escapes the cavity, there will be no

78

significant concentration on the wall and no model is required.

In the proposed model the virtual origin is shifted to the downwind wall of the upwind building. The model also adds extra initial spread $\Delta\sigma_o$ caused by plume trapping, extra vertical spread in the wake $\Delta\sigma_{z,wake}$, and a plume trajectory correction caused by building downwash Δz_{wake}. Appropriate functions for $\Delta\sigma_o$, $\Delta\sigma_{z,wake}$, and Δz_{wake} were given in Chapter 3. The total vertical spread used in the model is then

$$\sigma_{z,wake} = \sigma_o + \Delta\sigma_{o,wake} + \Delta\sigma_{z,wake} \tag{4.1}$$

where σ_o is the initial size without cavity trapping. There is no distance dependence of plume spread $\sigma_{z,wake}$ since it is always evaluated at the virtual origin of the plume. With undisturbed plume rise h, the effective plume height h_{total} is

$$h_{total} = h - \Delta z_{wake} \tag{4.2}$$

The dilution D at any distance z' above the concentration reflecting surface can be found from

$$\frac{DQ_e}{U_H H^2} = 2\pi \left(\frac{\sigma_y}{H}\right) \left(\frac{\sigma_{z,wake}}{H}\right) \left[\exp\left(-\frac{(z'-h_{total})^2}{2\sigma_{z,wake}^2}\right) + \exp\left(-\frac{(z'+h_{total})^2}{2\sigma_{z,wake}^2}\right)\right]^{-1} \tag{4.3}$$

In reality plume convection velocity U_c decreases and σ_y increases in the wake but the product $U_c\sigma_y$ is assumed to remain constant in the building wake so that dilution can be calculated using the values of $U_c = U_H$ and σ_y in the undisturbed plume. To obtain simple estimates of the dilution on the wall downwind wall of the upwind adjacent building, it was assumed a constant dilution existed over the wall. After trying several possibilities it was found that the best estimate for this average dilution was found by

taking the average of the concentrations at emitting and adjacent roof level. The roof of the emitting building was used as the mass-reflecting surface. For the emitting building roof $z'=0$, the normalized dilution at the emitting building roof height is, from Equation (4.3)

$$\frac{D_{emit}Q_e}{U_H H^2} = \pi\left(\frac{\sigma_y}{H}\right)\left(\frac{\sigma_{z,wake}}{H}\right)\exp\left(\frac{h^2}{2\sigma_{z,wake}^2}\right) \tag{4.4}$$

At the adjacent building roof the distance above the reflecting surface $z'=\Delta H$ where ΔH is the difference in roof heights, the normalized dilution at the adjacent building roof height is

$$\frac{D_{adj}Q_e}{U_H H^2} = \frac{2\pi\left(\frac{\sigma_y}{H}\right)\left(\frac{\sigma_{z,wake}}{H}\right)}{\exp\left(\frac{(\Delta H-h)^2}{2\sigma_{z,wake}^2}\right) + \exp\left(\frac{(\Delta H+h)^2}{2\sigma_{z,wake}^2}\right)} \tag{4.5}$$

Dilution is inversely proportional to concentration, so the average minimum dilution is

$$D_{min} = \frac{2D_{emit}\,D_{adj}}{D_{emit} + D_{adj}} \tag{4.6}$$

The model assumes constant dilution with height z', using the dilution from Equation (4.6) as the dilution over the entire wall. This is similar to the model used in EPA (1995b) for SCREEN3 assumes that the building recirculation cavity fills up uniformly with some concentration.

COMPARISON OF DILUTION DATA AND THEORETICAL MODEL

Dilution measurements for an emitting building of reference height H downstream of a $2H$ high building with a gap H wide between the buildings are shown in Figure 4.6. The plume was emitted from a short stack $h_s=0.175H$ at location 1 at six values of stack exhaust velocity to windspeed ratio M. The dilution decreases slightly with height for all values of M, but mixing in the recirculation cavity and the gap between the buildings produces a concentration profile that is more spatially uniform than would be seen in a gaussian plume. The slightly higher dilutions near ground indicate that the plume is not able to mix as easily down into the gap between buildings.

The solid lines in Figure 4.6 show predictions from the theoretical model for all 6 values of stack exhaust velocity to windspeed ratio M. The theoretical model assumes a constant concentration over the wall and makes no attempt to model the complicated mixing in the building recirculation cavity and gap between buildings. The data in Figure 4.6 shows increased dilution near the ground indicating that in fact the plume was not able to mix thoroughly down to roof level in the gap. This leads to a moderate underprediction of the dilution and overprediction of concentration near the ground.

The theoretical model also assumes that the entire exhaust is trapped and thoroughly mixed in the recirculation cavity. For low values of stack exhaust to windspeed ratio M, the predictions are close to the measured values and indicates that the plume is mixed thoroughly within the building recirculation cavity. For higher values of M the model underpredicts the dilutions indicating that these plumes had enough momentum for some of the exhaust to escape the building recirculation cavity without being trapped.

Effect of Stack Height

Figure 4.7 shows dilution data for an emitting building of reference height H downstream of a 2H high building with a gap H wide between the buildings. This is the same situation as Figure 4.6 except that a taller stack was used in Figure 4.7. The data shows the same effects as for the shorter stack with increasing dilution near ground level. Significantly higher dilutions are observed than predicted by the theoretical model for high values of exhaust velocity to windspeed ratio M. There is a small increase in dilution with the increase in stack height but this is not significant compared to the variation in dilution with M. The nominal values of the exhaust velocity to windspeed ratio M that are listed in Figure 4.7 are calculated using the windspeed in the approaching flow U_H. In reality, the windspeeds in the cavity behind the building will be significantly slower than in the approaching flow, leading to an increase in the effective value of M with increased plume rise and dilution.

Effect of Gap

Figure 4.8 shows dilution data for an emitting building of reference height H downstream of a $2H$ high building with a no gap between the buildings. The plume was emitted from a short stack $h_s=0.175H$ at location 1. This is the same situation as Figure 4.6 except that the gap between the buildings was removed. The dilution exhibited quite a large variation with height that was not seen when there was a gap present. Dilution increases significantly with height above the emitting building roof. The stack position was near the upwind edge of the building recirculation cavity where the actual flow speed will be much less than the undisturbed reference height windspeed U_H. This allowed the plume to jet up to the top of the cavity where it can become trapped near the edge of the adjacent building producing lower dilutions near the adjacent roof height. The current theoretical model is incapable of handling this, and instead assumes a constant dilution with height that still produces quite good predictions near the

emitting building roof but over predicts the dilution near the roof of the adjacent building.

Effect of Stack Location

Figure 4.9 shows the same situation as Figure 4.8 except the plume in now emitted stack 2 instead of stack 1. The dilution in this case does not show the drastic decrease with height as seen for the plume emitted from stack 1 and instead shows relatively uniform concentration with height. Stack 2 near the downwind edge of the wake recirculation cavity appears to allow the plume to mix more uniformly inside the cavity. In this case, the assumption of constant concentration with roof height is reasonable. The theoretical model correctly predicts increasing dilution with increasing M but fails to produce the proper range of dilution values.

Effect of Building Height

All previous cases have been for a adjacent building of height $2.0H$. Figure 4.10 shows data from a $1.5H$ upwind building with no gap between the buildings. Dilution has decreased with height above the roof, as was the case with a $2H$ tall adjacent building, but the effect was not as strong for the $1.5H$ adjacent building. The variation of measured dilution with M covers a larger range than the case of a $2H$ tall upwind building and this is indeed predicted by the theoretical model. However the model is only able to predict the correct effect of building height and does not predict the actual range correctly. The predictions are close for lower values of M but still underpredict the dilution for high values of M.

Figure 4.11 shows data for the stack at location 2 instead of location 1 for a $1.5H$ adjacent building with no gap between the buildings. The building recirculation cavity for a $1.5H$ tall adjacent building will be smaller than for a $2H$ building. The stack location in this case was near the downwind edge of the building recirculation cavity,

most of the stack exhaust would have escaped trapping, especially for high values of M.
As a result, the measured dilutions shown in Figure 4.11 were much larger than the
predictions of the model that assumes that 100% of the exhaust is trapped in the building
recirculation cavity. For plumes that are only partial trapped, the model underpredicts the
dilution by a factor of 10. The performance of the theoretical model is poor considering
the roof level model was able to predict dilutions within a factor of 2, although the fact
the model is always underpredicting dilution allows it to be used as a conservative
estimate in the absence of better information.

CONCLUSIONS

Using the average of the concentration at emitting and adjacent roof heights as the
concentration on the back wall of an adjacent building upstream of a lower emitting
building produces estimates that shows the correct relative effects of changing stack
height h_s, exhaust velocity to windspeed ratio M, and adjacent building height but with
significant underpredictions of the dilutions. The theoretical model should only be used
as an approximation as it in not able to fully simulate the complicated dispersion effects
caused by the building recirculation cavity. This is consistent with Chapter 15 of the
1997 ASHRAE handbook that recommends using gaussian dispersion theoretical model
only to obtain relative effects of changing different parameters.

REFERENCES

ASHRAE. (1997) "Air flow around buildings", Chapter 15 in 1997 ASHRAE Handbook
of Fundamentals. American Society of Heating, Refrigerating and Air-Conditioning
Engineers, Atlanta, Georgia.

EPA (1995b) "SCREEN3 model user's guide" U.S. Environmental Protection Agency,
Research Triangle Park, North Carolina, document EPA-454/B-95-004.
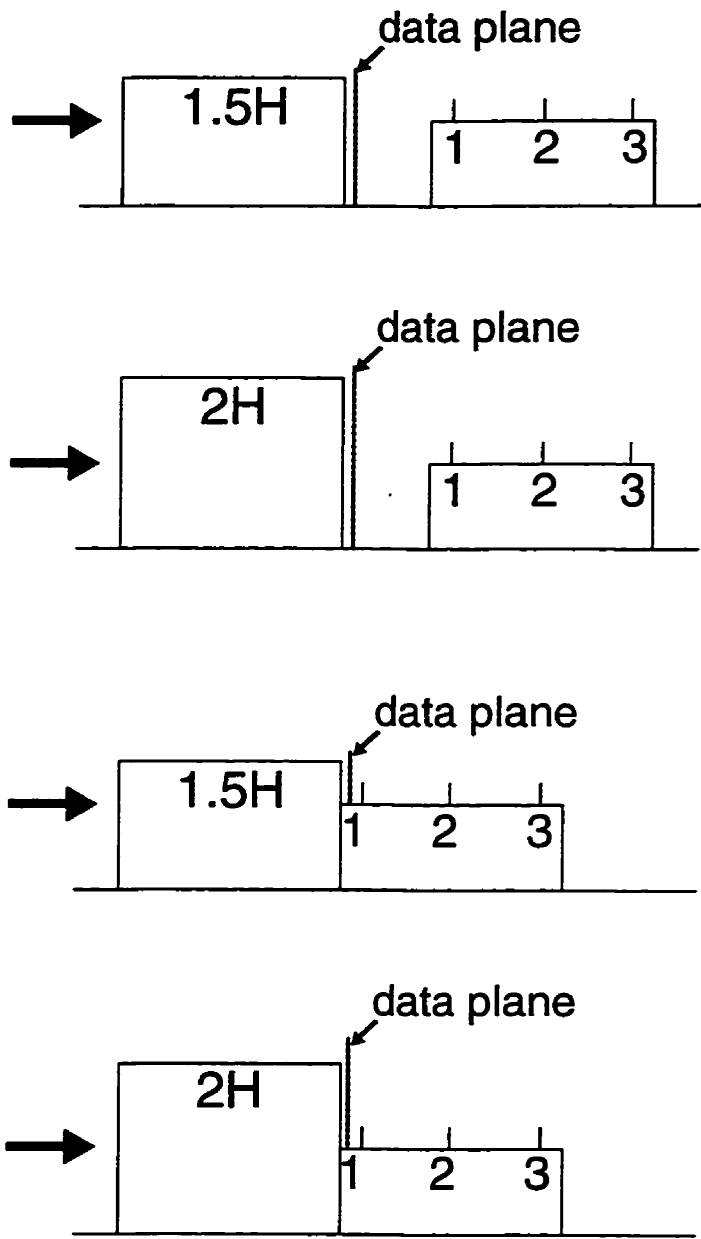
Figure 4.1   Building configurations used to investigate dilutions on downwind wall of a building with a lower downwind emitting building.

Figure 4.2   Schematic of water channel facility used to simulate atmospheric flow
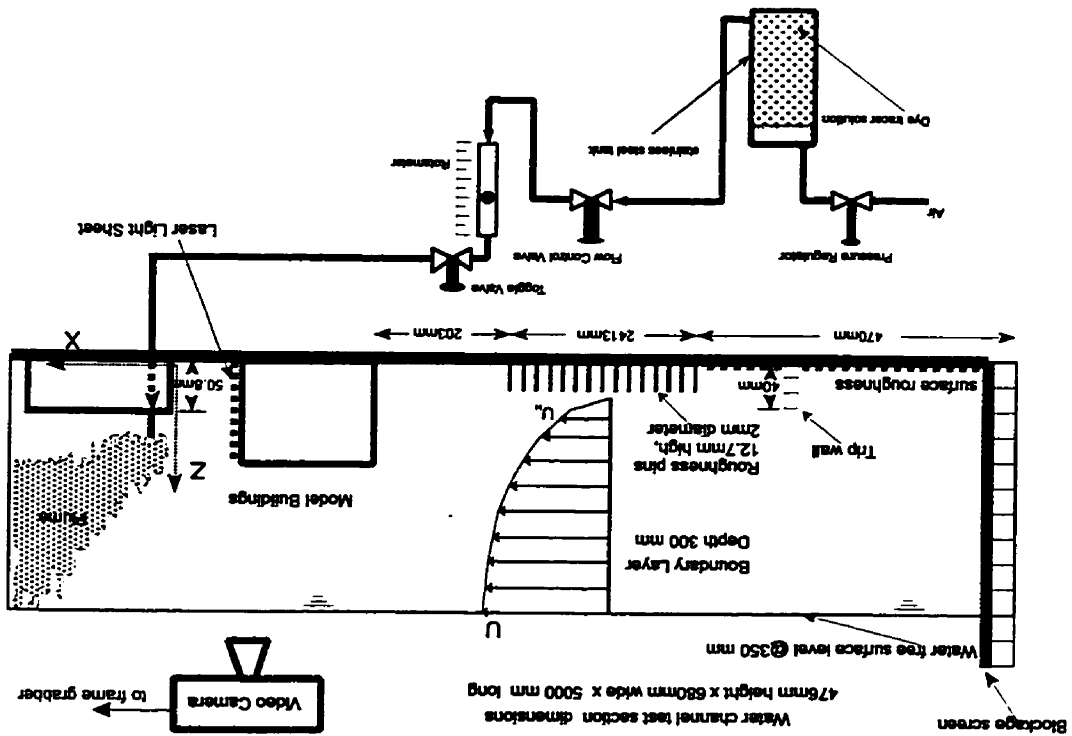
Actual Plume
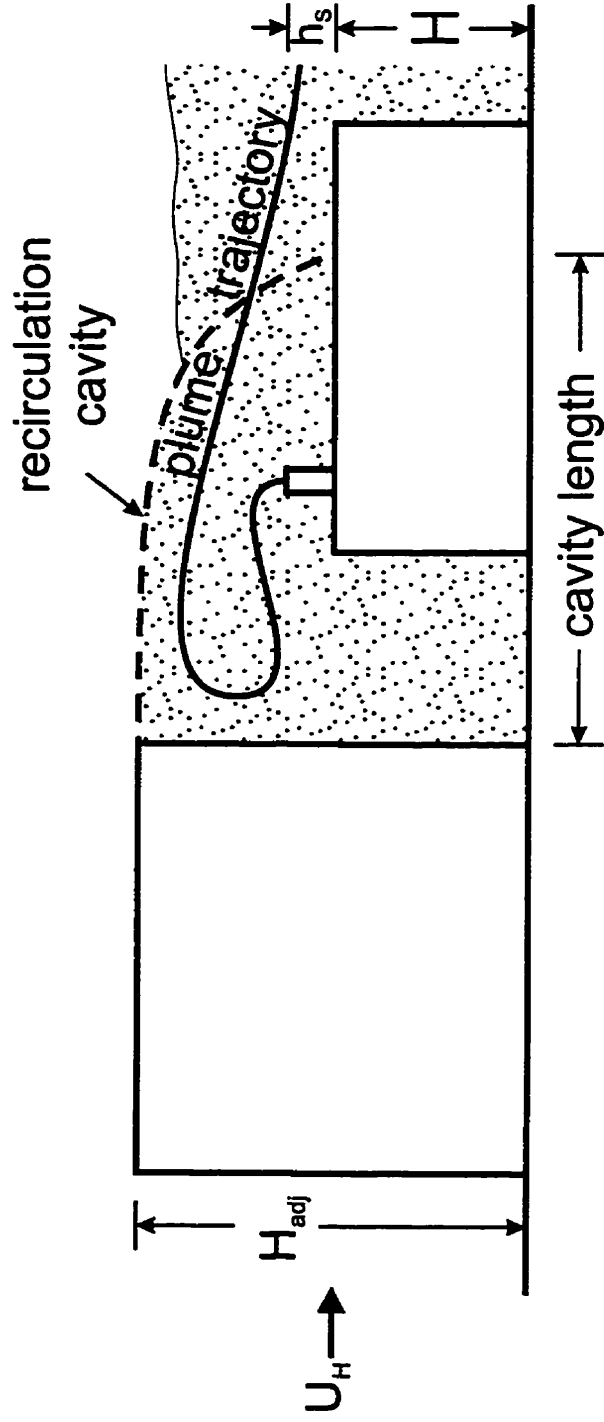
Figure 4.3   Actual plume behavior for a downwind emitting building when trapped in wake of a higher upwind adjacent building.

Wind

camera view of
building wall
in mirror

internal
45° mirror

glass roof
and wall

light sheet
aligned with
building wall
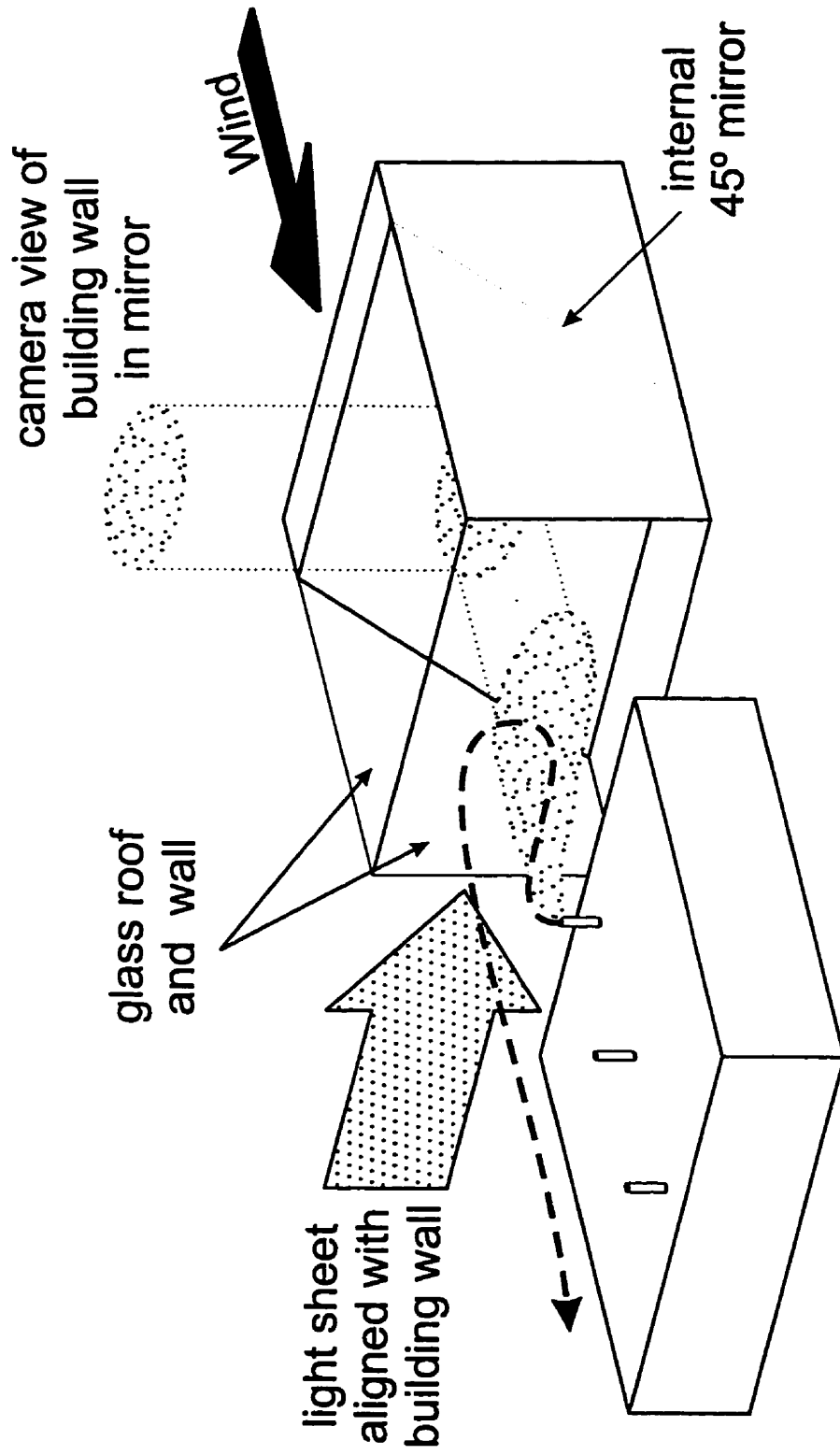
Figure 4.4   Schematic of method used to measure concentrations on the wall of the upwind
building.
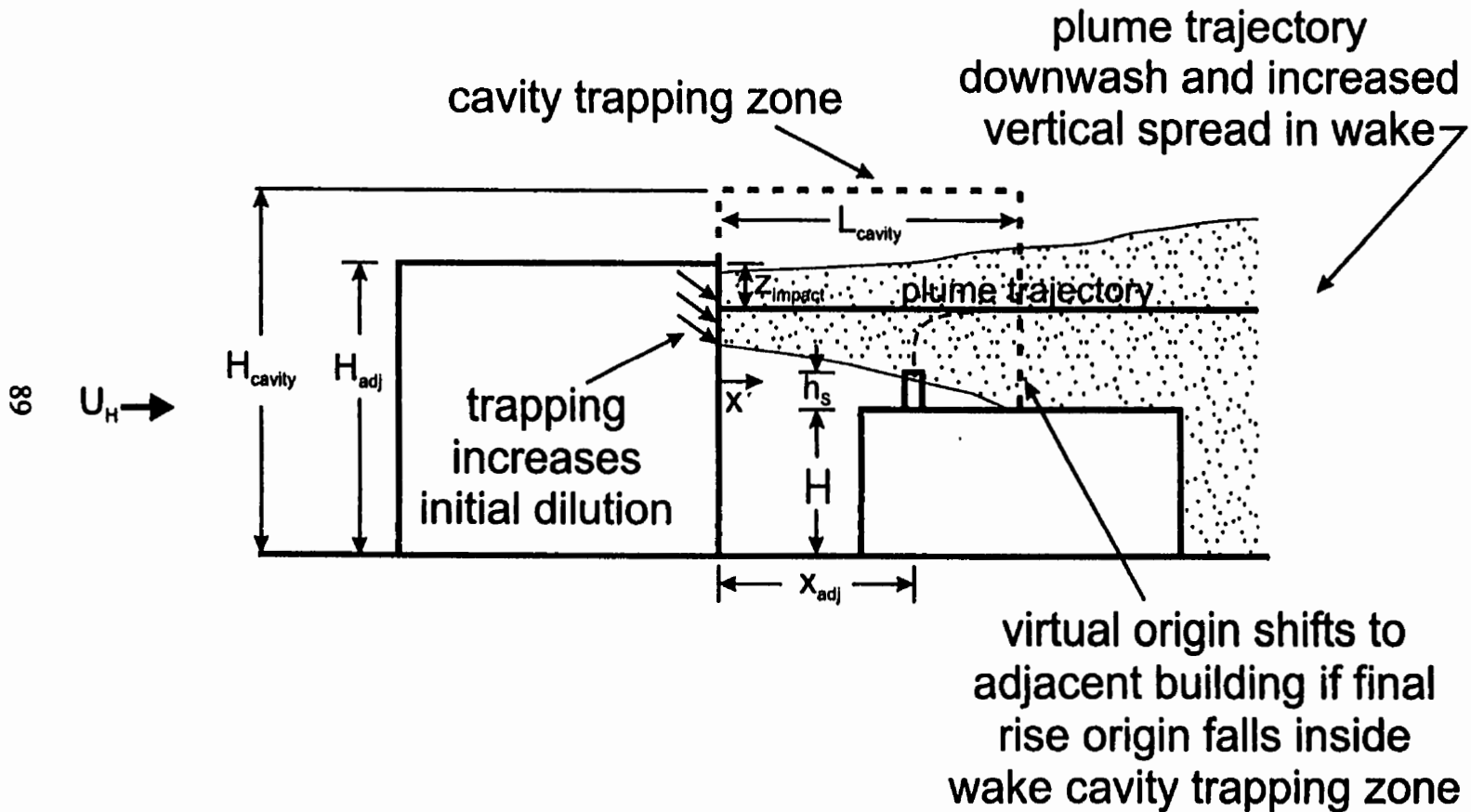
Figure 4.5 Proposed model to estimate dilutions on the downwind wall of the taller upwind building.
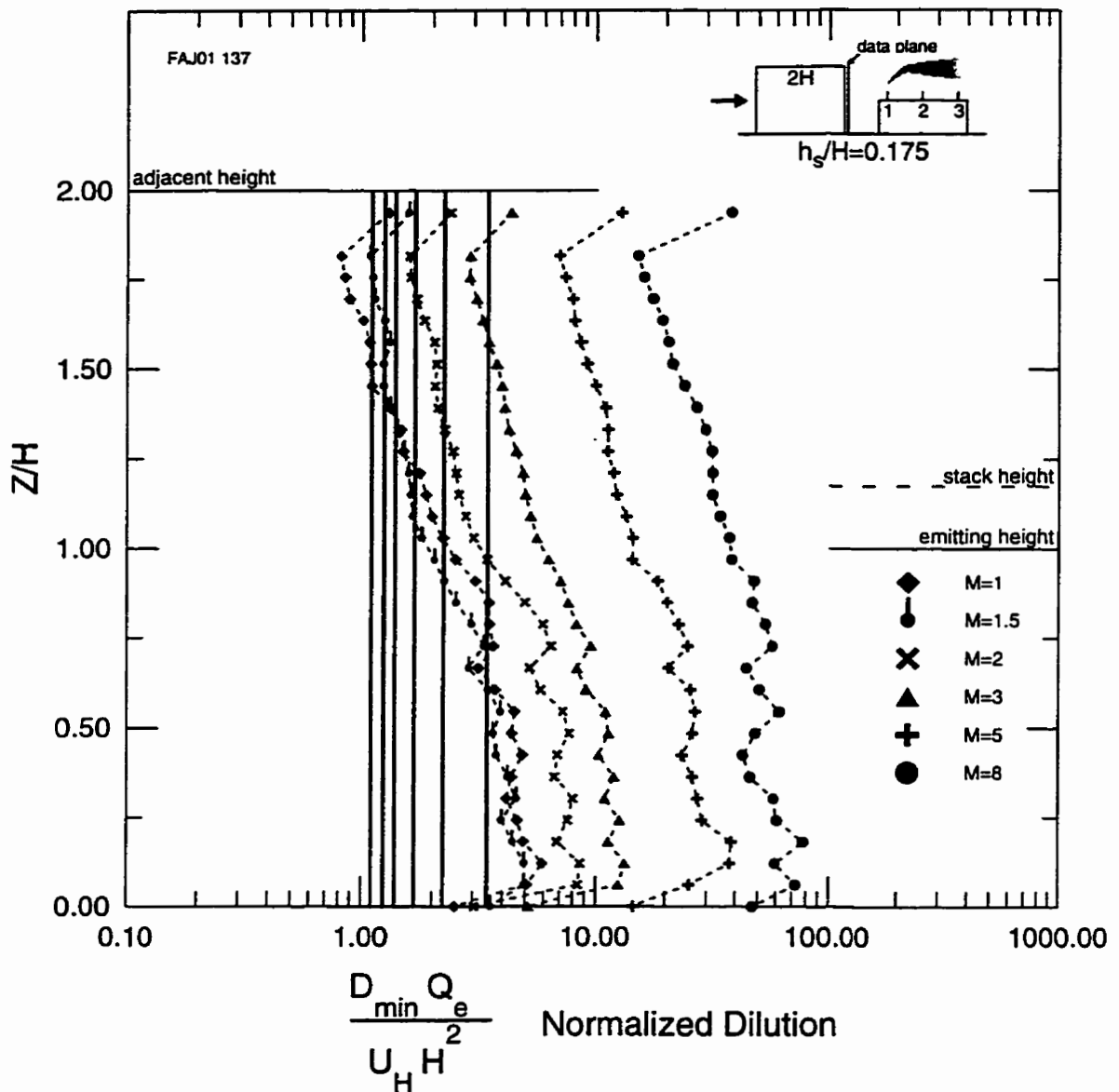
Figure 4.6   Normalized dilutions on the downwind wall of $2H$ high building with the emitting building downstream. The building were separated by a gap $1.0H$ wide. Stack height was $h_s=0.175H$ at location 1 (upwind stack) with six different values of exhaust velocity to windspeed ratio M. The ratio M increases from left to right on the set of theoretical lines.

90
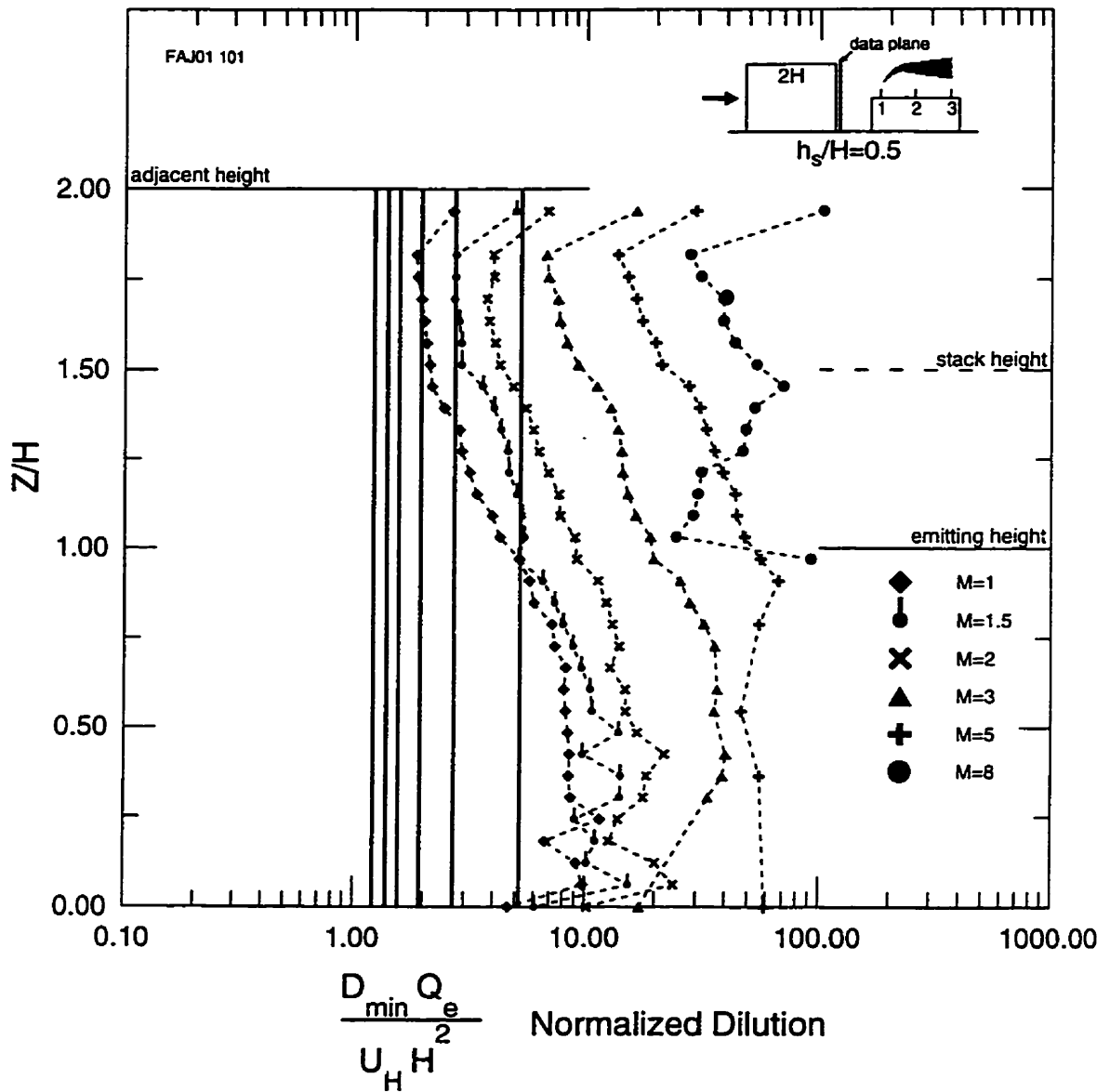
Figure 4.7   Normalized dilutions on the downwind wall of $2H$ high building with
the emitting building downstream. The building were separated by a
gap $1.0H$ wide. Stack height was $h_s=0.5H$ at location 1 (upwind stack)
with six different values of exhaust velocity to windspeed ratio M. The
ratio M increases from left to right on the set of theoretical lines.

91
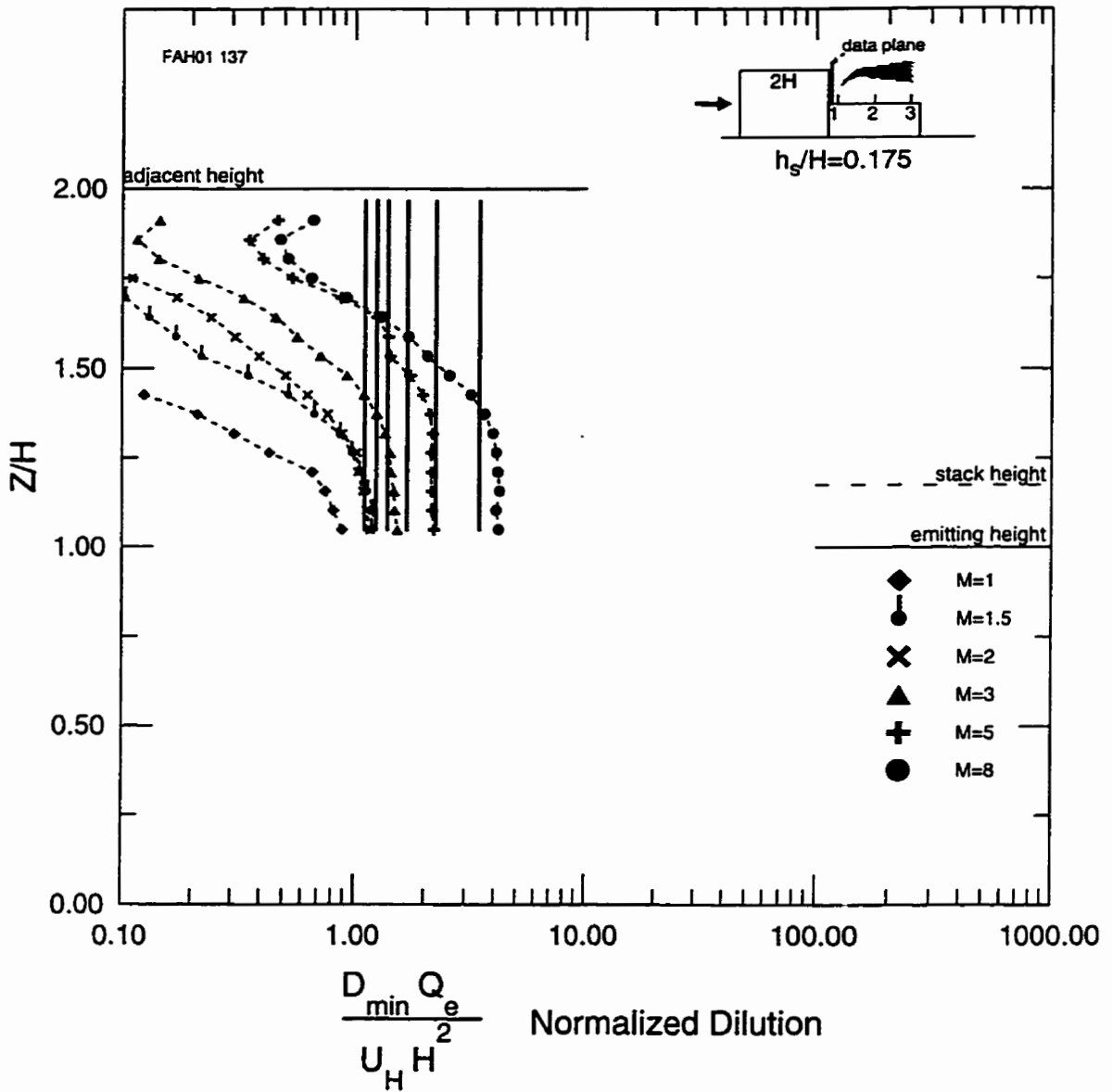
Figure 4.8   Normalized dilutions on the downwind wall of $2H$ high building with the emitting building downstream. There was no gap between the buildings. Stack height was h_s=0.175H at location 1 (upwind stack) with six different values of exhaust velocity to windspeed ratio M. The ratio M increases from left to right on the set of theoretical lines.
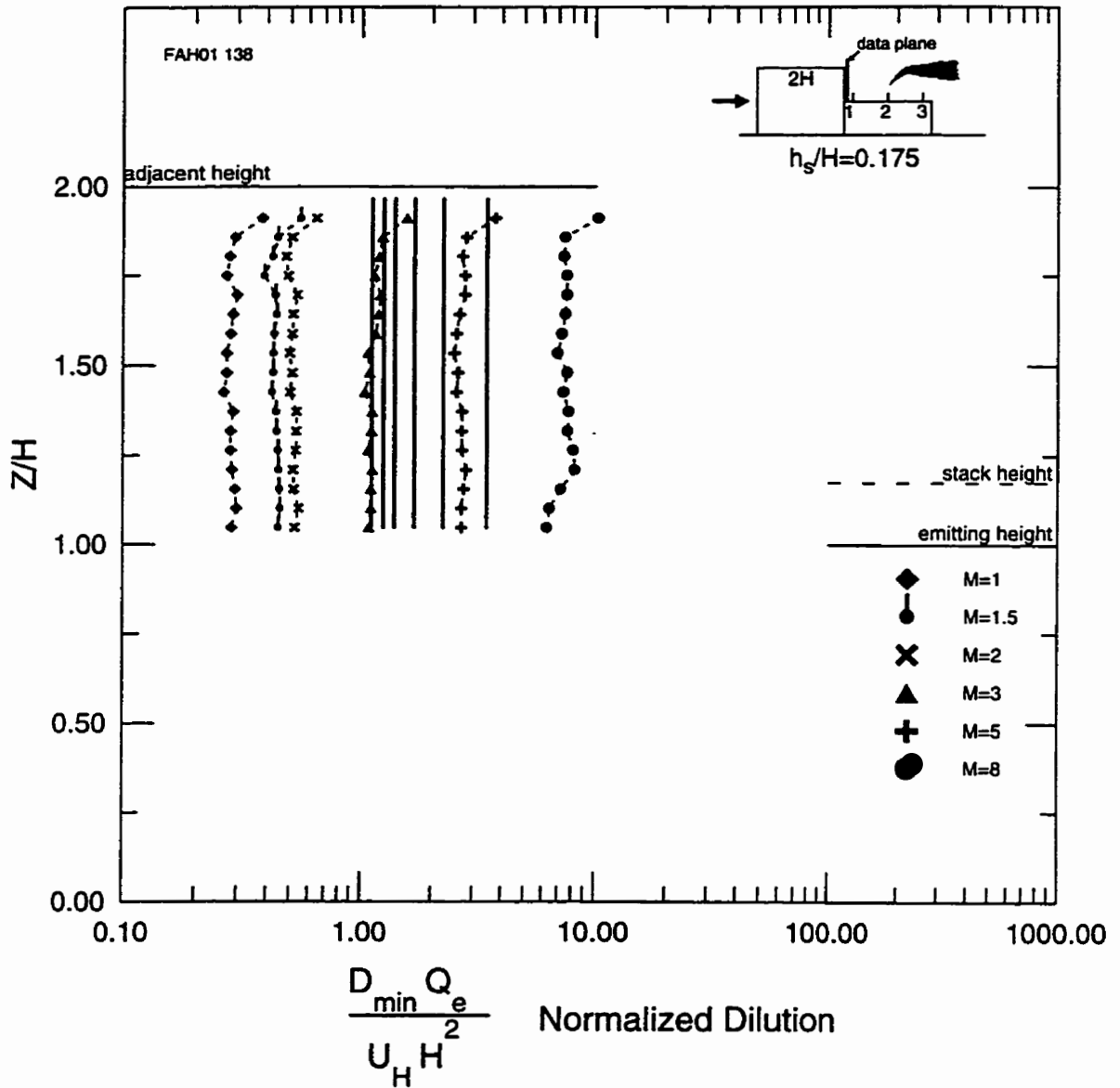
Figure 4.9   Normalized dilutions on the downwind wall of 2*H* high building with the emitting building downstream. There was no gap between the buildings. Stack height was h_s=0.175*H* at location 2 (central stack) with six different values of exhaust velocity to windspeed ratio *M*. The ratio *M* increases from left to right on the set of theoretical lines.

93
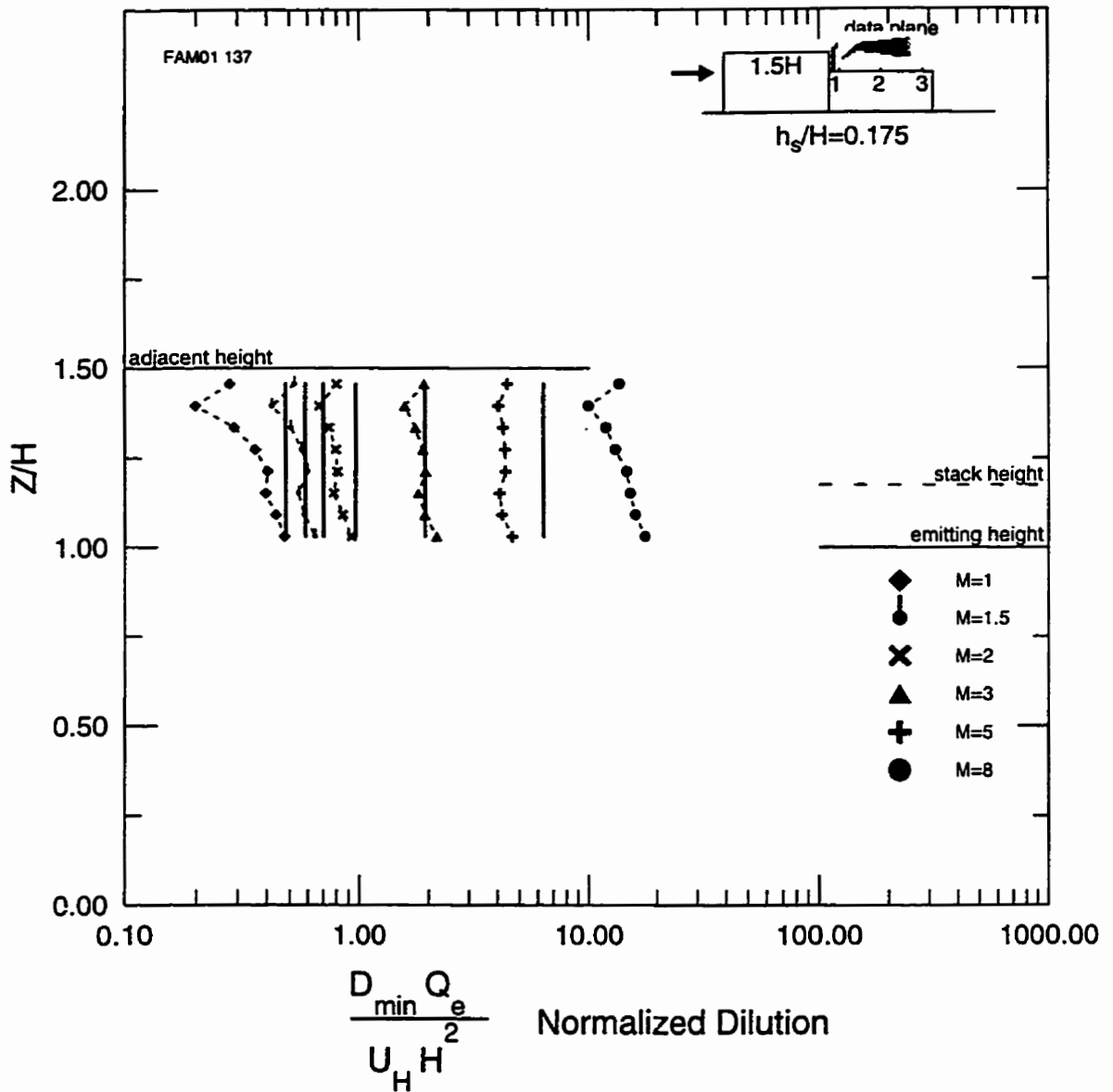
Figure 4.10   Normalized dilutions on the downwind wall of $1.5H$ high building with the emitting building downstream. There was no gap between the buildings. Stack height $h_s=0.175H$ at location 1 (upwind stack) with six different values of exhaust velocity to windspeed ratio M. The ratio M increases from left to right on the set of theoretical lines.

94
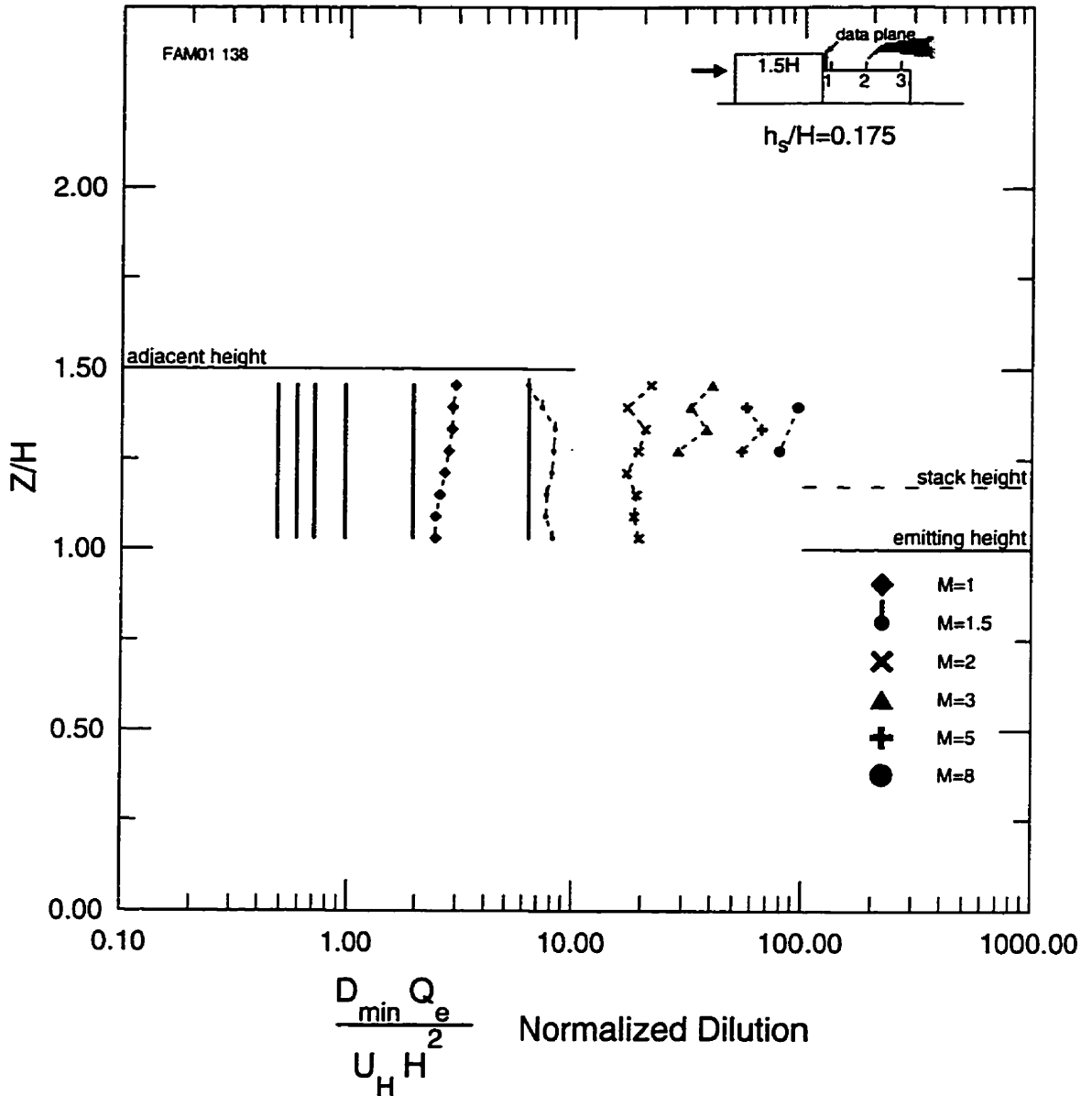
Figure 4.11   Normalized dilutions on the downwind wall of 1.5H high building with the emitting building downstream. There was no gap between the buildings. Stack height h_s=0.175H at location 2 (central stack) with six different values of exhaust velocity to windspeed ratio M. The ratio M increases from left to right on the set of theoretical lines.

CHAPTER 5
SUMMARY AND CONCLUSIONS

Three papers have been presented that address plume dispersion around closely-spaced adjacent buildings. Scale model simulations of plume dispersion using a flourescent dye tracer technique provided data for analysis and comparison with dispersion theory. The first paper considered two cases: plumes from stacks on flat roofed buildings and plumes from isolated stacks. The second paper considered dilutions on the roof of a building with exhaust stacks when a taller adjacent building is located upwind. The third paper considered dilutions on the wall of the taller upwind building with exhaust emitted from the downwind building. A gaussian dispersion model was developed to predict the measured dilutions in each of the three cases.

GAUSSIAN PLUME MODEL FOR ISOLATED STACKS AND STACKS ON FLAT ROOFED BUILDINGS

In the first paper, presented in Chapter 2, a final-rise gaussian plume model was developed for predicting plume dispersion for several building situations. These situations were: plumes emitted over long, flat roofed buildings; plumes emitted from a stack at ground level with no buildings present; plumes from an emitting building with an adjacent building of the same height downstream; and plumes from an emitting building with an adjacent building of the same height upstream.

The following conclusions were reached:

- A gaussian model with the plume at final rise height everywhere with a limit on the amount of dilution produced by plume height was suitable for predicting dilutions for all building situations investigated, and was shown to be more accurate and robust than a transitional gaussian plume model with

distance-dependent rise.

- For plumes emitted near the leading edge of building roof, stack exhaust is trapped in a front edge recirculation cavity requiring the plume to be modeled by locating its virtual origin at the upwind edge of the building, and adding some extra initial spread.

- Measurements of crosswind plume spread validated the linear plume spread with distance model, with the same spreading rate for a stack near ground level, a stack on the reference building and the step-across (same roof level) roof buildings with a gap between them.

The gaussian plume model developed in Chapter 2 to predict dilutions for the simple cases of dispersion from isolated stacks and stacks on flat roofed buildings serves as a starting point when dealing with more complicated building configurations in subsequent chapters.

ROOF LEVEL DILUTIONS WITH A LOWER EMITTING BUILDING DOWNWIND

The flow patterns in and around the building near-wake are quite complex, and significant simplifications were required to produce a stack design model for estimating dilution on the buildings. A dispersion model was developed in Chapter 3 for cases where a plume is emitted from a stack on a building downwind of a taller adjacent building upwind.

The measurements showed that:

- The amount of exhaust gas trapped in the recirculation cavity behind the

97

upstream building depends on stack location, stack height, stack exhaust momentum ratio, and the relative height difference and crosswind width of the buildings.

- For plumes whose height falls within an empirically-determined wake cavity trapping zone , part of the plume is carried upstream from the stack back toward the downwind wall of the adjacent building and is mixed in the recirculation cavity before finally escaping downstream. The plume dispersion can be simulated by shifting the virtual origin of the plume to the back wall of the upwind building to produce recirculation cavity concentrations upwind of the stack.

- The dispersion model should also include extra initial dilution, added vertical spread and a decrease in plume height caused by building downwash.

- Plumes that are not trapped in the wake should be given some extra initial dilution, added vertical spread and building downwash, with no shift in the virtual origin, because no concentration should appear upwind of the stack.

- The dispersion model gives estimates within a factor of two for the measured dilution when the plume is fully trapped in the flow recirculation cavity or fully escapes. The proposed model assumes all plume material is trapped in the near-wake recirculation cavity. When the plume is near the downwind edge of the cavity, with some concentration trapped and some escaping, the proposed model underpredicts dilution (overpredicts concentration) and so is conservative for stack design.

WALL DILUTIONS WITH LOWER EMITTING BUILDING DOWNWIND

Chapter 3 proposed a theoretical model to predict dilutions on the roof of an emitting building when there is a taller upwind adjacent building. The gaussian model used taller adjacent upwind building in Chapter 3 was extended in Chapter 4 to predict dilutions on the wall of the adjacent building. To adapt the roof level model to the wall, the average of the concentration at emitting and adjacent roof levels predicted by the gaussian model was used to approximate the concentration that existed at all heights on the downwind wall of the adjacent building. This simple approach was shown to produce the correct relative effects of changing stack height, exhaust velocity to windspeed ratio and adjacent building height, but produced only a rough estimate of actual exhaust to receptor dilution factors that existed on the wall when a high stack or high exhaust velocity allowed part of the plume to escape the flow recirculation cavity.

DIRECTIONS FOR FUTURE RESEARCH

There are several ways future research could be directed in order to extend the understanding of flow around buildings. Some of the more important areas left unaddressed in the current study are:

- The current study only dealt with wind directions normal to a building wall. Future research could consider flow at other angles to the buildings as it is expected that flow at angles other the $90°$ will produce roof edge vortices that can affect the flow.

- The buildings investigated in the current study had width greater than height, forcing most of the exhaust plume over the roofs of the buildings. If the adjacent building was a high-rise had greater height than width, the majority of the plume would pass around the sides creating different flow patterns than

in the current study. The next logical step would be reverse the aspect ratio and measure dilution over high-rise buildings with height 2.5 times the width and 5.0 times the width to the determine if theoretical model from the current study is applicable to buildings with height greater than width.

- The maximum spacing between buildings in the current study was one emitting building height. In order to determine how far downstream upwind buildings affect the flow, tests are needed with greater spacings between the buildings.

- All buildings in the current study were simple rectangular blocks. Tests of more complicated building shapes are needed to determine the sensitivity of dilution patterns to changes in building configuration.

- Tests should be made with buoyant plumes with the exhaust is at a lower density than the air to observe how the additional plume rise from buoyancy affects dilutions. In the current study, the density of the exhaust and ambient fluid were always the same. The ratio of stack exhaust velocity to windspeed used in the laboratory produced results that were applicable to and combination of exhaust velocity and windspeed that produced the same ratio. For buoyant plumes each combination of windspeed, exhaust velocity and fluid densities would correspond to only one full scale condition and a more extensive series of tests would be required.

- The theoretical model developed in Chapter 3 used for predicating roof level dilutions on an emitting building with a taller upwind adjacent building underpredicts dilutions when applied to the wall on the upwind building as shown in Chapter 4. This failure is likely due to the fact that the theoretical model assumes that the plume is either completely trapped or completely

escapes the building recirculation zone. Improvements to the model should be made to account for the fraction of the plume that escapes the building recirculation cavity and is not present on the downwind wall of the adjacent building.

APPENDIX A
BUILDING CONFIGURATIONS

Except for the reference building case, all configurations in the current study involve two neighboring buildings. The building with three exhaust stacks is referred to as the emitting building and the other building as the adjacent building. These configurations are categorized according to whether the emitting building is upstream or downstream of the adjacent building and according to the relative heights of the two buildings. Step-down refers to cases where the downstream building roof height is lower then the upstream building, step-up refers to cases where the downstream building roof height is higher than the upstream building, and step-across refers to cases where there is no change in roof height between the two buildings. This leads to the six different groups of building configurations. For each combination of emitting building upstream or emitting building downstream, and step-up, step-down, or step across, there were two possible spacings between the buildings: no spacing, or a gap of $1.0H$.

The reference building is a building with a long flat roof with three stacks located toward the upwind end of the roof. The reference building serves as a standard of comparison for the other building configurations. The reference building height H was chosen as a convenient length scale, and other dimensions are referred to in terms of the reference height H. In the present study the reference building $H=2$" (50.8mm) equal to about 40' in the full scale for a scale ratio of 240:1.

All emitting buildings were of height H, the same as the reference building. There were four different heights of adjacent building: $0.5H$, $1.0H$, $1.5H$, and $2.0H$. All emitting and adjacent buildings had a length (in the flow direction) of $2.5H$ except for the reference building that had a length of $12.5H$. Other than the reference building, each of the building configurations shown in Figure A.1 were tested in single-width and double-width combinations. For single width combinations the width (in the crosswind

102

direction) of 2.5*H*, equal to the building width. For double-width combinations, the width of the buildings was equal to 5.0*H* or twice the building length. In total this leads to 33 different building configurations for roof level measurements, although not all configurations are discussed in this thesis.

The building configurations addressed in Chapter 2 are shown in Figure A.1. All these configurations involve no change in roof height. Chapter 2 also addresses the case of a plume emitted from an isolated stack with no buildings present. Figure A.2 shows the building configurations dicussed by Chapter3. All these configurations involve an emitting building downstream of a taller adjacent building.

In addition to roof level dilution measurements, wall dilutions were investigated for several scenarios. Concentrations were measured on the downwind wall of an adjacent building when the emitting building when the emitting building was downstream, of the upwind wall of the adjacent building was upstream. These are the walls of the adjacent building upon which the largest concentrations would be seen. Building configurations shown in Figure A.3 for wall concentrations have the same dimensions as the corresponding configurations in Figure A.1 for roof level measurements with emitting buildings 1.0*H* and adjacent buildings 1.0*H*, 1.5*H*, 2.0*H* high. Chapter 4 of this thesis discusses dilutions on the wall of a taller upwind building. The building configurations used in this chapter are shown in Figure A.3

For each of the building geometries discussed above, there were three different possible stack location, three different stack heights and six values of exhaust velocity to windspeed ratio *M*. The three stacks were located along the centerline of the emitting building, at distances of 0.25*H*, 1.25*H*, and 2.25*H*, from the upstream edge of the emitting building. Each stack was constructed as a force fit allowing for easy height adjustment. The three stack heights used in the experiment were 0.175*H*, 0.25*H*, and 0.5*H*. The stack height of 0.175*H* corresponds to a height of 7' in the full scale, that is the

height many stacks are built to meet the minimum requirement of the fire code. The six different values of exhaust velocity to windspeed ratio M were 1, 1.5, 2, 3, 5, and 8. In total this led to 54 different combinations of stack height, stack location, and stack exhaust velocity to windspeed ratio M for each building geometry.
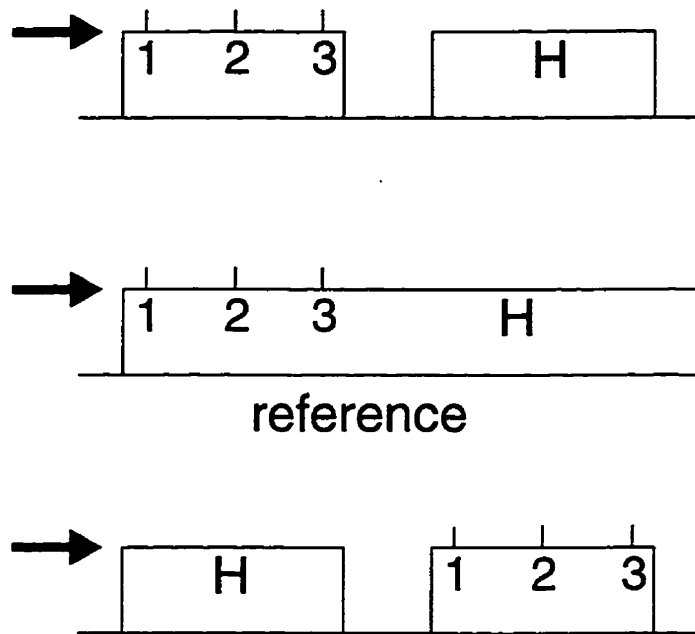
Figure A.1   Building configurations used to measure dilutions with same roof height
            buildings. These configurations are discussed in Chapter 2.
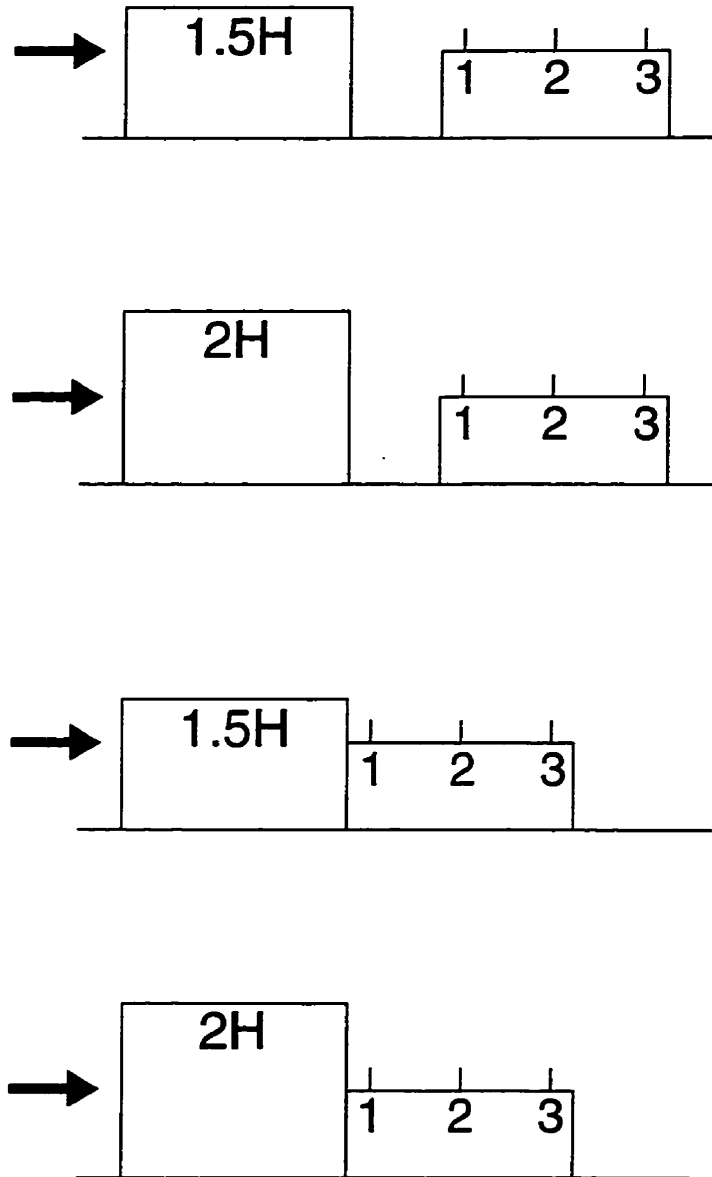
Figure A.2   Building configurations used to measure roof level dilutions in near-wake of a taller upwind building. These configurations are discussed in Chapter 3.

106
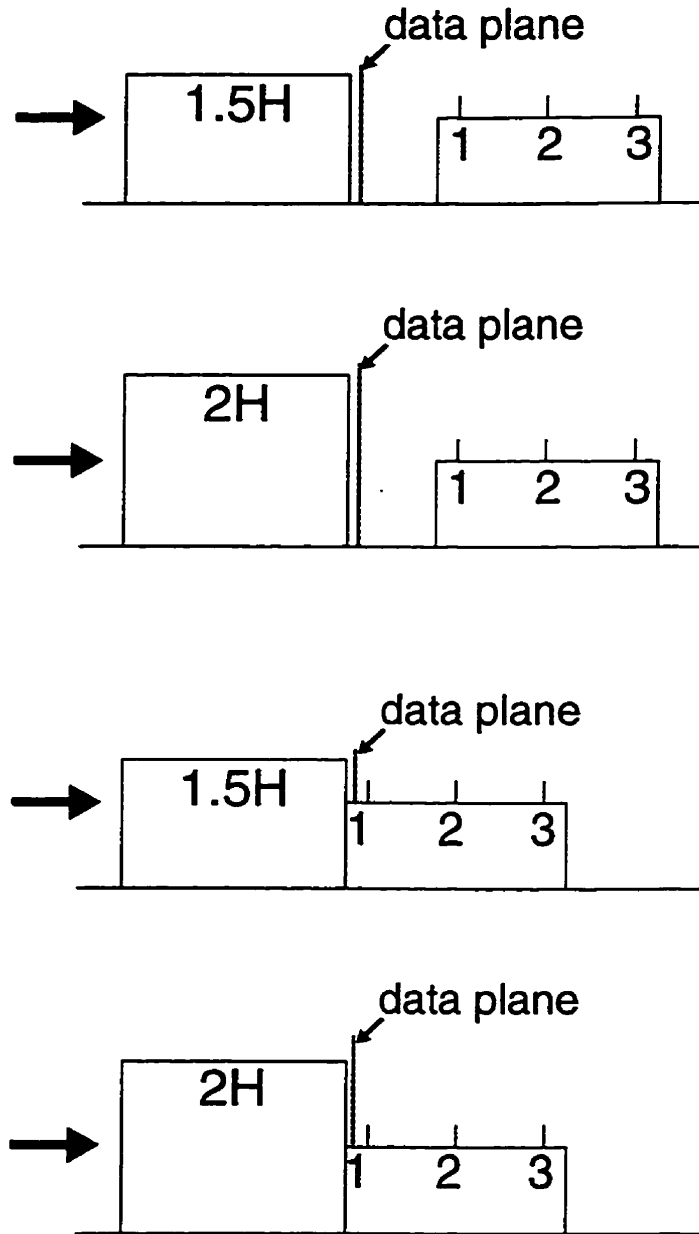
Figure A.3   Building configurations used to measure concentrations on the wall of a
taller upwind building. The dotted line shows the data plane upon
which concentration measurements were made. These configurations
discussed in Chapter 4.

APPENDIX B
MEASUREMENT OF PLUME DISPERSION AROUND MODEL BUILDINGS USING LASER INDUCED FLUORESCENCE

INTRODUCTION

The objective of the present study was to determine the effect of an adjacent building on the dispersion of a plume emitted from a neighboring building. To this end, scale model buildings were constructed to be used in a water channel simulation of the dispersion process. Flourescent tracer dye illuminated by laser light sheets was used to track the dispersion of the plume over the roofs of these buildings.

To record video images, a black and white Hitachi KP-MI CCD camera was placed roughly 1 m above the water surface overlooking the model buildings. Output from this camera was shown to be linear with light intensity (See Appendix F). The camera array was 640 by 480 pixels. Ten frames a second were grabbed from the camera onto computer by a Matrox Pulsar Board that digitized each pixel output to a value from 0 to 1023.

LASER INDUCED FLUORESCENCE

Disodium Fluorescein was used as dye tracer used in the water channel experiments. This flourescent dye was emitted out of the model stacks to simulate the plume. A 4 Watt argon-ion laser was used to illuminate the flourescent dye. When the dye molecules pass through the laser light sheet, the dye fluoresces and the resulting fluorescent light is detected with the video camera.

For measuring concentrations near the roof level of the emitting and adjacent buildings, two laser light sheets were placed 2mm above the roofs of the two buildings.

108

For cases where the emitting and adjacent buildings had different roof heights, one light sheet was placed at each roof level. The laser intensity decreases as one moves away from the center of the beam, so the brightest part of the each beam was placed near the center of the building roof. The edges of the light sheet were masked to prevent the edges from being present over the other light sheet at a different height. For cases where there was no difference in roof heights between the two buildings, the two light sheets were overlapped. This produced better light sheet uniformity.

For measuring concentration on the wall of an adjacent building, model buildings were constructed with internally mounted 45° mirrors. The wall of the adjacent building closest to the emitting building and the portion of the roof above the mirror were constructed of glass. A single laser light sheet was placed 2mm in front of the glass wall. This allows fluorescent light created by tracer dye passing through the laser light sheet to be reflected to the video camera above the water channel.

Dye tracer

Disodium Fluorescein dye was used as a tracer to simulate stack exhaust being dispersed on the adjacent and emitting buildings. The fluorescent dye was stored in a 75L tank connected to a pressure line. Flexible tubing carried the dye mixture from the tank through one of five rotameters to control the flow rate. The dye was then carried from the rotameter through flexible tubing underneath the base plates in the water channel to the stacks. Details of rotameter calibrations and settings can be found in Appendix C.

The fluorescent dye absorbs laser light most effectively at wavelengths around 488nm, and peak emission is around 515nm. This difference in emission and absorption wavelengths, allowed a band pass filter to be placed over the camera lens that passed light near the emission wavelength and blocked light near the absorption or laser wavelength, thus allowing the camera to see only flourescent light from the dye tracer and not see

reflected light from the laser. Noise is reduced by filtering out laser light reflected from micro bubbles in the water and other surfaces.

Temperature and pH Sensitivity

Fluorescein dye has the advantage of being relatively insensitive to temperature. Walker(1987) shows the variation of fluorescent intensity to be 0.3% per degree K. The dye has been shown, however ,to be sensitive to pH changes when the value of pH is below about 7.5. Carrying out a calibration before each set of runs accounts for possible day to day variations in pH level of the water. Values of pH measured in the water were typically around 8.0.

EXPONENTIAL DECAY OF BEAM INTENSITY

If the intensity of a coherent beam of laser light is I_e, the decrease dI_e is its intensity over a distance dy along the beam path is

$$dI_e = -\varepsilon C(y)I_e dy \qquad (B.1)$$

where $C(y)$ is the concentration at point y and ε is the extinction coefficient. Integrating along the path length from 0 to a point y gives

$$I_e = I_o \exp(-\varepsilon \int_o^y C(y)dy) \qquad (B.2)$$

I_o is the intensity of the beam at $y=0$. For the case where the concentration is uniform with y, Equation (B.2) becomes

$$I_e = I_o \exp(-\varepsilon C \Delta y) \qquad (B.3)$$

110

where Δy is the distance traveled by the beam through a region of constant concentration C. The intensity of fluorescent light I_{ij} received at a particular pixel ij in the camera is proportional to the incident intensity I_e at that point given by Equation (B.3), the quantum yield due to fluorescence φ, the extinction coefficient ε, the distance along the volume of space covered by the laser light sheet that is detected by pixel ij and the fraction F of the available light from this volume that is actually captured by pixel ij, and the concentration $C(y)$ at position y, so that

$$I_{ij} = I_e F \varphi L C(y) \tag{B.4}$$

The quantum yield due to fluorescence φ is the fraction of laser light captured by the dye molecules that actually results in the emission of fluorescent light, see Guilbault (1973).

For the fluorescein dye tracer used in the present study, the value of the attenuation coefficient ε was determined experimentally. The decay in fluorescent light intensity as a laser light sheet passed through a region of constant dye concentration in a tank was measured. An exponential function was fit to the decaying light intensity to determine the attenuation coefficient ε. The value of the attenuation coefficient was found to be dependent on concentration. The variation of the attenuation coefficient ε could be described by the equation

$$\varepsilon = \frac{1}{520 \, C^{0.3} + 734 \, C^{0.15} + 297} \tag{B.5}$$

where concentration C is in mg/L and the attenuation coefficient ε is in $[\text{mg/L}]^{-1}[\text{mm}]^{-1}$. Equation B.5 was used over a range of concentrations from 0.1mg/L to 10mg/L. For the concentration C_{cal}=0.04mg/L used to calibrate the system, this gives a value of $\varepsilon = 0.024$ $[\text{mg/L}]^{-1}[\text{mm}]^{-1}$. In determining the attenuation coefficient ε, no correction was made for the fact the beam sheet was diverging at an angle of $10°$. Equation B.5 thus accounts for

111

the decrease in laser light intensity due to attenuation and beam divergence.

ATTENUATION IN CALIBRATION BOX

The video imaging system was calibrated by placing a box constructed of glass and polycarbonate with an open top and bottom into the water channel and filling it with a known concentration of fluorescein dye. Figure B.1 shows a schematic of the arrangement of the calibration box. Before placing any dye in the box, 100 frames are taken to get a background image. Images were then taken at concentrations of 0.01mg/L and 0.04mg/L. At these concentrations the attenuation is non-negligible over the path length of the beam through the box.

For each pixel in the camera a gain is calculated that is know concentration C_{cal} divided by the intensity of the fluorescent light detected at that pixel I_{ij} divided by a correction factor for attenuation A_j. The attenuation correction factor A_j accounts for the fact that the intensity of the light beam I_{ij} point ij is has been attenuated by passing through regions of concentration C_{cal}. The intensity I_{ij} is less then the intensity would have been if the light sheet had not been attenuated before arriving at point ij that would be the case when observing actual plumes.

If the intensity at a point ij without attenuation would have been $I_{o,ij}$ then from Equation (B.3) the ratio observed intensity I_{ij} to $I_{o,ij}$ is

$$\frac{I_{ij}}{I_{o,ij}} = A_j = \exp(-\varepsilon C_{cal}\Delta y_j) \qquad (B.6)$$

In Equation (B.6) C_{cal} is the known concentration in the calibration box, and Δy_j is the normal distance from the edge of the calibration box to the point in question (see Figure B.1). The gain G_{ij} factor for each point is then

$$G_{ij} = \frac{C_{cal}}{I_{0,ij}} = \frac{C_{cal}}{I_{ij}/A_j} = \frac{C_{cal}\exp(-\varepsilon C_{cal}\Delta y_j)}{I_{ij}} \qquad (B.7)$$

Attenuation of the flourescent light is negligible as it passed through the water. The flourescent light is at a different wavelength than the laser light and is not absorbed by the dye. Experiments confirmed that this was the case (See Appendix D)

DATA ANALYSIS

For each combination of stack position, stack height and momentum ratio, 1000 frames were taken at 10 frames a second for a 100 second average. Before the run a 100 frame (10 second) background was taken. For each run, the average background image was subtracted from the 1000 frame plume image to get the average intensity above background at each of the 307200 pixels in the frame. The gain factors were then used to calculate the concentration at each point as

$$C_{ij} = G_{ij}I_{ij} \qquad (B.8)$$

From this the dilution D was calculated:

$$D_{ij} = \frac{C_{source}}{C_{ij}} \qquad (B.9)$$

A non dimensional dilution was then calculated

$$\frac{D Q_e}{U_H H^2} \qquad (B.10)$$

where Q_e is the volume flow rate at the source, U_H is the velocity in the approaching flow at emitting roof height H, and H is the height of the emitting building.

Of particular interest is the minimum dilution or maximum centerline

113

concentration along the roof or wall of the building. Concentration at each downstream position x' was found by taking the average at each point of the concentration at that point and two points on each side. The highest of these averages was taken as the maximum roof level concentration C_r. This five pixel smoothing was used to eliminate unreasonably high estimates of the concentration due to random variations from point to point. The maximum roof level was then used to find the minimum dilution D_{min} and normalized minimum dilution $D_{min} Q_e/U_H H^2$.

CONCLUSIONS

A reliable method for measuring concentrations on a building surface was developed for water channel simulation using a laser induced fluorescence technique. This technique not only provided flow visualization but an quantitative measure of concentrations at a large number of points over the building surface.

REFERENCES

Guilbualt G.G. (1973) "Practical Flouescence" New York, Marcel Deker Inc.

Johnston, C.R. and Wilson, D.J. (1996) "A vortex pair model for plume downwash into stack wakes" Atmospheric Environment 30 (accepted May 7/96) 8 journal pages.

Liu, F. (1996) "Plume dispersion around a building from a ground-level source" Department of Mechanical Engineering, University of Alberta, Edmonton, AB, 147 pages.

Walker, D.A. (1987) "A fluorescence technique for measurement of concentration in mixing liquids" J. Physics E: Scientific Instruments, 20, 86-94
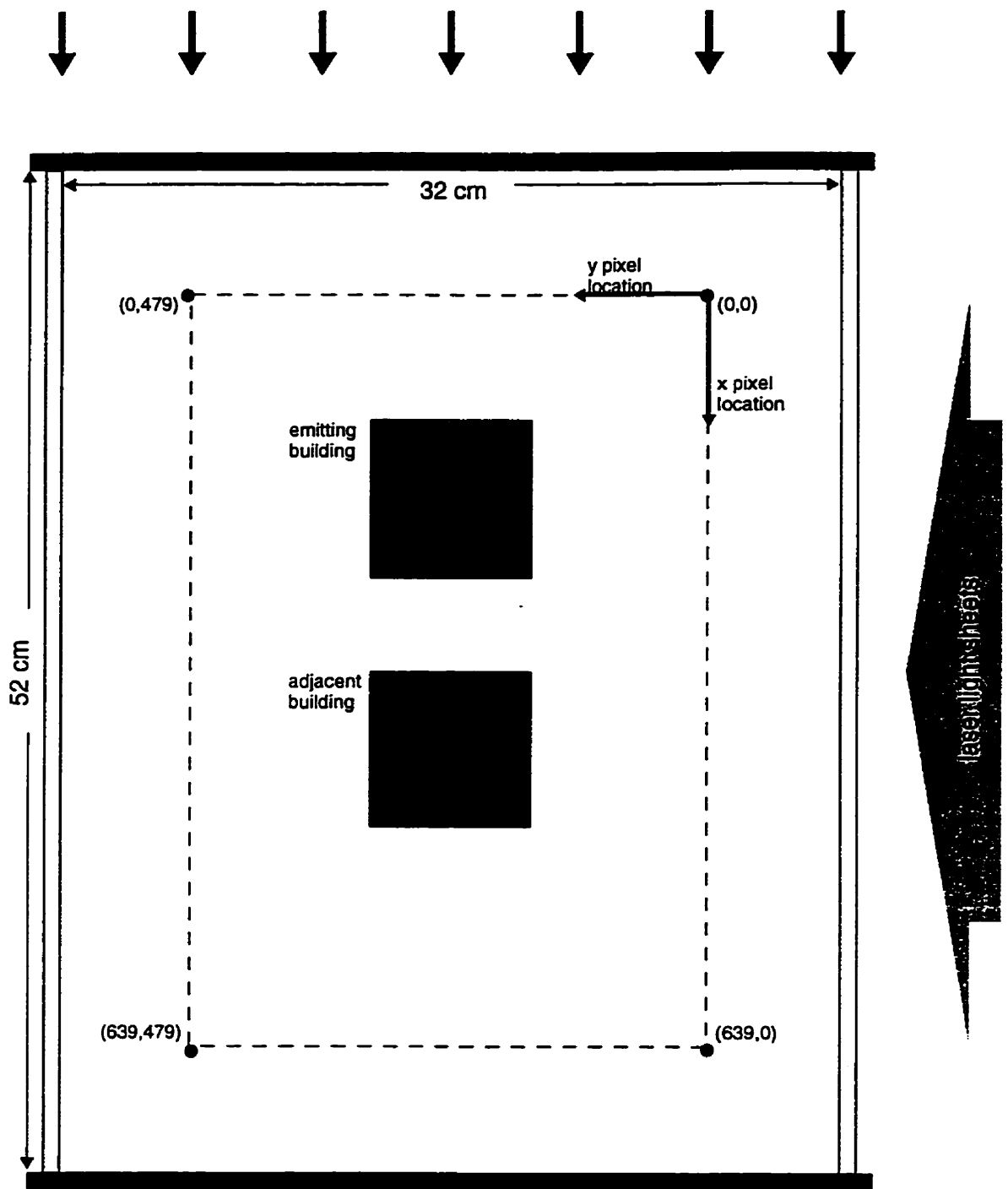
Figure B.1   Top view of calibration box arrangement

APPENDIX C
FLOW RATES AND ROTAMETER CALIBRATION

INTRODUCTION

Stack exhaust flow rates for the water channel building models used in the present study were regulated by a control panel containing 5 rotameters and 9 toggle valves. Each of the 9 toggle valves was in series with a fine adjustment valve. Flow through each of the toggle valves was adjusted before any experiment to the proper flow rate so that during any experiment, the correct flows were available and could be changed by simply opening and closing the toggle valves. This eliminated the need to find the correct setting on the rotameter each time the flow was changed.

EXPERIMENTAL SETUP

Fluorescein tracer dye was stored in a tank with a volume of approximately 75 Litres. Air above the dye mixture in the tank was pressurized by connecting a valve on the top of the tank to a pressure line maintained at around 30 psi. The pressurized air forced the tracer dye out of the tank through an opening at the base to a hose leading to the control panel. The flow passed into a manifold on the front of the control panel that had outlets to 9 toggle valves. Each toggle valve was in series with a fine adjustment valve. Flow proceeded through the toggle valve and fine adjustment valve to one of five rotameters. Some of the rotameters were connected to more than one toggle valve. Outlets from the rotameters led to a second manifold on the back of the control panel. The outlet from the manifold led to a four way valve that allowed selection of one of three possible stacks or a drain line. Flow was carried to the stack through flexible rubber hoses that ran along the inside edge of the water channel and under the base plates at bottom of the water channel. A hole in the base plates underneath the emitting building allowed the three hoses to be connected the stacks in the model emitting building.

116

To calibrate each of the 5 rotameters, a beaker was placed on a weight scale. Flow from the drain line was ejected into the beaker and the time taken to fill the beaker with a particular volume of water was measured. Readings were taken at a number a settings over the range of each rotameter. Figures C.1 toC.5 show plots of the calibration points for each of the five rotameters. A second order polynomial was fitted through the calibration points for each of the rotameters. These polynomial functions were then used to find the required rotameter setting for a given flow rate in subsequent experiments. Listed below are the calibration functions for each rotameter along with the rotameter type for each tube. X_{rot} is the setting on the rotameter setting and Q_{rot} is the rotameter flow rate in mL/second.

Tube 1: Brooks R 6-15 A: $\quad Q_{rot} = 0.9228X_{rot} - 0.2345$ $\hspace{2cm}$ (C.1)

Tube 2: Matheson 603: $\quad Q_{rot} = -6.0 \times 10^{-5} \, X_{rot}^2 + 0.0236 \, X_{rot} - 0.0323$ $\hspace{1cm}$ (C.2)

Tube 3: Matheson 603: $\quad Q_{rot} = -6.0 \times 10^{-5} \, X_{rot}^2 + 0.0237 \, X_{rot} - 0.0224$ $\hspace{1cm}$ (C.3)

Tube 4: Brooks R 2-15 B $\quad Q_{rot} = -0.0021 \, X_{rot}^2 + 0.1013X_{rot} - 0.1268$ $\hspace{1cm}$ (C.4)

Tube 5: Brooks R 2-15 A $\quad Q_{rot} = 0.0002 \, X_{rot}^2 + 0.02X_{rot} - 0.0629$ $\hspace{1cm}$ (C.5)

Equations (C.1) to (C.5) were used to find the appropriate rotameter setting for a given flow rate. The flow rates were calculated to give a chosen range of values of stack exhaust velocity to windspeed ratio M defined as

$$ M = \alpha_m^{1/2} \left(\frac{\rho_e}{\rho_a} \right)^{0.5} \frac{W_e}{U_H} \hspace{2cm} (C.6) $$

where W_e is the mean stack exhaust velocity and U_H is the windspeed at the reference height H in the undisturbed approach flow. The reference height H is the height is the height of the reference building and is used to non-dimensionalize dilutions in the present study. ρ_e is the density of the stack exhaust, and ρ_a is the density of the approaching flow. For all cases in the current study the density of the exhaust gas and the approaching flow were equal so that for the laboratory simulations. The factor $\alpha_m^{1/2} = \sqrt{2}$ is used to correct the laminar velocity profiles in the laboratory to the correct full scale turbulent value, see Johnston and Wilson (1996), so for the current study

$$M = \sqrt{2} \left(\frac{W_{e,lab}}{U_{H,lab}} \right) \tag{C.7}$$

The mean exit velocity W_e is the volume flow rate from the stack Q_e divided by the area so

$$W_e = \frac{Q_e}{\frac{1}{4}\pi d^2} \tag{C.8}$$

where d is the inside diameter of the stack. Inserting this into Equation (C.7) and solving for the volume flow rate gives

$$Q_e = \frac{MU_H \left(\frac{1}{4}\pi d^2 \right)}{\sqrt{2}} \tag{C.9}$$

A laser doppler anemometer was used to measure the velocity profile in the water channel. The measurements were with no buildings present to find the velocity profile when undisturbed by the presence of any buildings. The measurements were made on the centerline of the water channel at a point 4 inches downstream from the end of the

118

roughness elements used to generate the correct turbulence in the flow. The velocity U in the approaching flow as a function of height z above the position of the bottom of the water channel was found to be

$$U = 62.6\,z^{0.26} \qquad\qquad (C.10)$$

for velocity U in mm/sec and z in mm. For the velocity U_H at reference height H=50.8mm, Equation (C.10) gives the velocity U_H =174mm/sec. Using this in Equation (C.9), along with d=0.1" (2.54mm) and α_m=2 the stack exhaust flow rate Q_e in mL/sec in terms of the exhaust velocity to windspeed ratio M is

$$Q_e = 0.6245\,M \quad [mL/\text{sec}] \qquad\qquad (C.11)$$

Most experiments in the current study were performed using performing windspeed ratios of M = 1, 1.5, 2, 3, 5, and 8. For each value of the velocity ratio M the required flow rate was calculated from Equation (C.11) and an appropriate rotameter was chosen. The correct setting for each rotameter was calculated from the polynomial fit for that rotameter, see Equations (C.1) to (C.5). Table C.1 gives a summary of the rotameters and settings used.

Table C.1 Rotameter Flow Rates and Settings

M	Q_s [mL/sec]	Rotameter	Setting
1	0.6245	Tube 4: R215B	9.15
1.5	0.9368	Tube 3: 603	46
2	1.2490	Tube 2: 603	65
3	1.8736	Tube 2: 603	113.5
5	3.1227	Tube 1: R615A	3.65
8	4.9963	Tube 1: R615A	5.65

REFERENCES

Johnston, C.R. and Wilson, D.J. (1996) "A vortex pair model for plume downwash into stack wakes" Atmospheric Environment 30 (accepted May 7/96) 8 journal pages.

Tube 1: Brooks Tube Size R-6-15-A

$Q_{rot} = 0.9228 X_{rot} - 0.2345$
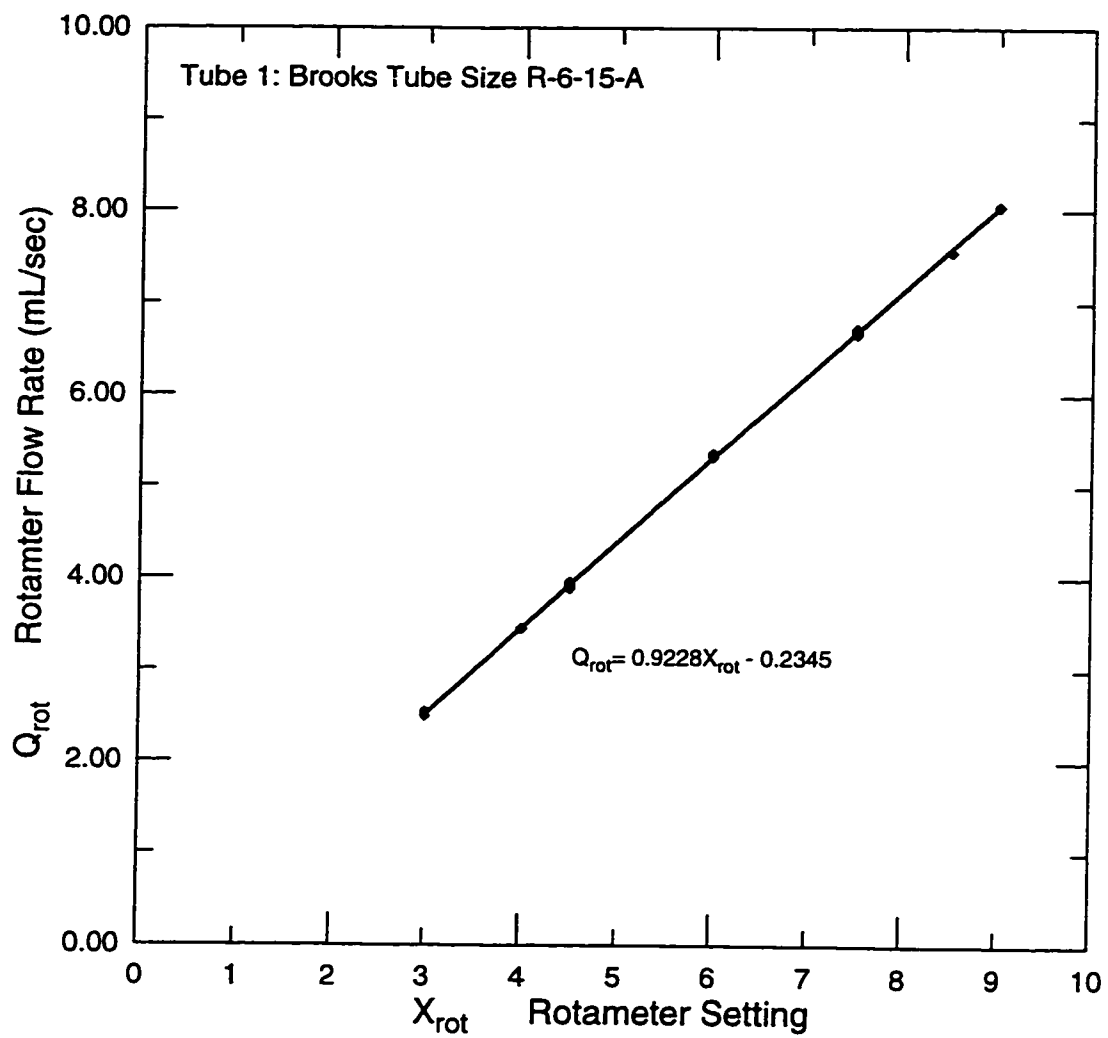
Figure C.1   Calibration curve for rotameter tube 1

121

The figure shows a calibration curve plotting Q_{rot} Rotameter Flow Rate (mL/sec) on the y-axis against X_{rot} Rotameter Setting on the x-axis. The plot is titled "Tube 2: Matheson 603" and includes the equation:

$$Q_{rot} = -6 \times 10^{-5} X_{rot}^2 + 0.0236 X_{rot} - 0.0323$$
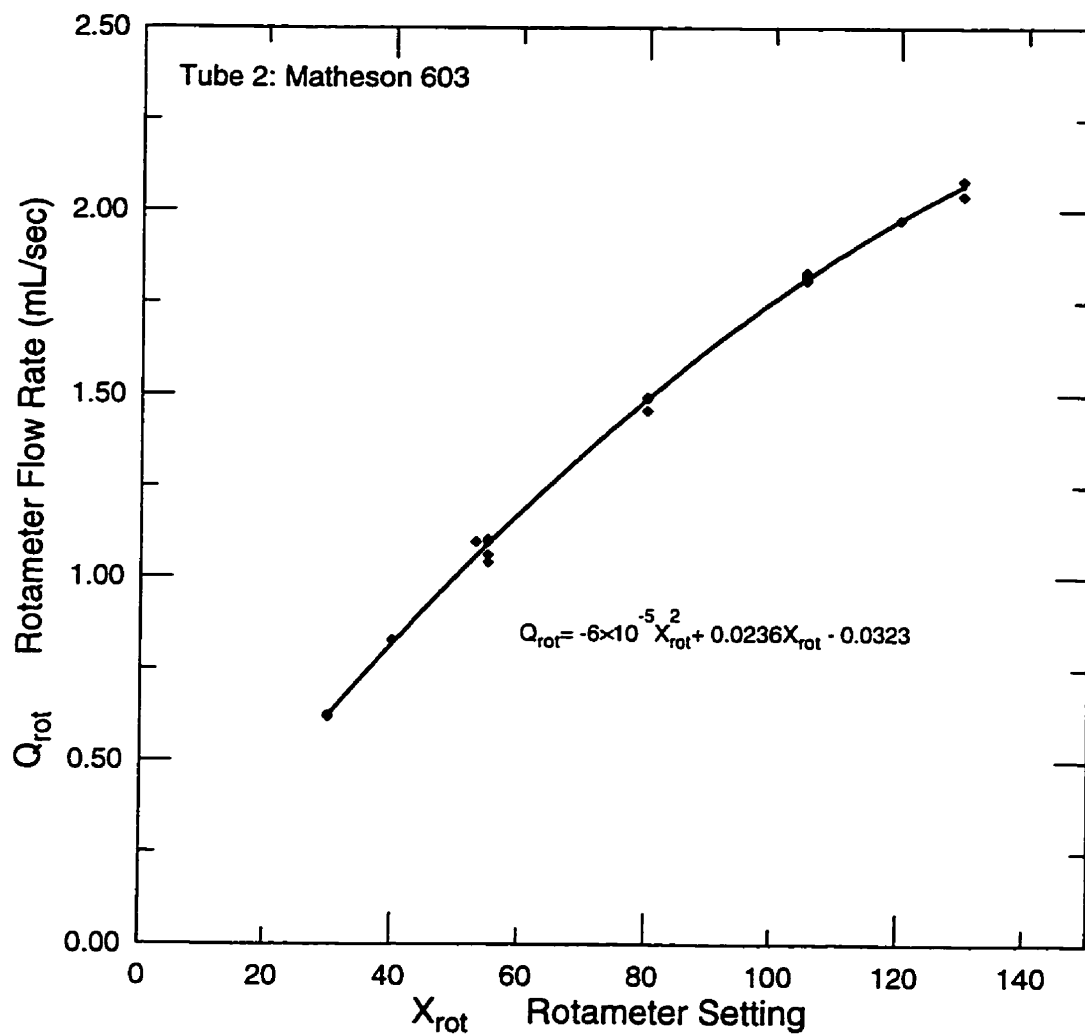
Figure C.2   Calibration curve for rotameter tube 2

122
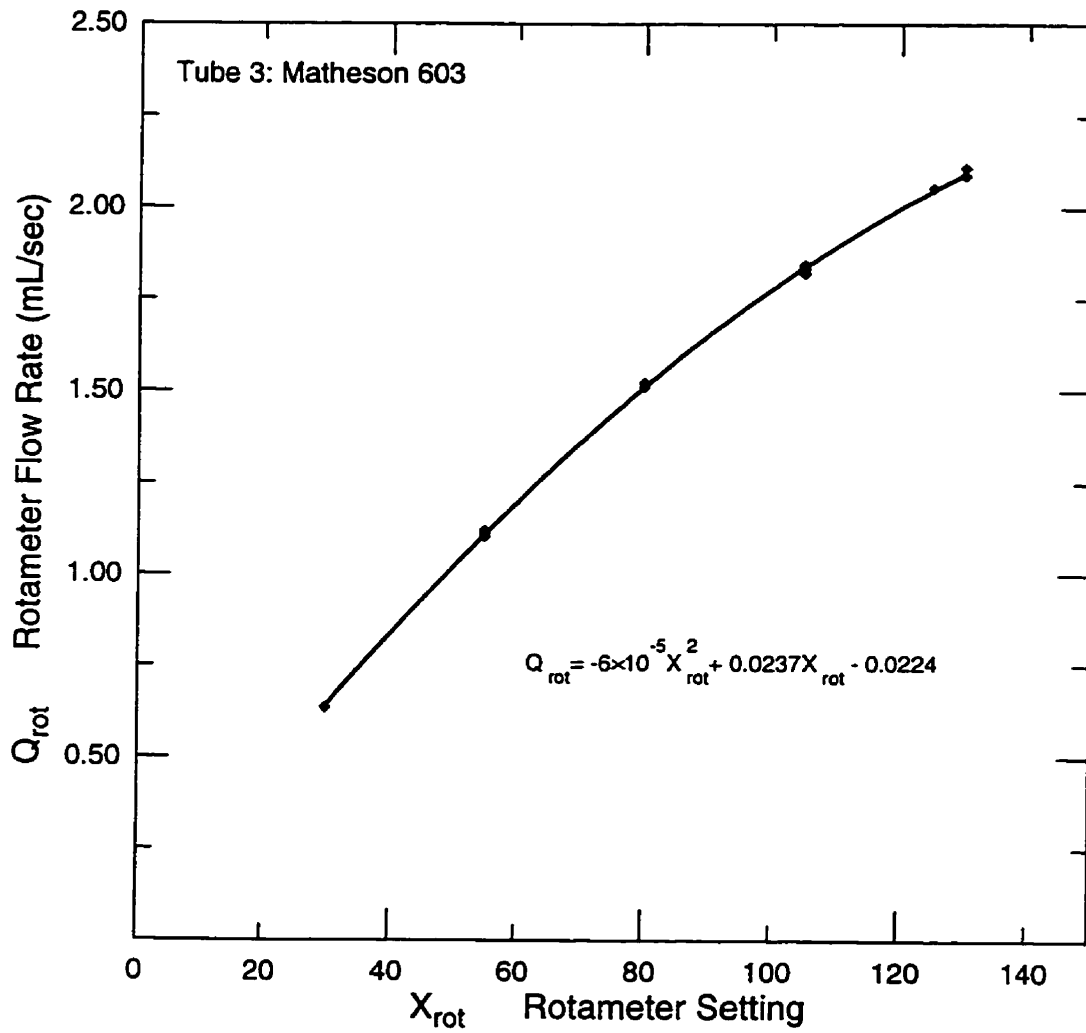
Figure C.3   Calibration curve for rotameter tube 3

The curve is labeled "Tube 3: Matheson 603" with the fitted equation:

$$Q_{rot} = -6\times10^{-5}X_{rot}^{2} + 0.0237X_{rot} - 0.0224$$

The y-axis is labeled Q_{rot} Rotameter Flow Rate (mL/sec) and the x-axis is labeled X_{rot} Rotameter Setting.
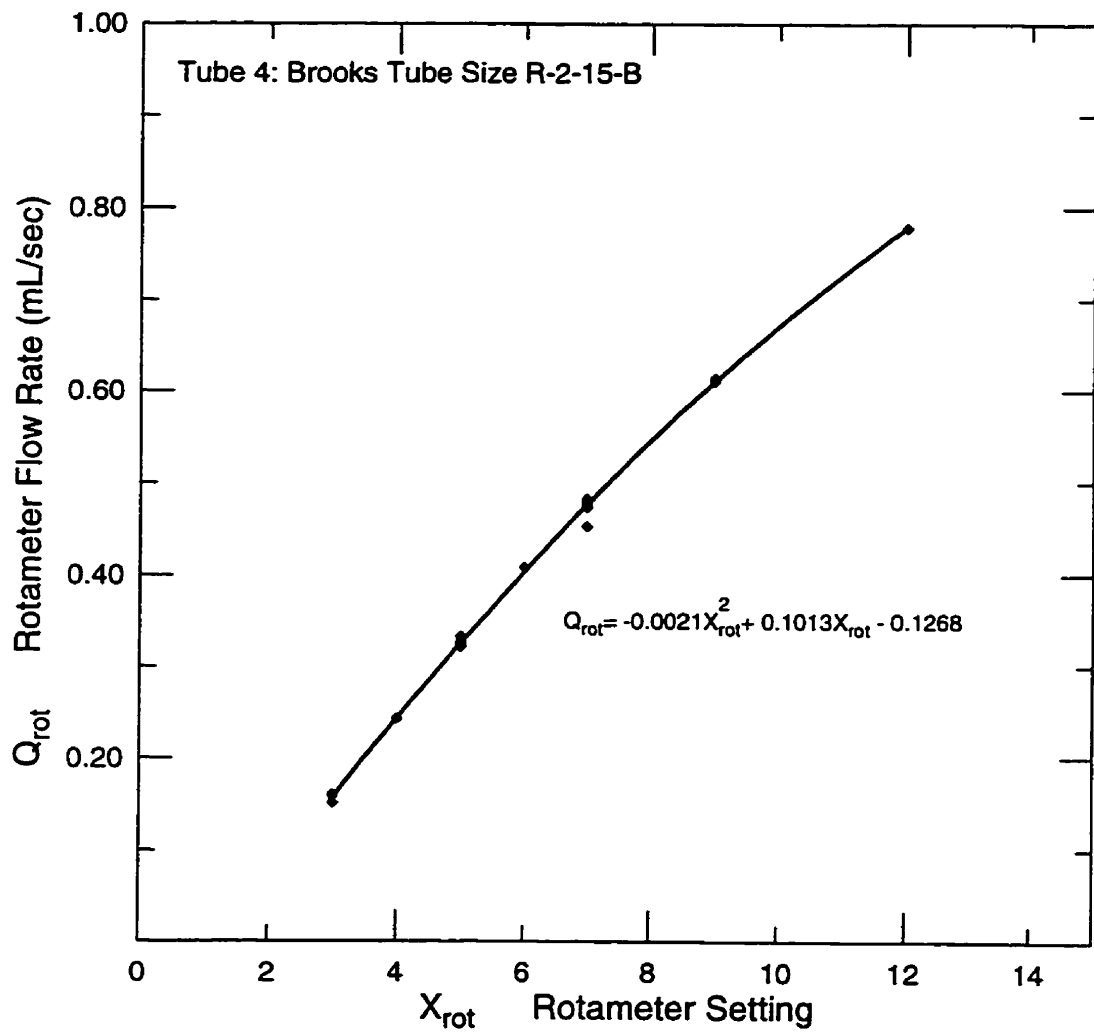
Figure C.4   Calibration curve for rotameter tube 4

The chart shows a calibration curve with axes labeled:
- Y-axis: Q_{rot} Rotameter Flow Rate (mL/sec), ranging from 0.00 to 0.25
- X-axis: X_{rot} Rotameter Setting, ranging from 0 to 14

Title on chart: Tube 5: Brooks Tube Size R-2-15-A

Equation on chart: $Q_{rot} = 0.0002X_{rot}^2 + 0.02X_{rot} - 0.0629$

Figure C.5   Calibration curve for rotameter tube 5

125

APPENDIX D
ATTENUATION OF DYE FLUORESCENCE LIGHT

INTRODUCTION

Flourescent light emitted from dye passing through a laser light sheet had to travel from the point at which the dye intersected the light sheet up through the water in the channel above that point to the camera above. If the water through which the light traveled also contained significant concentrations of dye then there was the potential problem that the flourescent light could be attenuated traveling between the laser sheet and the camera. In this appendix it will be shown that the attenuation of fluorescent light traveling the concentrations of tracer dye was negligible and did not need to be accounted for in the experiments.

PEAK ABSORPTION AND PEAK EMISSION

Light in laser sheets is absorbed by the flourescent dye molecules and re-emitted at a lower frequency. All the experiments for this thesis used Disodium fluorescein as the tracer dye. The peak absorption for fluorescein is at a wavelength of $\lambda_a = 488$nm. The peak emission is at a wavelength of $\lambda_f = 515$nm. The laser was operated in multiline mode meaning that a range of wavelength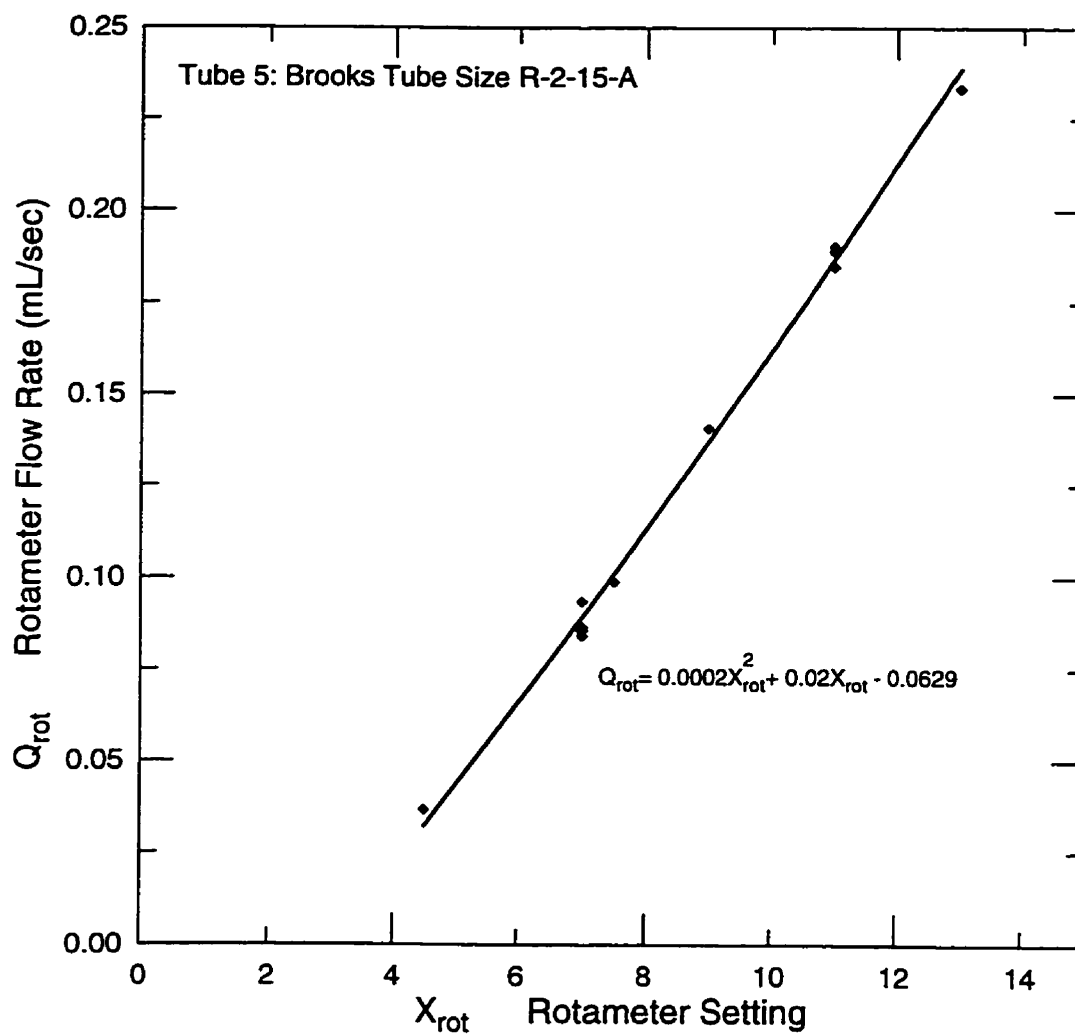s were emitted from the laser although only wavelengths around 488nm would be effectively absorbed by the dye. The fluorescence is at a lower wavelength of 515nm that is not effectively absorbed other dye molecules in the water over the 350 mm path length through which the light travels.

Experiments were performed to verify that indeed the fluorescent light was not reabsorbed by dye in the channel. A transparent bottle of dye was fixed in a position on the bottom of the water channel. A laser sheet was shone in the side of the bottle to illuminate the dye with large glass tank was placed above the bottle. The amount of dye

in the tank was raised in increments to observe the effect of the dye on the light reaching the camera. Figure D.1 shows the light intensity in counts detected by the camera as the amount of dye in the tank is increased. One can see that there is a negligible decrease in the light intensity detected by the camera, and from this it was concluded that the fluorescent light it not significantly affected by the concentration of dye through which it passes.
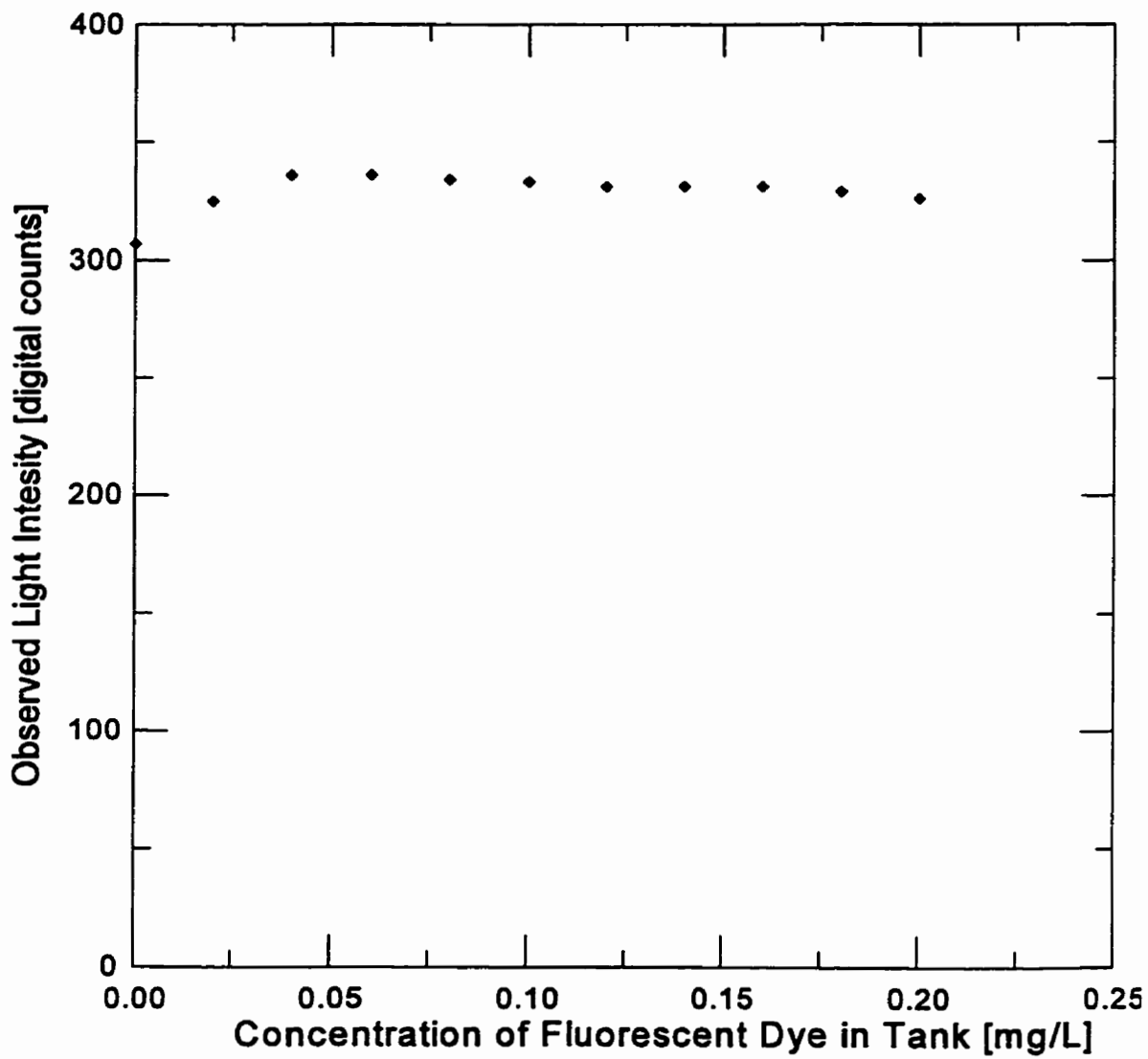
Figure D.1   Change in light intensity with increasing concentrations of fluorescent dye in tank above laser light sheet

128

APPENDIX E
LASER LIGHT ATTENUATION THROUGH A PLUME

INTRODUCTION

As a coherent beam of laser light travels through a concentration of fluorescein dye, the intensity of the beam gradually decreases as photons are absorbed by the dye particles. The attenuation of the beam at a certain point depends upon the concentration profile over the entire path length up to that point. For a plume with a highly intermittent concentration profile, correcting for laser beam attenuation would be very difficult as it would require knowledge of the concentration profile at each point in time. The experiments were arranged therefore, so that the concentrations in the plume would never be large enough to cause significant attenuation.

ATTENUATION IN PLUMES

Negligible attenuation through the plume was arranged for all experiments by fixing the source concentration. To estimate the attenuation through a plume, consider a source of diameter d_s emitting at a uniform concentration C_s. The size of the plume grows roughly in proportion to downstream distance from the stack x'.

$$d_{plume} = d_s + 0.16x'$$

(E.1)

Mass conservation then requires that the concentration C_x a downwind position obey the relation:

$$C_x \frac{\pi d_{plume}^2}{4} = C_s \frac{\pi d_s^2}{4}$$

(E.2)

129

.

For a coherent beam of laser light, the decay of beam intensity I_e goes like

$$I_e = I_o \exp(-\varepsilon \int_o^y C(y)dy)$$ (E.3)

where I_o is the initial intensity of the beam at $y=0$, see Appendix B. The attenuation will be negligible if the integral of concentration with distance is less than some critical value:

$$\int_0^y C(y)dy < crit$$ (E.4)

The critical value will depend on what maximum acceptable concentration across the plume is required. For a uniform concentration C_s at the source, the integral on concentration across the source diameter is

$$\int_0^{d_s} C_s dy = C_s d_s$$ (E.5)

Then at the any downstream position x:

$$\int_0^{d_{plume}} C_x dy = C_x d_{plume}$$ (E.6)

from Equation (E.2)

$$C_x d_{plume} = C_s \left(\frac{d_s^2}{d_{plume}} \right)$$ (E.7)

Since d_{plume} is always larger that d_s , from Equation (E.1) then

$$C_x d_{plume} = C_s d_s \left(\frac{d_s}{d_{plume}} \right) < C_s d_s \qquad\qquad \text{(E.8)}$$

Then if $C_s d_s$ < crit then $C_x d_{plume}$ < crit, then by fixing the value of C_s so that there is negligible at the source then this ensures that there is negligible attenuation at all downstream locations.

In the current study the source concentration was fixed at 4mg/L. The diameter of the source was 0.1"=2.54mm. At this concentration the attenuation coefficient calculated from Equation B.5 was ε=0.0055[mg/L]$^{-1}$[mm]$^{-1}$. This gives an attenuation of

$$\frac{I_e}{I_o} = \exp(-\varepsilon C(y)d_s) = 0.95$$

or 5% attenuation across the source which was determined to be acceptable. At all downstream positions the attenuation will be less than 5%.

APPENDIX F
VIDEO CAMERA LINEARITY

INTRODUCTION

Test were performed to determine whether or not camera response was linear with dye tracer concentration, since camera linearity greatly simplifies calibration. As well, tests were performed to determine the resolution of the camera.

CAMERA LINEARITY

Clear bottles of fluorescein dye placed on the bottom of the water channel and were illuminated by laser light sheet. The bottles contained know concentrations of dye ranging from 5 mg/L to 0.00390625mg/L, about a 250:1 range. Each bottle of dye was placed in an identical location and the observed average intensity from a 10 by 10 area of pixels in the camera was recorded. Figure F.1 shows a plot of camera intensity vs. concentration. The data is plotted on a log-log scale because concentrations varied over several orders of magnitude. Linearly related data should fall parallel to a 45° line on the log-log scale. For the most part the data does display this trend indicating that the camera response can be considered linear over the range of concentrations shown. At higher values of concentration, some of the data show lower concentrations than would be expected from a linear relationship. This can be attributed to the fact that, at higher concentrations, the laser light sheet is attenuated by the dye in the calibration bottle. The decrease in observed intensity is due to a decrease in the intensity of the laser light sheet intensity and not a decrease in camera response.

CAMERA RESOLUTION

Output from the camera is digitized to a value between 0 and 1023. Since output

of the camera was shown to be linear with light intensity and the intensity of light emitted from the fluorescent dye was shown to vary linear with light intensity, calibrations of camera output could done using a single known concentration. For the present study, all calibrations were done using a calibration concentration of 0.04 mg/L. The source concentration for all of the experiments was 4 mg/L so that all calibrations were done at a dilution of 100:1.

For a typical calibration the camera output for a concentration of 0.04 mg/L was roughly 250 counts depending on what region of the laser light sheet was being viewed by the camera. This gives a sensitivity of 0.00016 mg/L per count. This means the system could detect dilutions between 25:1 and 25000:1.

To estimate the amount of noise in the system the intensity of a point in the calibration box was collected 50 times. The concentration in the calibration box and the laser power remained constant so that the light intensity should have remained constant. From the 50 separated readings, the standard deviation in the measurements was determined to be ±5 counts. During the actual experiments the reading were averaged over 1000 frames. Since the error is inversely proportional to the square root of the number of counts $\sqrt{N}$, the error for 1000 frames works out to ±1.118 counts, roughly a dilution of 22361:1

133

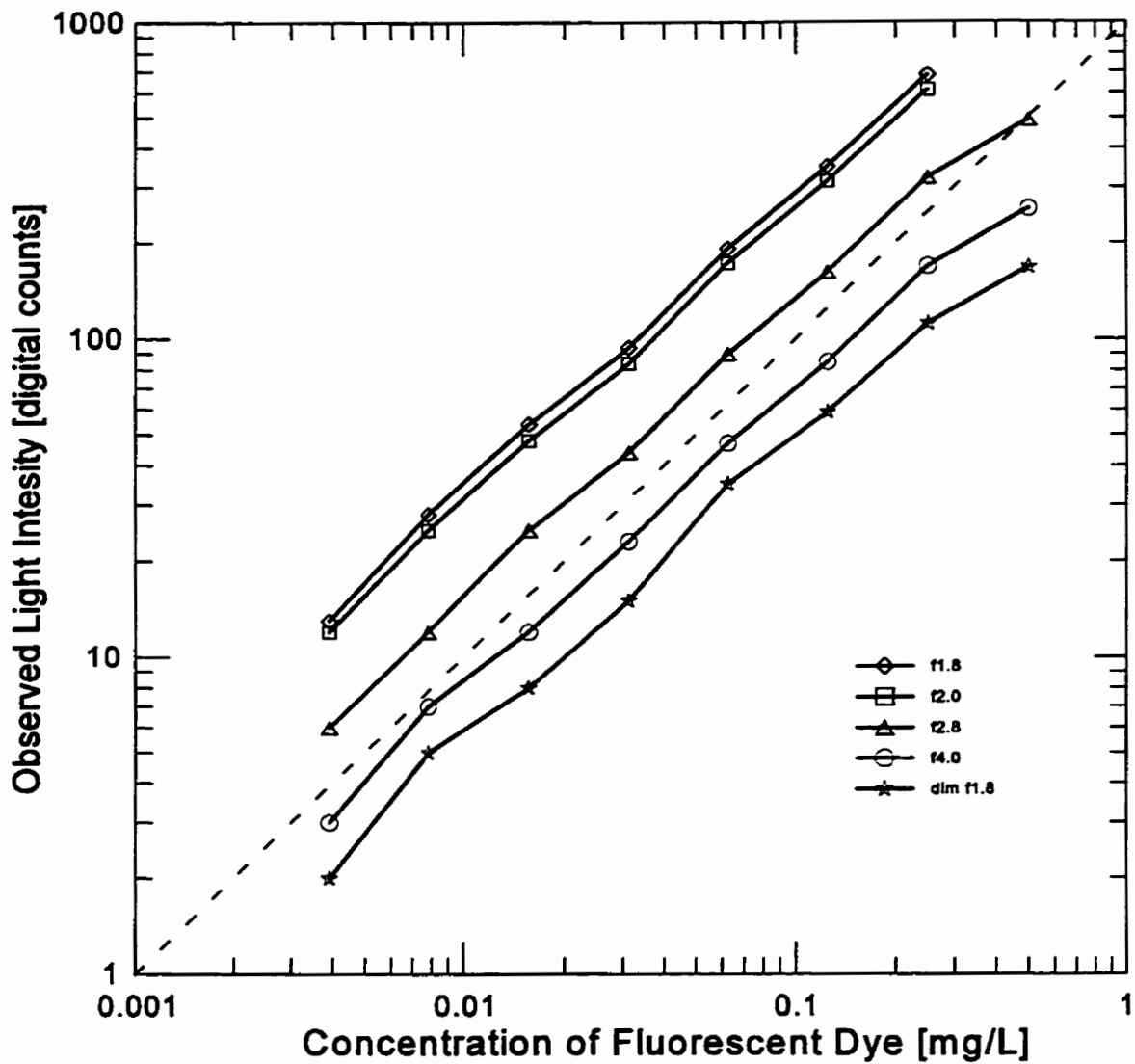Figure F.1   Intensity observed in the camera with increasing concentration showing
              camera linearity. Linear functions are parallel to the 45° on the center
              of the graph. Different sets of data were taken with different camera f
              stop settings on the camera. The set marked "dim f1.8" was done with
              of laser light sheet of lower intensity than the other cases.

134

APPENDIX G
DATA ANALYSIS PROCEDURES

INTRODUCTION

For each building configuration, all possible combination of stack height, stack location and exhaust velocity to windspeed ratio M, were performed together on the same day as a set of 54 runs. The water in the channel was refilled before each of these runs. Before each of these sets of runs a calibration was performed to determine the camera response to changes in concentration for that particular scenario. This changes from run to run due to slight differences in laser power, distance between camera and the light sheets, different height of the light sheets and different amount of zoom on the camera. Performing a calibration before each set of 54 runs accounts for small changes in each of these parameters.

LOCATIONS

The corners of the buildings provided reference points from which the distances between points in the camera could be determined. At the beginning of each calibration, the locations in terms of camera pixels were recorded using the "locate" computer program. Each corner was recorded with its label and the x and y location in pixel number. Location in the x direction varied from pixel 0 to 639, and Location in the y direction varied from pixel 0 to 479. The corners of the emitting building were always labeled A, B, C, and D starting with point A the top left corner and moving around the building clockwise with the camera looking down from above The corners of the adjacent building were always recorded as E, F, G, and H with point E in the top left corner and moving around the building clockwise with the camera looking from above.

For the mirrored buildings, the corners of the area of the face of the building upon

which concentrations were being measured that was visible in to the camera were recorded as J, K, L, and M starting with J in the top left corner and moving around the building in the clockwise direction. For the cases were there was a gap between the emitting building and an adjacent mirrored building all of the face of the mirrored building closest to the adjacent building should be visible in the mirror. This put points J and M at the ground and L and K at the roof if the adjacent building was downwind of the emitting building. If the adjacent building was upwind of the adjacent building, then points J and M would have been at the roof and points K and L would be at the ground. In reality, the entire face of the building was not visible in the mirror due to the thickness of the by the metal used to make the sides of the building and the glass used to construct the top of the building in front of the building.

For the cases where there was zero gap width between the emitting and adjacent buildings then data would only be available on the portion of the wall of the adjacent building that is above the height of the emitting building. This puts points J and M at the emitting building roof level if the adjacent building is downstream of the emitting building. If the adjacent building is upstream of the emitting building then points J and M would be at the top of the adjacent building with points K and L at the emitting building roof level.

In addition to the corners of the buildings, the locations of the three stacks were recorded. The stacks were labeled 1, 2, and 3 with 1 being the most upstream stack. Note that these locations were only recorded for roof level measurements. If there was a split in the level of the light sheets then the location of the split was recorded and given the label S. Only the x position on the split was important, and location was only relevant for roof level measurements were there was a difference in building heights. All of these locations were stored in a single text file with a ".LOC" extension.

CALIBRATION IMAGES

The calibration box was placed around the buildings in question so that the entire are to be viewed by the camera would be enclosed by the calibration box. The box was placed roughly in the center of the water channel so with its sides parallel to the sides of the water channel. A small submersible pump was placed in the corner of the box outside the view of the camera to continuously stir the water inside the box during the calibration process and prevent dye bleaching.

After the laser had been turned on and properly aligned and all the buildings were in the correct position, a background image was taken using the "Backsht" program. The program took 100 frames at 10 frames per second and stored the sum of the counts recorded at each pixel for the 100 frames. Since the water was refilled before each calibration, the water in the box contained no fluorescent dye.

After the background had been taken, calibration images were taken with two different concentrations of fluorescein dye the calibration box. In theory, only one concentration was required for calibration since the camera response was linear, but a second concentration was used to see if one known concentration could be reproduced from the other. The was a useful check to ensure that nothing had gone wrong during the calibration process.

The two concentrations used for all calibrations in the present study were 0.01mg/L and 0.04mg/L. The inside dimensions of the calibration box were 52 cm long by 32 cm wide with length in the direction of the flow (when the water channel was operating) and width in the crosswind direction. The height the water in the box was 35 cm that is the height at which the channel operated during actual runs. This yields a box volume of 58240 mL minus the volume of the buildings minus 250mL for the volume of the fish pump. From the volume of the box, the amount of fluorescein dye

required to produced concentrations of 0.01mg/L and 0.04 mg/L could be calculated. The fluorescent dye introduced into the calibration box came from a previously mixed stock solution of 400mg/L. The appropriate amount of dye was measured by weight on an electronic balance. The 400mg/L stock solution used to create the correct concentrations in the calibration box was the same solution used to mix the 4mg/L source solution that was used emitted from the stacks during the plume simulations.

The calibration images were taken at 10 frames per second, for 10 seconds using the "Calsht" program. This program stored the sum of all counts at each pixel taken over 100 frames. The operations of the program "Calsht" is identical to the operation of the "Backsht" program used to take background images except that the "Calsht" program asks the user for additional information to be stored with the file. The program asks for:

- concentration used in calibration
- The location file containing the corners of the building, stack locations and split
- The length and width of the emitting and adjacent buildings.
- The distance from the inside edge of the calibration box the nearest building edge of the adjacent and emitting buildings.

From the length and widths of the emitting and adjacent buildings the program calculated the mm per pixel in the x and y directions over the emitting and adjacent building roofs since the number of pixels between building corners could be found from the location file. The mm per pixel was stored for both the emitting and adjacent buildings if they are at different heights due to the fact that the number of mm per pixel were not be the same if they were at different distances from the camera.

The distance from the inside edge of the calibration box to the nearest building edge was used to calculate the distance from the inside edge of the calibration box

138

through which the laser light sheet enters to the first row ($y=0$) in the camera. This distance was calculated for both the emitting and adjacent building. This distance was used in the attenuation correction in the gain calculation discussed in the next section.

GAIN

A gain G_{ij} was calculated for each pixel so that the concentration at any point C_{ij} and is related to the observed intensity I_{ij} as

$$C_{ij} = G_{ij} I_{ij} \qquad \text{(G.1)}$$

The program "Findgain" takes a calibration image and a background image and creates a binary file containing the gain at each pixel. The program takes the calibration image and subtracts the background image in the box. If either the calibration image or the background image has a value greater than 1000 counts (on a scale of 0 - 1023) the point is considered overloaded and a value of 1000 time the calibration concentration is stored for that point. This value of 1000 times the calibration concentration is an arbitrarily chosen large value used to mark overflowed points. If the calibration image minus the background has a value of less than 0.1 at any point then the point is considered to have under flowed and a gain and 0 is stored for that point to mark it as an underflow.

The remaining acceptable pixel outputs need to be corrected for attenuation as the laser light sheet decays as it passes through the box. The observed intensity needs to be adjusted to the value that would have been seen at a particular point if the laser light sheet had reached that point without being attenuated by passing through any concentration of fluorescein dye. If the initial intensity of a coherent beam of laser light was I_o then the intensity after passing through a distance Δy of constant concentration C then the intensity of the beam is I_e is

$$I_e = I_o \exp(-\varepsilon C \Delta y) \qquad \text{(G.2)}$$

If it is assumed that the initial intensity of the beam I_o is the same as the intensity of the beam that would have been observed at point ij if the beam had not passed through any concentration before reaching point ij, call this intensity $I_{o,ij}$, then the actual observed intensity at point ij would be

$$I_{ij} = I_{o,ij} \exp(-\varepsilon C_{cal} \Delta y_j) \qquad \text{(G.3)}$$

where C_{cal} is the known concentration in the calibration box and Δy_j is the distance from inside edge of the box to row j. This is calculated from the pixel number j times the mm per pixel in the y direction and the boxdistance from the calibration file that gives the distance from the inside edge of the calibration box to row $y=0$ in the camera.

The camera gain for each pixel should then be the known concentration in the calibration box C_{known} divided by the unattenuated fluorescence intensity $I_{o,ij}$ since this is the intensity that will be present in the actual plume simulations where there is negligible attenuation through the plume (see Appendix E), therefore using Equations (G.1) and (G.3)

$$G_{ij} = \frac{C_{cal}}{I_{o,ij}} = \frac{C_{cal}}{I_{ij} / \exp(-\varepsilon C_{cal} \Delta y_j)} \qquad \text{(G.4)}$$

This gain is stored in a gain file with a ".GN1" extension. This file is a binary file of double precision real numbers.

PLUME CONCENTRATIONS

All plumes were averaged over 100 seconds (1000 frames at 10 frames per

second). The program "threshavg" was created to acquire this data. The program stores the total counts for each pixel acquire over 1000 frames and in addition calculates the intermittency at each pixel. The intermittency is the percentage of the time there was a reading at that point above a certain threshold. For the plume simulation performed in the current study the threshold was 5 counts above the background image taken before the plume image. The program also prompted the user for the stack number, stack height and the flow rate which was stored along with the plume image.

The next step in the process was to use the gain file to extract concentrations from the intensity readings in the plume image. For each point ij, the concentration at that point C_{ij} was the gain G_{ij} times the observed intensity at that point I_{ij}
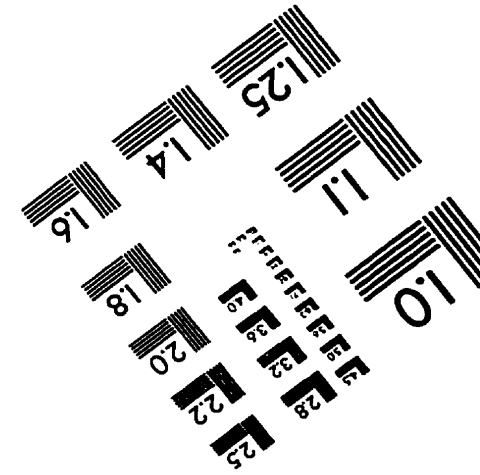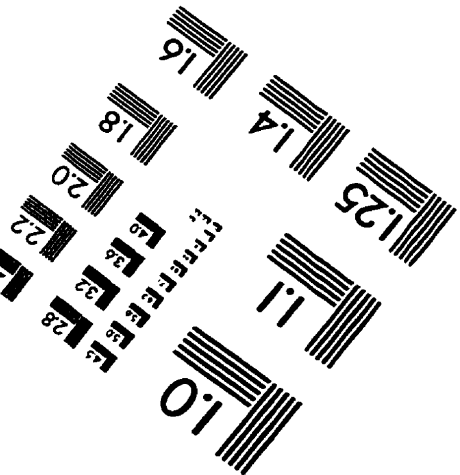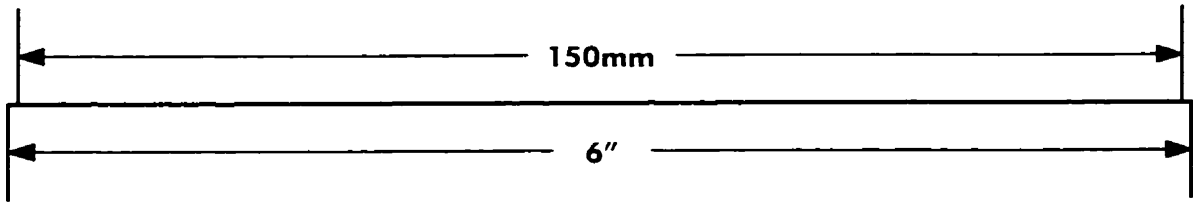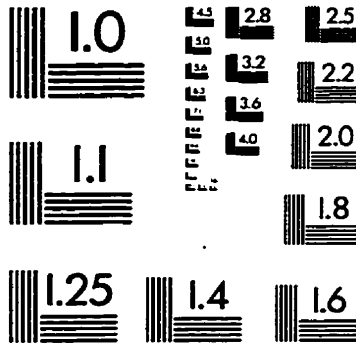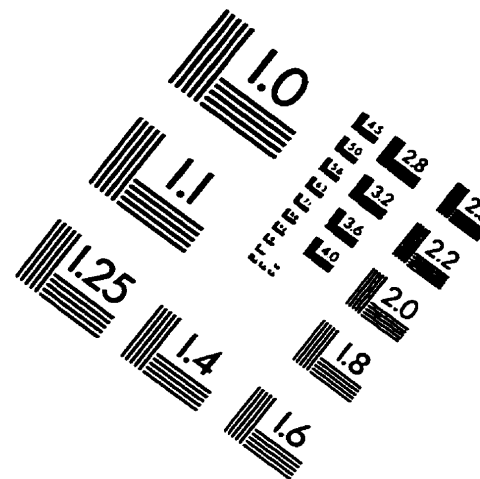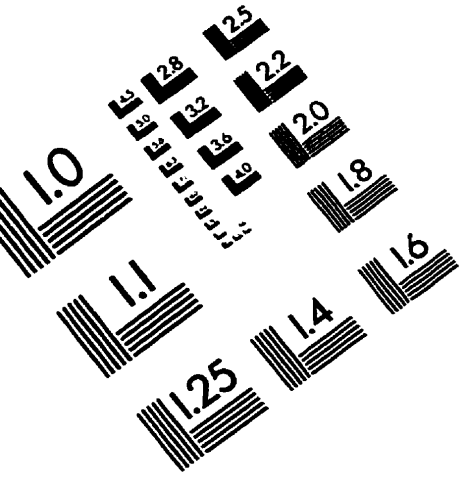
If either the plume image or background image at any point had an average intensity above 1000 the point was considered to have overloaded and the point was assigned a concentration of 1000 times the source concentration, or if the gain at any point had a value of 1000 times the calibration concentration calibration having been marked as an overflowed point in the calibration image, it was given a value of 1000 times the source concentration. Similarly if any point had a gain of zero having been marked as an underflow in the calibration image, it was also give a value of 1000 times the source concentration. The value of 1000 times the source concentration was an arbitrarily chosen large value used to mark all bad points.

Each calibration ".CN1" file is a binary file containing the concentration at each point stored with double precision real variables. Data from these files is extracted using the "Surf" program to create data that can be used for contour plots and the "mindilut" program to create data that can be used for plots of minimum (centerline) dilution. The "Surf" program takes the concentration ".CN1" and uses every fifth point to create columns of data that can be used to create contour plots. Every fifth point is used since this gives adequate resolution at reduces the time required to process the data. Each row

in the file contains x pixel location, y pixel location, x position in mm, y position in mm, concentration, dilution, and normalized dilution. These files are ASCII text files.

IMAGE EVALUATION
TEST TARGET (QA-3)

150mm

6"